Optimal design of reinforcement of masonry arches = Progetto ottimo di rinforzi di archi in muratura

Department of Architecture, Construction and Design
Ph.D. Program:
KNOWLEDGE AND INNOVATION IN HERITAGE DESIGN
SSD: ICAR/08–Structural Mechanics

Optimal design of reinforcement of masonry arches

by
Mariaceleste Lasorella

Supervisors:
Prof. Mario Daniele Piccioni
Prof. Aguinaldo Fraddosio
Prof. Elio Sacco

Coordinator of Ph.D. Program:
Prof. Carlo Moccia

Course n°35, 01/11/2019-31/10/2022

Dipartimento Architettura, Costruzione e Design
CORSO DI DOTTORATO:
CONOSCENZA E INNOVAZIONE NEL PROGETTO PER IL PATRIMONIO
SSD: ICAR/08–Scienza delle Costruzioni

Progetto ottimo di rinforzi di archi in muratura

Dottoranda
Mariaceleste Lasorella

Tutor:
Prof. Mario Daniele Piccioni
Prof. Aguinaldo Fraddosio
Prof. Elio Sacco

Coordinatore del Corso di Dottorato:
Prof. Carlo Moccia

Corso n°35, 01/11/2019-31/10/2022

CONTENTS

INTRODUCTION

Italy has a rich architectural heritage that requires ongoing interventions for the preservation of its historical significance and structural integrity.

Conceived to withstand gravitational loads through their geometric configuration, masonry constructions are vulnerable to instabilities caused by external actions such as differential foundation settlements, seismic action, and long-term deformations.

Recent studies, questioning the well-established conception of masonry as unable of withstanding the above-mentioned load conditions, largely fueled by the Elasticity Theory [1] defining structural safety in terms of material strength rather than stability, have recognized masonry constructions a certain capacity of triggering *rocking* mechanisms to accommodate these external actions and thus exhibiting an additional resistance to seismic actions [2] [3].

Even considering this *rocking* mechanism, the level of structural safety has not always been sufficiently high as evidenced by the devastating effects of the recent seismic events, which highlighted the weak mechanical behavior of masonry structures under seismic action and thus the need for strengthening interventions.

Nevertheless, as recent seismic events demonstrated, current strengthening techniques proved ineffective in preserving masonry constructions and, in some cases, even contributed to the global collapse of the construction by triggering unexpected mechanism in historical masonry structures, as evidenced by the collapse of San Marco [4], the Basilica of Santa Maria Paganica [5], the Basilica of San Francesco in Assisi [6] and the Basilica Santa Maria in Collemaggio [7].

Since any strengthening intervention alters the mechanical response of masonry, ensuring the structural safety of masonry constructions is rarely reconciled with the need for

conservation. These two purposes are frequently incompatible, as providing the adequate level of structural safety has often resulted in the adoption of inappropriate strengthening solutions.

Being the gap between structural safety and preservation still an open issue, the scientific community has been actively involved in a constant search, which has never exhausted, for both new approaches for the structural assessment [8] and new strengthening systems for historical constructions. This also reflected in the framework of the most recent regulatory developments underlying the design of strengthening techniques and professional practice [9] where a higher emphasis on the conservation aspects of architectural heritage is given [10].

To address this need, innovative strengthening materials, such as Fiber Reinforced Cementitious Matrix composites (FRCM), have been developed and have gained increasing endorsement as an alternative to more well-known FRP due to more compatibility with the substrates being reinforced [11]. However, experimental results have demonstrated that the presence of reinforcement substantially alters the structural response of masonry and different collapse mode become possible, such as crushing or sliding between joints [12] [13]. Moreover, since not only rocking but also sliding mechanisms are allowed, it is not possible to rely on the simplified Heyman's model [14] but it is necessary to reformulate the problem for defining the safety level of masonry structures in the more complex framework of the non-standard Limit Analysis [15].

In an attempt to provide a solution for bridging this antinomy between structural safety and preservation, the main purpose of the present thesis is to define a design procedure for the reinforcement of masonry arches to suitably increase the value of the collapse multiplier, without completely constraint the structural system and preventing the sliding mechanisms. The idea is to design a reinforcement defined as "optimal". The term "optimal" here means that the reinforcement has to provide the arch with the sufficient safety capacity by defining a proper localization of the reinforcement, located at the intrados or the extrados, thus allowing the arch to accommodate the displacement due to the seismic action or settlements with a four-hinge mechanism.

This thesis is divided into three parts. In Part I, the purpose that motivated the thesis topic is defined and framed within the current research scenario. In this first part, some case studies demonstrating the limited effectiveness of the current strengthening strategies are reported and effective solution for the conservation of historical masonry construction are proposed. In Part II, the computational approaches and modelling strategies that are typically employed to assess the safety level of existing historical constructions are shown with a focus on limit

analysis approaches underlying the main advantages of this methods in describing the structural behavior of unreinforced and reinforced masonry.

In part III, the limit analysis problem with non-associative flow rule for the design of reinforcement is reformulated. An algorithm for solving limit analysis problem with both the Coulomb criterium with associative flow rule (dilatancy associated to the sliding) and a non-associative Coulomb criterium (sliding without dilatancy) is defined. In particular, the approach to solve the limit analysis problem for the non-associative case involves the solution of the nonlinear programming (NLP) as a sequence of linear programming problems (LP). Then, this algorithm is enhanced with an additional constraint equation in the linear programming problem to take into account the inserted reinforcement.

The MATLAB code implementing the nonlinear programming problem is validated through numerical simulations. In these simulations, the collapse mechanisms of the unreinforced and reinforced configurations are thoroughly analyzed for masonry block systems to assess the effect of the reinforcement on the increase in collapse load multiplier and the resulting collapse mechanism. Moreover, for the design of the optimal reinforcement two different mechanical responses of the reinforcement will be considered: elastic reinforcement and elastic-perfectly plastic reinforcement.

A first solution considered is the use of an ideal "elastic" reinforcement preventing a hinge to occur on the opposite side of the interface where the reinforcement is applied. In the limit analysis problem, the introduction of elastic reinforcements leads to a full constraint for relative displacements, reducing in such a way the degrees of freedom of the structural system. This allows for an initial assessment of the arch response and the definition of potential areas for reinforcement placement.

A second option is to employ elastic-perfectly plastic reinforcements that give the structure some degree of ductility. The introduction of elastic-perfectly plastic reinforcements is accounted in the equilibrium equation. By incorporating the concept of "plastic behavior", the reinforcement design will accommodate for localized displacements and optimal redistribution of forces.

Through a sequential design approach, a comprehensive understanding of the reinforcement design process is provided, offering insights into both elastic and elastic-perfectly plastic behavior. Consequently, this investigation has facilitated the identification and the proposal of potential reinforcement strategies that effectively enhance safety while preserving the fundamental characteristics and the collapse mechanisms of masonry arches.

PART I PRESERVATION OF ARCHITECTURAL HERITAGE: THE ANTINOMY BETWEEN SAFETY AND CONSERVATION

Chapter 1
Structural safety of masonry constructions: the importance of preservation

Italy is renowned for its varied and rich architectural heritage with a storied past. However, it is also prone to earthquakes, and these natural disasters have had devastating effects on its constructions due to the weak mechanical behavior of masonry under seismic action. Notable earthquakes include those that occurred in 1997 in Umbria and Marche, 1980 in Irpinia, 2009 in L'Aquila, 2012 in Emilia, and 2016 in central Italy, as these events have had a significant impact.

It is widely recognized that equilibrium in historic masonry constructions is a problem of stability. Although masonry can withstand external static actions through its geometrical configuration, it is vulnerable to instabilities caused by differential foundation settlements, seismic activity, and long-term deformations. Therefore, preserving these structures and ensuring that they can withstand earthquakes is crucial for their conservation.

Due to this vulnerability of historic masonry constructions, several strengthening techniques have been employed over time to improve their safety. Given the limitations of the current techniques, an update in assessment and intervention approaches is necessary. As a result, numerous technological approaches have been developed to address the specific challenges in the safety assessment of historic structures. This is reflected in the most recent regulatory developments and conceptual frameworks underlying the design of consolidation interventions and professional practice [9] [10].

Indeed, the scientific community has been actively involved in addressing the challenges posed by the numerous earthquakes that have affected historic centers and tested the outcomes of post-earthquake emergency interventions. The limitations of traditional and current reinforcement techniques have highlighted the need for a substantial and rapid update:

- of the scientific knowledge,
- of the technical regulations,
- of the practical design methodologies.

The following section examines the lessons that can be learned from these experiences to improve the preservation of heritage buildings.

1.1. Masonry structural behavior in seismic zones: insights from recent earthquakes

The importance of preserving Italian architectural heritage and ensuring structural safety in seismic zones has been highlighted by recent seismic events. In the wake of these events, measures have been taken for the preservation of the rich cultural and historical heritage of the country.

Figure 1: Santa Maria ad Nives Church in Osoppo (left), Ognissanti di Ospedaletto Church in Gemona (right) after Friuli earthquake of 1976.

Following the Friuli earthquake of 1976 (Figure 1), a process of continuous search for new materials and strengthening techniques for historical constructions began, which has never been exhausted. In fact, this was the crucial event that led to the spread of a new generation of methodologies for the structural assessment, in the static and seismic analysis.

The seismic events that occurred in the following decades, however, have exposed the limitations of these recent interventions, whose design was influenced by the scientific and

cultural context of the time, without a comprehensive understanding of the actual structural behavior of masonry buildings. In fact, the 1997 earthquake in Umbria and the 1980 earthquake in Marche, followed by the L'Aquila earthquake in 2009 and the Emilia Romagna earthquake in 2012, has brought to light the vulnerability of much of Italian historic built environment (Figure 2). The earthquakes subjected masonry structures to strong forces, resulting in extensive damages. Furthermore, many existing masonry structures were made even more vulnerable by previous interventions. The combination of these factors resulted in widespread and severe damages.

Figure 2: Mulino church in San Felice, after the 2012 earthquake and St. Maria Church in Paganica, damaged by 2009 L'Aquila earthquake.

Researchers have dedicated their efforts to develop approaches that enhance the understanding of the mechanical behavior of masonry during seismic events. A structural damage survey was conducted to identify the behavior and vulnerabilities of different type of structures, focusing on the study of the kinematic mechanisms of the macro-elements that compose a masonry building and act as monolithic units [16]. The damage assessment conducted revealed that the masonry monolithic behavior was not always observed, often due to the poor quality of the material which caused entire walls to collapse as illustrated in Figure 3.
Brandonisio et al. [17] studied the seismic behavior of masonry churches that were damaged during the 2009 earthquake. Lagomarsino [18] conducted a more comprehensive assessment of the damages sustained by over 700 churches to identify the collapse mechanisms of different architectural elements. In [19], Lagomarsino et al. proposed a new methodology for assessing seismic damage in the churches of Umbria and the Marche.

Furthermore, with regards to the structural damage caused by the seismic events of the 2016-2017 Central Italy seismic sequence, an extensive database was compiled based on in situ surveys conducted during that period, as documented in [20] [21] [22], providing valuable insights into the inherent vulnerability of masonry churches when subjected to seismic activity.

Figure 3: S. Biagio church in L'Aquila [17] (left), S. Maria Assunta Church in Montesanto [19] (centre), the apse of S. Eusanio Martyr church in S. Eusanio Forconese [18] (right).

The earthquakes occurred in Italy have highlighted the necessity for enhancing the seismic resistance of historical structures to prevent future damage. Many of the technological solutions proposed in the years following the earthquakes, such as resin, reinforced injections and replacing wooden structures or vaults with reinforced concrete structures, did not withstand subsequent earthquakes unharmed. The post-earthquake surveys have confirmed the importance of designing and implementing appropriate strengthening interventions.

1.2. Current approaches for the structural safety: design principles and limitations

Before the Friuli 1976 and Irpinia 1980 earthquakes, strengthening interventions, which were frequently invasive and inadequate, were conducted in an effort to comply with building code requirements for standard construction introduced in [23] [24], then integrated and updated in [9]. However, the current approach places a higher emphasis on the conservation and preservation of architectural heritage [10]. In fact, defining criteria for classifying safety levels and intervention approaches for masonry structures is still an ongoing challenge, even in the context of the recent technical standards.

Ensuring the structural safety of masonry constructions, particularly those located in earthquake zones, is rarely reconciled with the need for conservation. These two purposes are frequently incompatible, as a strong emphasis on safety has often resulted in the adoption of inappropriate design solutions.

One of the issues that has significantly hindered the intervention approach on masonry structures is a context heavily influenced by well-established theories, such as the Elasticity Theory [1]. While this theory may be effective for certain types of structures (such as steel or reinforced concrete), it fails to accurately depict the behavior of masonry, leading to the perception of masonry as lower in strength and hence the implementation of interventions that alter its structural functioning in an attempt to bring it to the level of safety of reinforced concrete structures. On the other hand, the approach based on numerical values, such as the *nominal life*, which is relevant for new constructions but not applicable to existing and historic ones.

Considering the problem of the preservation of historical buildings even only from the point of view of structural safety, hence ignoring the aspects related to the preservation of historical and artistic values, any idea of achieving significant and reliable effects through technological solutions that substantially alter the mechanical properties of materials and the structural behavior must be abandoned.

The definition of the level of safety according to the criteria of the regulatory framework represent only a few aspects of the design of strengthening interventions on masonry structures. Another fundamental aspect, that will be comprehensively discussed in the following, is the definition of physical models and thus of the analytical and numerical methods needed to quantify this level, as well as the techniques for carrying out interventions that are reliable and consistent with the interpretative models of the complex mechanics of historical structures.

1.3. Main requirements for the preservation of historical structures

The current principles of architectural preservation have been formalized in various guidelines (ICOMOS Charter [25], Carta Italiana del Restauro [26], [27]) and in Cesare Brandi's Theory of Restoration in 1977 [28] . These principles, which must be applied in the practice of an architectural restoration project, include:

- *Recognizability*: any restoration work should be clearly distinguishable from the original material of the artifact or structure, without disturbing the overall appearance of the object.
- *Minimum intervention*: restoration should interfere as little as possible with the original material of the object or site and should only be carried out to the extent necessary to preserve its cultural value.
- *Reversibility*: any restoration interventions should be reversible, meaning that they can be undone in the future if necessary.
- *Compatibility*: any interventions or treatments carried out on an object or site should be compatible with the original material and its cultural significance. In other words, the restoration should not introduce materials or techniques that are incompatible with the original, as this can undermine the authenticity and cultural value of the object or site.
- *Interdisciplinarity*: a restoration project may involve professionals from diverse fields, all of whom bring unique insights to the project.

Moreover, architectural restoration should prioritize the preservation of the *integrity* and *authenticity* of the structure. This involves using appropriate materials and techniques that respect the historical and cultural significance of the structure and avoiding any alterations or damages to the original material or the removal of any essential elements. In order to achieve these goals, as mentioned above, the restoration should be reversible and minimally invasive. Ultimately, to effectively protect architectural heritage, a comprehensive strategy must address both conservation and safety concerns. It is crucial an in-depth understanding of both these aspects in relation to the specific construction. The approach outlined in the Italian guidelines for interventions on cultural heritage focus on conservation and monitoring, while minimizing structural interventions ensuring structural safety through proper design, maintenance, and testing.

1.4. An introduction to the concept of improvement and reparability

The need to overcome the limits of the current intervention methodologies highlighted by recent seismic events, has profoundly changed the way of conceiving interventions both from a theorical and technical point of view. In fact, one of the key aspects in the context of the most recent developments in technical standards was the introduction of new approaches to ensuring the structural safety of historic buildings.

The first one, known as *improvement*, meaning the improvement of the building's structural response, was developed as a way to balance the need for structural safety with the need for conservation of historical structures. As specified in 2008 Building code [29] and fully explained in the 2011 Guidelines[9] an intervention of *improvement* provides the possibility of operating with lower safety levels, as conventionally defined and quantified in modern standards, than those required for new constructions. As noted by Modena et al. [30], the approach to the structural safety of historical constructions based on the concept of *improvement* in the sense of valorization of the original constructive characteristics, is not only a regulatory expedient implemented to avoid interventions that are too invasive and compromise conservation but is the most appropriate way to operate. In fact, it allows to resort, where strictly necessary, to interventions of minimal entity and minimal impact, that is, local and very targeted.

The second aspect is the concept of *reparability*: a design criterion for conservation where preservation can be ensured if it is possible to deliver to each post-earthquake reconstruction phase a historic structure that, however inevitably damaged or otherwise reinforced, can be repaired. The first effect of reparability is to prefer minimized interventions in consideration of the capacity of innovative materials to significantly modify, even when used in moderate quantities, local mechanical behavior, and structural responses.

The interpretation of the design criteria oriented to guarantee the structural safety of historical constructions and inspire the conservative approach, i.e. the non-invasiveness and compatibility of interventions, offers the cue for interesting operational proposals. Substantially implicit in traditional methods and considering that there is no historic structure in a seismic zone that has not undergone several repairs works overtime, the proposed criteria can play a significant role in the design of interventions using innovative techniques.

Therefore, *improvement* and *reparability*, guarantying the implicit consequence of non-invasiveness, compatibility, removability, and minimization that, as illustrated in the previous section, are the basic principles of conservation.

Chapter 2
Strengthening techniques for masonry constructions: state of the art

Advances in the regulative requirements have significantly impacted the approach towards the preservation of masonry structures. To minimize the risk of damage, interventions aimed at increasing the structural safety should be evaluated within the overall framework of conservation. This involves a comprehensive assessment of the compatibility, durability, and reversibility of any new techniques or materials used.

Interventions that integrate with the existing structure should be preferred. With the aim of not radically altering the original behavior of the construction, these interventions have the prerogative of being as reversible as possible, non-invasive and respectful of traditional techniques and materials. Thus, the need emerged for a re-evaluation of traditional materials and techniques, recognized not only as a historical reminder of a way of building, but also for their anti-seismic effectiveness. Moreover, some innovative interventions may be incompatible with the existing materials, potentially compromising the stability of a masonry structure. Therefore, it is crucial to evaluate the potential impacts of any proposed intervention before proceeding.

The section that follows will present a comprehensive analysis of both traditional and innovative intervention techniques aimed at enhancing the safety of historic buildings while preserving their historical and artistic value.

2.1. Effective structural response: box behavior activation in existing structures

The activation of the so-called *box behavior* [31] can improve the seismic response of existing masonry structures (Figure 4). Good connections between horizontal and vertical structural elements are crucial in ensuring satisfactory global behavior under seismic action, as they help prevent the detachment and overturning of walls subjected to out-of-plane forces and facilitate the transfer of seismic forces from floors to vertical walls. In the past, earthquakes have demonstrated that the lack of effective connections can lead to the total or partial collapse of historic buildings. On the other hand, if connections are effective and overturning is prevented, walls will be able to resist forces within their own plane. To prevent wall overturning, the insertion of ties, confining rings, or other elements suitable for connecting floors and walls can help distribute horizontal loads more effectively. While strong connections between structural components can limit damage, the layout of historic buildings, the discontinuities resulting from successive transformations over time and the lack of maintenance can often lead that is quite different from box behavior [32].

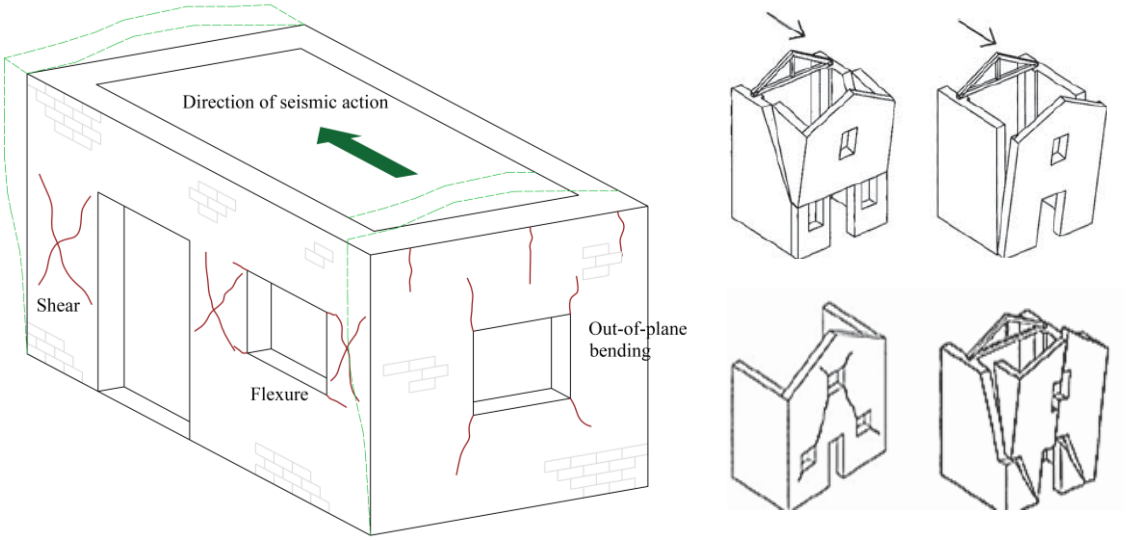

Figure 4: Activation of the box-like behavior(left) possible overturning mechanisms [9](right).

2.2. Unreinforced masonry arch collapse modes

Masonry arch is composed of an assemblage of rigid blocks without tensile strength at the interface. Therefore, masonry arch can only resist external actions through its geometrical configuration. In other terms, the arch is in equilibrium through compression when the thrust line, the load path of the resultants, is comprised in the thickness of the arch and the limit analysis safe theorem is respected. Under static loads, there are essentially four modes in which a masonry arch can become unstable:

- the activation of a mechanism,
- the sliding of one voussoir over the other,
- the crushing of the voussoir,
- the displacement of the arch supports.

An arch can collapse when enough internal hinges occur in the arch for the activation of a mechanism. Since a masonry arch is a three-times hyperstatic structure, for a collapse to occur it is necessary for at least four internal hinges to form, that is when the so-called four-hinges mechanism occurs (five hinges in the symmetrical case), see Figure 5.

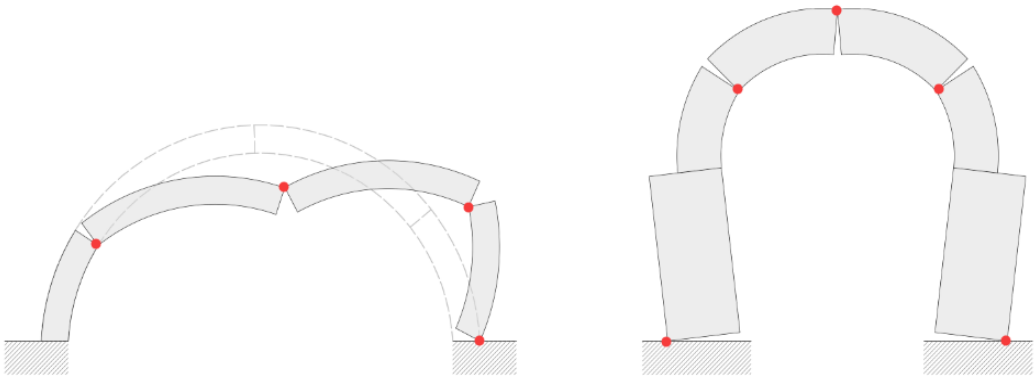

Figure 5: Four-hinges mechanism (left), five-hinges mechanism with symmetric load condition.

Internal hinges occur at the interfaces where the thrust line is close to the boundaries, at the intrados or at the extrados. In these interfaces, the compressive stress is concentrated on a small portion of the section around which rotation can occur, while the rest of the section is almost entirely cracked. This type of mechanism occurs when the material has a compressive strength that allows for localized rotation without causing crushing in the reacting portion.
The second mode of collapse concerns the sliding of one voussoir over the other (Figure 6). While this was once considered the primary cause of arch or vault collapse, according to early treatises on arches by De La Hire [33], it is now understood that sliding of the voussoir is typically not significant to cause collapse.

The third failure mode, which involves the crushing of compressed masonry, is actually very rare. It is almost never observed due to the high compressive strength of the stone itself.

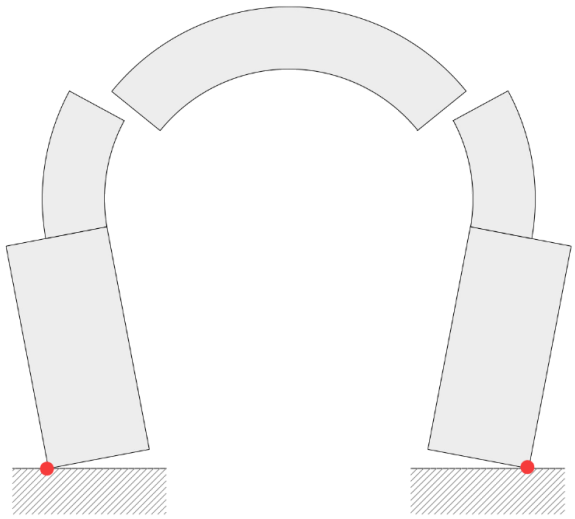

Figure 6: Sliding mechanism of a masonry arch.

The displacement of the arch buttresses, or supports, involves the formation of internal hinges to accommodate the displacement of the supports. Therefore, the capacity of the arch to adapt to changes in load conditions and preserve equilibrium is related to the interaction of the supports with the other structural elements composing the construction. Even though the structure as a whole remains in balance, the thrust line can reach the edge of a section in one or more points, and hence cause additional hinges to form and weaken the structural stability.

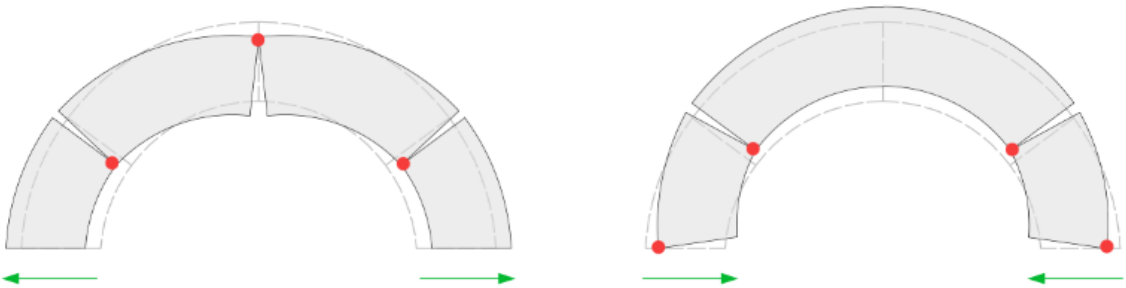

Figure 7: The formation of three internal hinges to accommodate the displacement of the supports.

A comprehensive analysis of the structural behavior of masonry arches is reported in [34] Some authors applied limit analysis approaches, developed for gravitational loads, to study the effects of seismic loads that can be represented by a horizontal inertial force proportional to the weight of the arch [35]. The limit condition of stability occurs when the thrust line becomes tangent to the arch (Figure 7). If it comes out, the arch is unable to withstand the

applied loads. In this case, a reinforcement is necessary to increase the safety level of the arch.

The mechanism shown above are typical of unreinforced arches under static load, such as gravitational loads and displacement due to settlements. In the following, will be shown what changes in the presence of reinforcement and what are the prevailing modes of collapse.

2.3. Well-established approaches for the safety of historical structures

In order to enhance the structural integrity and stability of masonry structures, researchers are currently focused on identifying and testing materials and technologies that can improve the safety level of masonry. This section will feature some representative examples of interventions.

As shown in Figure 8, one effective intervention example is the use of *scuci-cuci*, which aims to restore the continuity and quality of masonry walls. This technique involves the local replacement of cracked or heavily damaged masonry elements with new elements that are similar in form and material to the original ones. Proper techniques and materials are crucial for *scuci-cuci* repairs to be durable. Thorough assessment of the extent of damage and surrounding masonry condition is also important, as more extensive repairs may be needed in some cases.

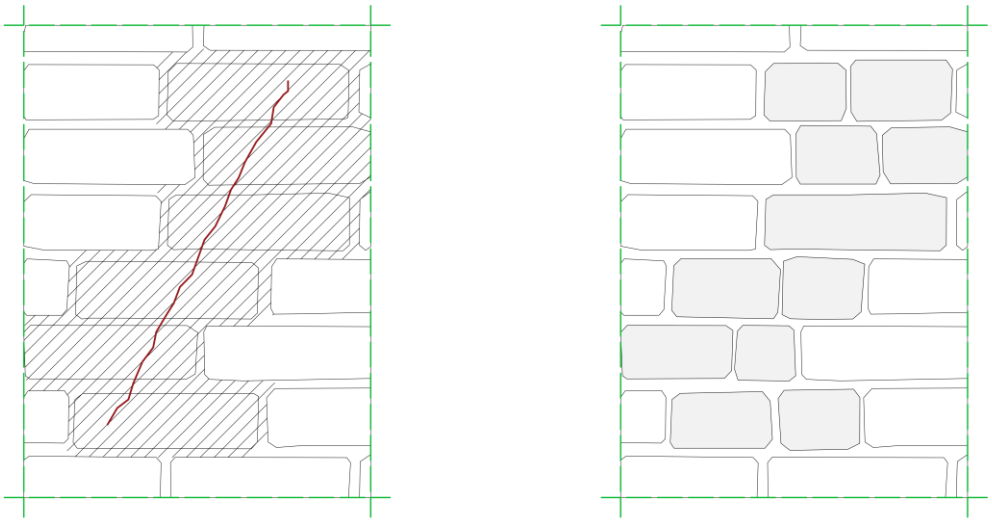

Figure 8: Scuci-cuci intervention on masonry wall with regular ashlars.

Another example of effective intervention is the use of *injections* (Figure 9). This technique can improve the strength of masonry by filling cracks or voids with a durable material. This can increase the compactness and strength of multi-leaf masonry walls, restoring their stability and preventing further damage. The type of material used for injections in masonry restoration depends on the specific features of the masonry construction and the nature of the

damage being repaired. They are often used in conjunction with other repair techniques, such as *scuci-cuci*, to provide an effective solution for restoring masonry structures. The efficiency of this type of intervention is discussed in [36].

Figure 9: Intervention of injection to improve the compactness and the strength of masonry walls.

Horizontal bearing elements, such as roofs, have a fundamental structural function under seismic action. If well connected with the vertical components, floors inhibit out-of-plane mechanisms contributing to the redistribution of horizontal loads. Since the total substitution with inadequate interventions can drastically alter the original behavior causing even collapses, traditional techniques to rebuilt horizontal components have to be preserved assuring a suitable choice of material and a proper stiffening effect.

Arch and vaults are vulnerable to seismic action, and hence, strengthen them represents one of the most frequent interventions that prevents local or global fail avoiding out-of-plane collapses induced to walls by their thrusts. This category of masonry structures can be strengthened by employing traditional techniques such as inserting tie-rods which compensate the thrust applied on bearing walls. Tie-rods are inserted to collect the thrust of the arch and prevent the piers from overturning. An example of this kind of intervention can be found in [37]. Tie-rods are effective in providing support to the arch when placed at or just above the springing, but their location inside may not always be practical. In such cases, alternative locations may need to be considered. Placing tie-rods at the extrados outside the walls can be combined with *frenelli*, small walls built above the vault, to prevent horizontal displacement of the springing walls during seismic action, see Figure 10.

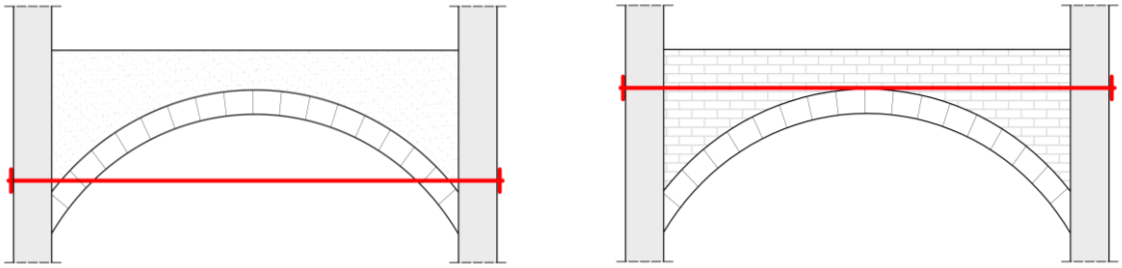

Figure 10: Insertion of a tie-rod in a masonry arch.

In order to improve structural safety, it is essential to incorporate buttresses and piers of an adequate width to counteract seismic forces [38]. Historically, masonry buttresses have been designed to withstand vertical forces resulting from gravity loads and horizontal forces generated by the thrust of the arch. However, during an earthquake, the horizontal seismic force can augment the thrust of arches and vaults in masonry structures, leading to collapse mechanisms due to overturning. As shown in Figure 11 the inclusion of buttresses in renovation interventions can enhance the structural safety of masonry constructions while preserving their identity and historical significance [39].

Figure 11: The inclusion of buttresses in renovation intervention, Madonna della Pietà church, Irsina (Matera) [39].

.

2.4. Counterproductive interventions in masonry structures

In the past, invasive structural interventions and the underestimated structural safety of masonry structures have led to irreparable damages. As highlighted by Borri in [40], it is possible to categorize these issues as "damages induced by Code application" as they were the direct result of the guidelines that were in effect at that time.

In general, current techniques of intervention should be avoided unless it has been carefully determined that traditional techniques are not feasible, and hence the intervention is suitable for the specific case meeting the criteria of compatibility, reversibility, and durability. Therefore, as indicated in [9], interventions such as those described below should generally be avoided due to their high level of invasiveness, potential material incompatibility, and uncertain effectiveness and durability. While these interventions may be effective at addressing specific issues, they may also have a detrimental impact on both the structural integrity (for example, by introducing overly rigid elements) and the preservation of the original materials of the ancient structure.

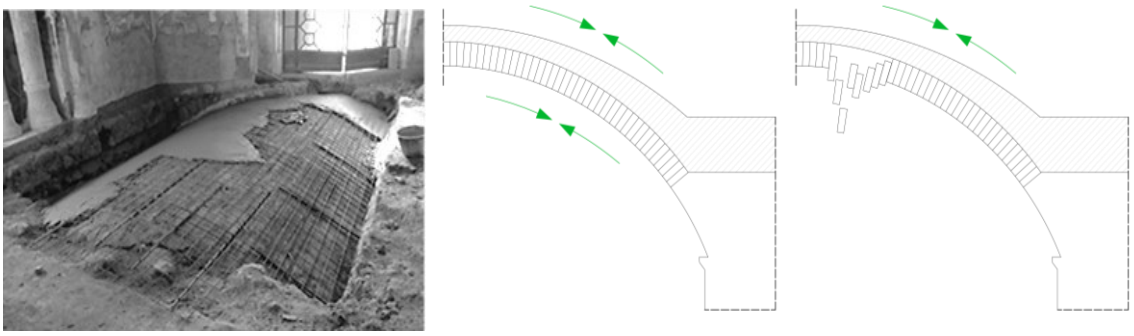

Figure 12: Insertion of a concrete cap over the existing masonry structure (left), effect on the structural behavior (right).

A common method for reinforcing arches and vaults involves exposing the extrados and casting a concrete cap over the existing structure. While this technique has been widely used in the past and can significantly increase the load-bearing capacity of the structure, it is important to minimize the thickness of the casting to avoid transferring compressive stress predominantly to the more rigid concrete structure and causing decompression of the vault (Figure 12). One main limitation of this type of intervention is the significant increase in weight and inertial mass, which can lead to increased horizontal forces during seismic events. Furthermore, these invasive and irreversible strengthening often deprive the masonry arch or vault of its structural function, leading to hybrid masonry and reinforced concrete systems. Another common intervention in historic structures is the removal of light timber-beam floors and their replacement with concrete. This practice can have negative effects on the structural integrity of the building. The removal of the timber-beam floor causes vertical

stresses to migrate to the external wall leaf, and the subsequent construction of the new concrete floor generates high compressive stresses in the walls (Figure 13). This can lead to punching shear action of the floor and the overturning of the external wall leaf during an earthquake. It is important to carefully consider the potential consequences of such interventions and to prioritize the preservation of original structural elements whenever possible.

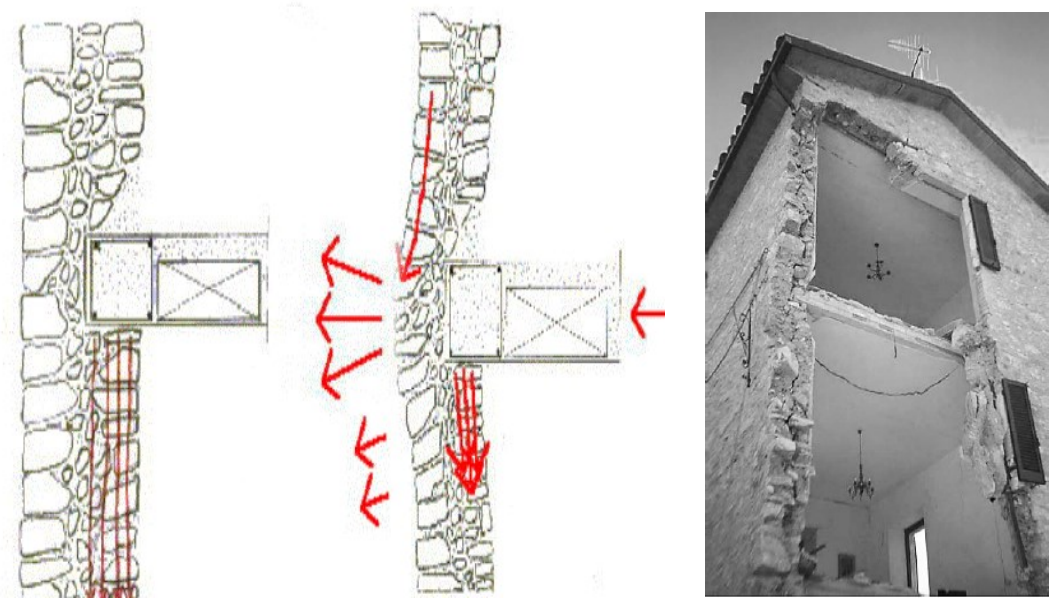

Figure 13: The removal of timber-beam floors and the subsequent reconstruction with concrete (left), damages due to the replacement of timber floors (right) [40]

2.5. Negative effects of current improper strengthening intervention

Over time, there has been a persistent search for new materials, as well as innovative techniques in an effort to address the challenges posed by masonry structures for their preservation. However, this search has often been frenetic and has not yielded many concrete results. In fact, the recent seismic events have highlighted the limits of the strengthening interventions on masonry structures that have sometimes led to unpredictable and difficult-to-quantify behaviors.

Generally, the masonry construction, whatever reinforced, exhibits local mechanical behavior and overall structural responses where the weakest link is the element with minimum structural strength capable of triggering the collapse of the entire structure. In fact, the seismic events in recent decades have provided an opportunity to test and validate the seismic response of strengthening interventions for masonry structures. In some cases, these interventions, although locally effective, had negative consequences on the overall structural response of the construction, by introducing excessively rigid elements or by compromising the integrity of the original structure.

Figure 14: The modern roof made by precast elements and unreinforced concrete slab in Santa Maria Paganica church in L'Aquila [5]*, inside view of San Marco church in the historical centre of L'Aquila* [4]

The severe consequences of such structural behavior can be witnessed in the aftermath of the Umbria-Marche and Abruzzo earthquakes. Significant examples arise from the improper use of reinforcement techniques, reiterated for a long time in the field of the so-called "structural restoration" with the aim of replacing entirely (by creating reinforced concrete frames embedded in the masonry) or, more frequently, partially (with the replacement of wooden floors and roofs with reinforced concrete structures, or with the creation of reinforced plaster alongside the walls) the existing structures. Recent research highlights the impact of

invasive interventions on historical masonry structures, as evidenced by the collapse of San Marco [4] and the Basilica of Santa Maria Paganica [5], see Figure 14.

In some cases, simple repairs, reinforcements, or partial reconstructions (along with enlargements and modifications) contributed to the vulnerability, due to the discontinuity in the masonry wall, increased height, and poor connections. The wrong use of reinforced concrete is also evident in the replacement of wooden trusses in the roofs and the substitution of timber floors with reinforced concrete.

The Basilica of San Francesco in Assisi is a first example of the severe consequences that can arise from interventions on masonry structures. The event had significant consequences for the preservation of the basilica. The 1997 earthquake in Assisi resulted in the collapse of the two vaults (Figure 15). The cause of the collapse is believed to be either the accumulation of damage from previous earthquakes or the retrofitting work done on the structure, including an intervention in 1958 that may have disrupted the monolithic static behavior of ancient structures. The collapses caused further damage to the structure and subjected it to deterioration, threatening its cultural value and significance. To this day, the event continues to be examined, as demonstrated in [6].

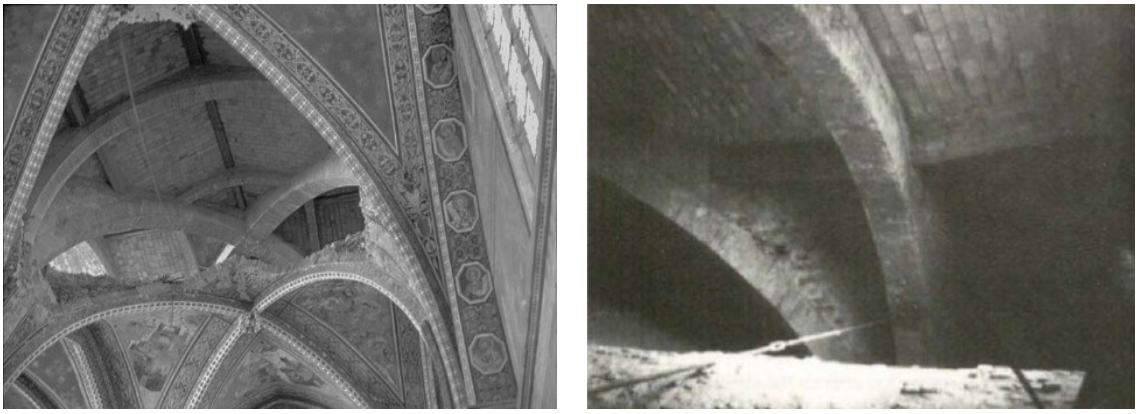

Figure 15: The consequence of the intervention on the Upper Basilica of San Francesco (left), tie-rod installed during the 1958 [41]*(right).*

The damage suffered by the basilica of Santa Maria in Collemaggio during the earthquake in L'Aquila in 2009 highlights challenges posed by seismic events in masonry structures [7]. The damage in this case primarily affected the dome and pillars at the intersection of the transept and nave and was caused by the lack of a classical box-like behavior between the structural elements and the unexpected seismic response of a strengthening intervention that had been carried out in 2000. The basilica of Santa Maria di Collemaggio was outfitted with a steel damper reinforcement system designed to dissipate energy during seismic events. However, this system ended up increasing the stiffness of the structural elements that comprise the nave, resulting in a torsional effect that caused the collapse of the two transept pillars, see

Figure 16. The strengthening system had moved the center of stiffness away from the center of mass, making the two pillars with the larger diameter (which were also the most rigid) the weak link in the structural system. This incident illustrates the challenges of predicting the local mechanical behaviors and overall structural responses of masonry structures, particularly when they have been strengthened.

Figure 16: The basilica of Santa Maria in Collemaggio after the L'Aquila earthquake in 2009.

Overall, these examples suggest that collapses of historic masonry structures can result from the incompatibility of modern materials with existing structures, as well as the increased seismic loads caused by adding mass and stiffness to the structure. This demonstrates the importance of carefully evaluating the potential impacts of strengthening interventions on the stability and preservation of masonry structures. Therefore, these events highlighted the need for a careful balance between structural safety and conservation requirements.

2.6. Fiber reinforcement materials for masonry strengthening: FRP and FRCM

In recent decades, there has been a significant progress in understanding the structural behavior of masonry constructions and devising approaches to minimize damage due to instabilities caused by differential foundation settlements, seismic activity, and long-term deformations.

Among the strengthening techniques employed for preserving masonry structures there is the use of composite materials such as Fiber Reinforced Polymers (FRP). These materials are made by inserting fibers (such as carbon, basalt, or steel) into a polymer matrix [42] [43] and may represent a solution for certain structural issues, particularly when combined with other techniques such as injections or tie-rods. In fact, these materials have the potential to provide advantages over heavier traditional materials such as steel or concrete. While the use of this kind of fiber reinforced materials systems allows for a decrease in weight compared to other interventions, significant issues must be considered regarding the durability of the matrix, which is not breathable and is highly sensitive to moisture and high temperatures. Furthermore, experimental evidence [44] [45] [46] demonstrates that the application of FRP reinforcement, while increasing resistance to loads, results in an excessive increase in stiffness in the areas where it is applied, leading to the emergence of much higher stress levels, particularly during the seismic action. This can lead to collapse mechanisms (such as crushing, sliding or debonding) that are unusual for unreinforced masonry.

Due to the low compatibility with the supporting materials and the alteration of the structural behavior of the masonry, the use of FRP reinforcement is considered an irreversible intervention. In fact, if these local strengthening are made of materials with significantly different properties, they may increase local pressure weakening the dynamic response of the structures.

Figure 17: Collapse mechanisms (crushing, sliding or debonding) for a reinforced arch with FRP [46]

For this reason, in recent decades, FRP composites have been outspread alongside new Fiber Reinforced Cementitious Matrix composites (FRCM) that, due to more compatibility with the substrates being reinforced has also gained increasing acceptance as an alternative to more well-known FRP. This reflected in the recent regulations [11].

In [47] are reported the results of experimental tests on the effectiveness of different fiber reinforced material composite systems. In fact, inorganic matrix composites overcome the problems that affect the FRP systems. The cementitious matrix, while being less effective in ensuring adhesion with the fibers, on the other hand, presents some advantages in terms of material compatibility, being the characteristics of the matrix similar to those of the support. Specifically, since the cementitious material is more compatible with masonry materials than polymer matrices, FRCM have excellent high-temperature resistance, good permeability, and good hygroscopic capacity. The combination of these advantages justifies the great interest that this system generates in the field of strengthening of masonry construction. Moreover, FRCM can be tailored to the specific operating conditions, geometric configuration, and reinforcement needs of a masonry construction. This results in ensuring a negligible invasiveness, reparability, and reversibility of the intervention allowing for its replacement if necessary.

Figure 18: Some examples of strengthening intervention with FRCM [11].

2.7. Structural issues of reinforced arches and possible solutions: optimal reinforcement

It is found that in many cases the safety level of masonry arches is insufficient, although recent studies have demonstrated a certain capacity of masonry structures to withstand seismic action through *rocking* mechanism [2] [3]. As claimed by Como, while steel and reinforced concrete structures can withstand seismic action trough ductility, masonry constructions resist earthquake trough *rocking*. In particular, *rocking* mechanism consists in the capacity of masonry rigid blocks systems to accommodate the motion due to a horizontal load moving sideways through a mechanism defined by four hinges. The rocking mechanism, although in presence of local damages, allows masonry structures to have a certain level of seismic capacity. In some cases, this capacity may not be sufficient, and a strengthening intervention is needed.

Innovative methods for strengthening arches, such as reinforcements with FRCM, typically aim to provide the masonry with the sufficient level of safety to resist load such as settlement and seismic action introducing tensile strength into the structure.

The presence of reinforcement significantly impacts the behavior of masonry arches. Depending on the location of the reinforcement, it can prevent the collapse mechanisms that are characteristic of unreinforced structures by inhibiting the formation of hinges on the side opposite the reinforced side. For example, if the reinforcement is placed at the intrados, the thrust line can fall outside the arch without causing any structural collapse [43]. This can prevent hinge formation and transform the arch into an isostatic three-hinged structure. The presence of reinforcement alters the collapse mode, which hence depends on the strength limits of the materials rather than the geometry. Experimental evidence shows that the use of reinforcement elevates the range of resistance to loads but results in much higher stresses than in an unreinforced arch, especially during seismic loads. Then different collapse modes become possible, such as crushing or sliding between joints (Figure 19).

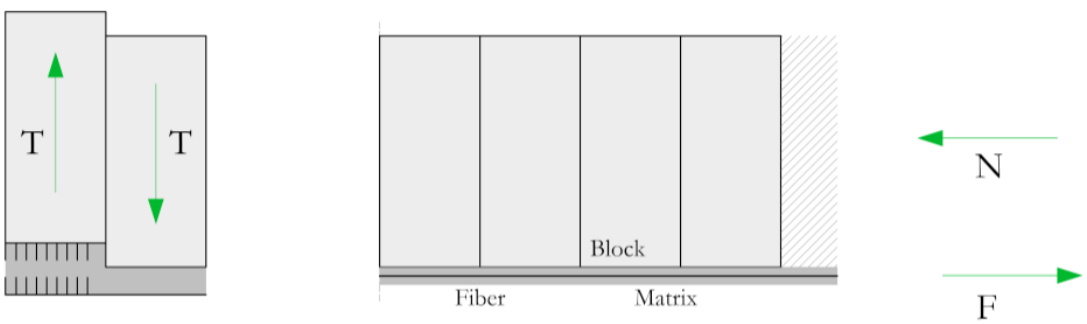

Figure 19: Tensile strength increment in presence of reinforcement and collapse mode with sliding displacement due to the increase in shear at the interface.

In fact, the reinforcement may generate problems preventing rocking to occur and turning parts of the structure into monolithic elements leading to the emergence of unexpected collapse mode shown in [12] and [13]. In a reinforced arch, the collapse mode is different. As can be seen in Figure 20, there is a consistent increase in shear at the base and sliding displacement at the keystone. In addition, as acceleration increases, while in the unreinforced arch, although there is still different behavior from that predicted by the Heyman's model, it does not behave as a rigid body. The reinforced arch behaves as a rigid body only initially.

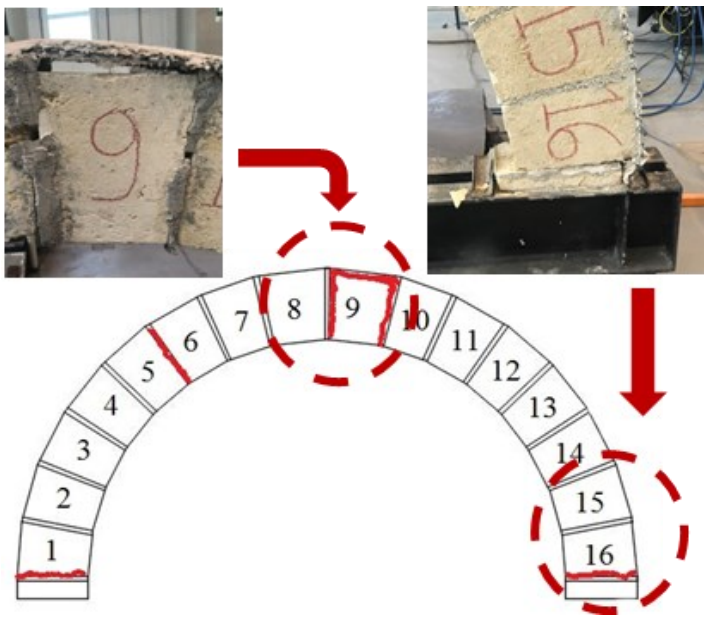

Figure 20: Collapse mechanism of a reinforced arch [12]

In light of the issues outlined, a key purpose of the thesis is to develop a design procedure for appropriate reinforcement interventions capable of suitably increasing the value of the collapse multiplier, without completely constraint the structural system and alter the collapse mechanism. The idea is to design an "optimal" reinforcement meaning that the reinforcement has to provide the arch with the sufficient safety capacity without preventing rocking. This is possible by defining a proper localization of the reinforcement at the intrados or the extrados that allow the arch to accommodate displacement due to the seismic action or settlements with the four-hinge mechanism. This will be properly illustrated in Chapter 6.

PART II LIMIT ANALYSIS FOR STRUCTURAL ASSESSMENT OF MASONRY STRUCTURES

Chapter 3
Modelling and structural analysis approaches for masonry structures

The computational approaches and modelling strategies that are typically used to assess the safety level of new structures may not be suitable for existing historical constructions. In particular, in the design process of strengthening interventions on historical constructions, the definition of the appropriate analytical and numerical methods to determine the safety level, is just one of the aspects that must be considered. In fact, the computational analysis of masonry structures results in an even more challenging task due to its heterogeneity and complexity.

In the last decades, a consistent effort of the entire scientific community was spent to evaluate different approaches for the description of the mechanical behavior of masonry and hence find the most effective tools for their structural assessment. In particular, the formulation of a comprehensive computational approach is particularly difficult due to a patchy knowledge of the geometrical and material features that plays a crucial role for accurately simulating the behavior of masonry structures. The next section will provide a comprehensive overview of current modelling and structural analysis strategies, highlighting the most significant aspects.

3.1. The role of geometry and material properties in masonry structural simulation

The structural masonry response is strictly influenced by both the geometric properties of masonry, such as the size, shape, and arrangement of each brick or stones, and the mechanical properties of masonry materials, such as their strength, stiffness, and the state of damage. These aspects play a key role in determining the behavior of masonry structures and a comprehensive knowledge is crucial for predicting how masonry structures will respond to external forces. Therefore, to achieve reliable structural simulation results for masonry structures, it is essential an accurate geometrical and structural survey [9]. The geometrical survey is typically based on the acquisition of 3D point clouds and the drawing of the geometry in a computer-aided design (CAD) environment. The point clouds provided by the geometric survey can be used to create two-dimensional maps and three-dimensional models and can be easily integrated with other surveying techniques and software. It is worth pointing out that, since recent software for computer graphics allow to model very complex three-dimensional shapes, the employability of this geometry in structural analysis is still an issue due to some errors emerging during the re-meshing process. Moreover, in historical buildings that have undergone multiple renovations and modifications, the original structure may have been altered, and the documentation may be incomplete or inaccurate. As a result, engineers may need to rely on site investigations and non-destructive testing techniques to better understand the geometry of the structure and ensure accurate modeling in structural simulations.

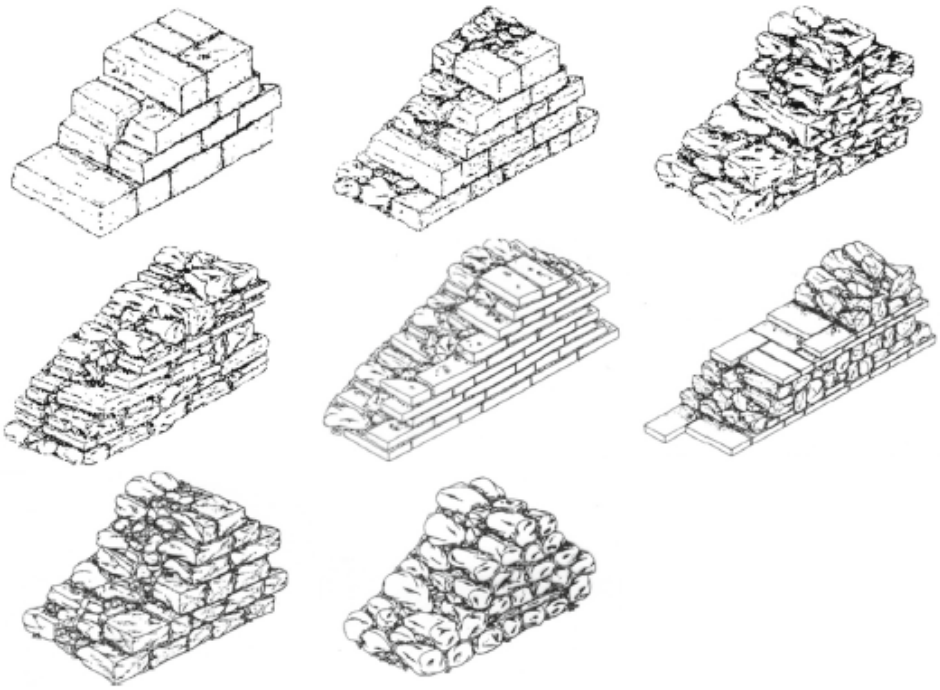

Figure 21: Some examples of typologies of historic masonry characterized by different mechanical behavior [48].

Another issue concerns the identification of the structural system governing the building geometry at both local and global scale. In fact, it is possible to identify two scales of representation of the mechanical behavior of masonry: the material scale and the structural element scale. Concerning the structural element scale, the interaction between each structural element, in other terms the topology of masonry [48] , see Figure 21, has a significant importance in determining the mechanical response of the entire construction. Generally composed by blocks bonded with mortar, masonry structures are built with a large variety of materials and assembled in different ways. Blocks are usually disposed with a certain pattern and made of material with a quasi-brittle response in tension and compression, while mortar is the bonding component characterized by cohesive-frictional behavior. In Figure 22 some masonry failure mechanisms at structural scale are depicted [49].

Figure 22: Masonry failure mechanisms at structural scale: diagonal cracking, sliding, crumbling, crushing.

The possible failure mechanisms that involve the whole masonry structure are of two types: out of plane rocking and in-plane shear, which are typically associated with seismic action. Out of plane rocking can be caused by self-load or the presence of a heavy pushing roof or floor and is usually the result of poor design or unwise modifications. In well-designed structures, in-plane shear failure is more likely to occur due to horizontal actions on the shear-resistant elements. For this reason, a deep knowledge of the historical evolution of the masonry structure can help to identify the presence of toothing between orthogonal walls, the quality of connections with horizontal elements or adjacent buildings.

The arrangement of blocks and their interaction with mortar is a crucial aspect defining the level of anisotropy. Brick masonry with a regular disposition of block exhibit different strengths along with different directions, while in random stone masonry anisotropy is less significant (Figure 23).

Figure 23: Disposition of blocks exhibiting different level of anisotropy .

The method proposed by Borri [50], referred to as the *Masonry Quality Index*, highlights the correlation between various typologies of masonry and their corresponding mechanical characteristics. The *Masonry Quality Index* method evaluates the presence or absence of certain aspects defining the mechanical properties of the wall. The estimation process requires a thorough understanding of historical construction methods and the categorization of the wall leaf connections, horizontality of bed joints, and brick shape (Figure 24).

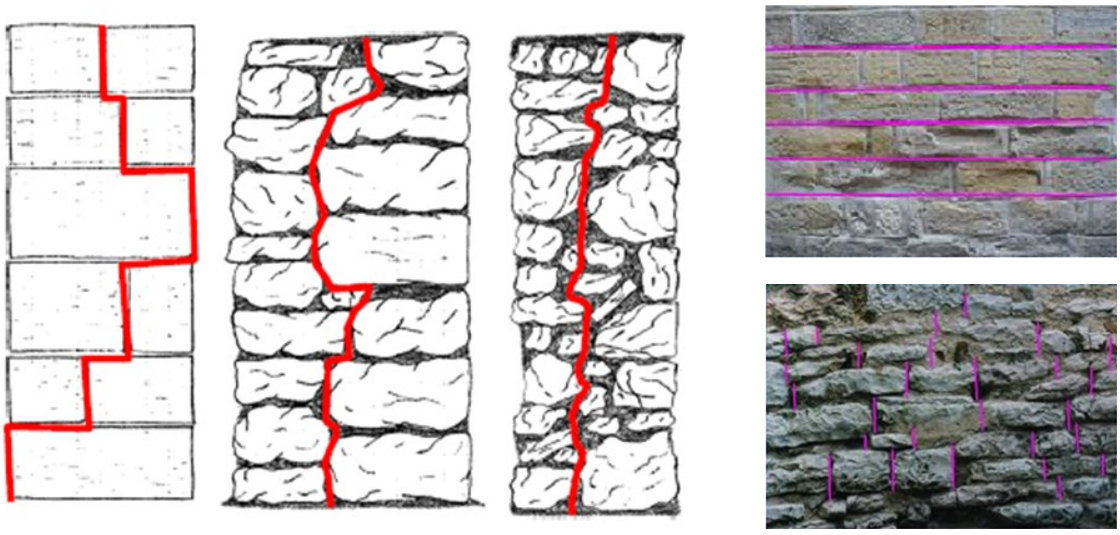

Figure 24: Some parameters counted in the Masonry Quality Index: wall leaf connections, horizontality of the bed joint, stagger properties of the vertical joints [50].

Due to its heterogeneity, masonry structural response is usually complex to describe from a mechanical point of view and is strictly dependent by the mechanical properties of its components. In particular, the combination of blocks with a higher value of strength in compression then in tension and mortar with weak cohesion contribute to a highly nonlinear response of masonry. Due to this consistent difference in strength between blocks and mortar, cracks typically run along the weaker element (i.e., the mortar joints) and hence local failure mechanisms can be classified in three modes: detachment, mixed mode (detachment

and sliding) and crushing [49]. The first one is essentially connected to the brittleness of the material and occurs with detachment fractures, such as those reported in Figure 25. The most frequent and usually irrelevant, this type of cracks emerges without any material failure but with just the separation of blocks at joints and have the positive effect of contributing to the accommodation and release of stress. The second mode results from the combined effect of detachment and sliding. This mechanism arises in masonry under high compressive loads and shears. The third one is the so-called crushing of the material and occurs in masonry subjected to compression. These two last modes are due to critical, or even collapse, load. In particular, the crushing mode is the most dangerous since it is associated to a sudden failure under compression.

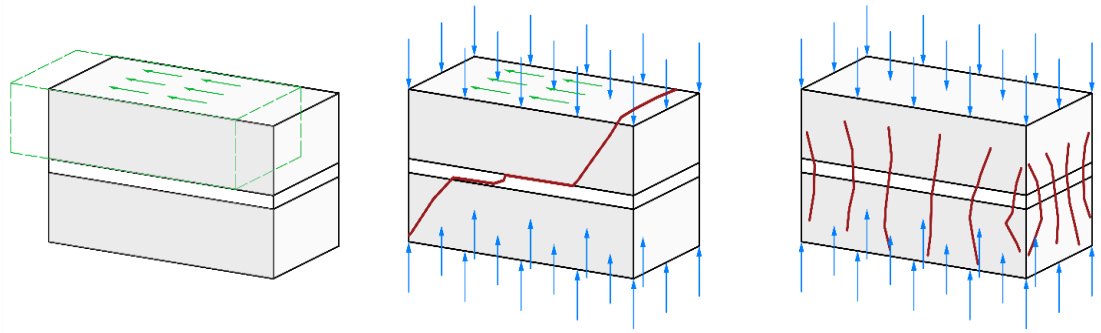

Figure 25: Typical failure modes of masonry at a two-block masonry assemblage scale: detachment, mixed mode (detachment and sliding) and crushing [49].

Regarding the material scale, the experimental characterization of blocks and mortar mechanical properties and their interaction from the single wall to the full-scale masonry construction is a challenging task. To ensure the conservation of the integrity of the historical structure and hence limit the invasiveness, indirect methods, such as non-destructive tests, have been proposed to characterize masonry materials and provide a fair structural assessment. The utilization of non-destructive testing methods allows for the acquisition of crucial information without causing damages to the building, however, it presents a limitation in obtaining accurate material characterization.

In-situ experimental characterizations of masonry construction have a limited effectiveness in clearly determining mechanical properties when compared to laboratory tests. For this reason, being semi destructive methods not always valuable, an estimation of the mechanical properties of a masonry construction can be done through a combination of in-situ testing and laboratory testing.

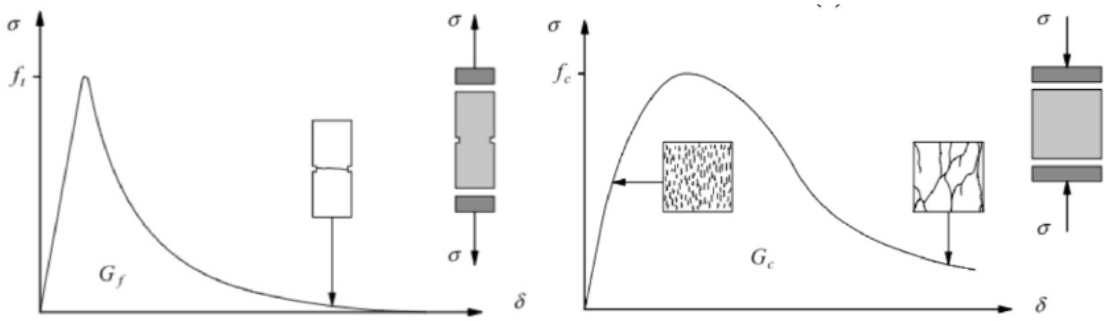

Figure 26: Uniaxial compression and tension tests on masonry walls [51].

The methodology commonly employed in the assessment of masonry material properties involves laboratory tests on sample specimens that are representative of the actual construction. Among the various test methods, compression testing is relatively straightforward to execute and provides valuable insights into the general material characteristics. As depicted in Figure 26 the results of uniaxial compression and tension tests on masonry walls are typically represented in the form of stress-strain curves.

By using a combination of both in-situ and laboratory test, it is possible to obtain a more comprehensive understanding of the mechanical properties of the blocks and mortar, as well as their interaction within the masonry construction. This can provide valuable information for assessing the structural behavior.

3.2. Classification of modelling strategies for masonry structures

The widespread adoption of computer-based elastic analysis methods in the late 1980s, aided by the emergence of FEM (Finite Element Method) solvers, contributed to the widespread use of methods proved inadequate for accurately predicting the behavior of masonry structure.

As shown in Section 3.1, due to their highly non-linear structural response and geometrical heterogeneity, masonry constructions are effortful to analyze by the structural point of view. The choice of a modeling strategy for masonry structures depends on the specific goals and constraints of the structural analysis, as providing a more accurate representation of the behavior of the masonry can also be computationally intensive. In fact, it is important to consider the trade-offs between accuracy and computational efficiency when selecting a modeling approach. For this reason, being hard the identification of a unique approach for assessing the safety of masonry structures, different modelling strategies and analysis approaches have been proposed that take into account their complex mechanical behavior.

In general, analytical models can be useful for quick and approximate analyses of masonry structures, while numerical models can provide more detailed and accurate predictions of the behavior of the structure. There are various numerical models that can be employed to analyze the behavior of masonry structures. A first classification of numerical models for masonry structures was proposed by Lourenco [51] in his PhD thesis. Numerical models for masonry structures can be broadly divided into two categories as illustrated in Figure 27: *macro-models*, or *continuum models*, in which the behavior of masonry is represented using a constitutive model that approximates masonry as a continuous material, and *micro-models* or *meso-scale models*, or *discontinuum models*, in which discontinuities are explicitly represented using constitutive models for masonry joints.

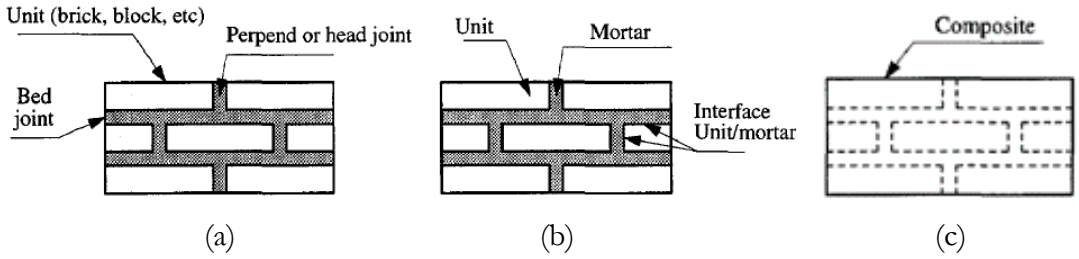

Figure 27: Modelling strategies for masonry structures: masonry unit (a), micro-models (b), macro-models(c) [51].

Macro-models are well-known for their low computational burden. However, they are limited in model typical discontinuities in masonry structures such as joints or cracks. On the other hand, *micro-models* are generally more accurate but have a significantly higher computational

cost. It is important to carefully consider the trade-offs between accuracy and computational efficiency when selecting a modeling approach for masonry structures. This first classification provides a framework for understanding the different approaches that can be used to model the behavior of masonry structures using numerical techniques. A selection of modeling approaches within this category can be found in reference [52].

The development of new structural analysis models for masonry structures has continued in response to the need for more effective tools to represent their behavior. This has resulted in a significant increase in the variety of available modeling approaches, as reported in [8] where a comprehensive classification of both existing modeling strategies and analysis approaches is provided and is here reported in summary form. The modelling strategies for masonry constructions can be distinguished into four categories:

- Block-based models
- Continuum models
- Macro-element models
- Geometry-based models

To analyze the behavior of masonry, *block-based models* can be used which provide insight into the material microstructure. This is done by considering the main heterogeneity of the material at the scale of blocks that are assembled with mortar or dry joints. This approach is effective in capturing the intrinsic anisotropy and failure patterns of masonry as it takes into account the actual masonry texture. By representing the masonry bond and its intrinsic structural and anisotropy properties, this modelling strategy is useful in characterizing the mechanical properties of masonry from small-scale experimental tests and in understanding various failure modes such as in-plane and out-of-plane responses. However, the use of this approach may be challenging when applied to complex structures due to the significant computational demands required.

The classification of *block-based models* in masonry structural analysis is based on the method of formulating the interaction between blocks:

- *Interface element-based approach*: the mortar joints are modeled as zero-thickness interface elements, while the masonry units are represented using smeared crack elements, within the framework of a Finite Element (FE) method. A significant development in this method was proposed by Lourenço and Rots [53], who introduced a multi-surface interface-based model that concentrates all nonlinearities at the interfaces. This approach provides a more accurate representation of the interaction between the masonry units and the mortar joints and captures the nonlinear behavior of the masonry units. This, in turn, results in a more realistic representation of the overall

behavior of the masonry structure. Some applications of this approach are reported in [54] [55]

- *Contact-based approaches*: these approaches are built upon the principles of contact mechanics, where rigid or deformable (linear or nonlinear) blocks interact based on frictional or cohesive-frictional contact definitions. These models are mainly implemented using the Distinct Element Method (DEM), originally proposed by Cundall and Stack [56] for the analysis of granular assemblies and implemented in the UDEC code [57]. The contact-based approach uses penalty formulation and explicit integration schemes. These methods have been used in several studies on real masonry structures [58] [59] [60] using rigid or linear elastic blocks.
- *Textured continuum-based approaches:* these continuum models [61] utilize the Finite Element Method (FEM) with nonlinear elements to model blocks and joints separately, without any interface between them. This allows for nonlinear deformation characteristics of both materials and the possibility of failure of blocks, mortar, or mortar joints by bond. Mesh discretization examples are shown [62] [63]
- *Block-based limit analysis approaches*: a reliable method for predicting the collapse load and failure mechanism of masonry structures, this approach has been developed over the past two decades, with various 2D and 3D models created. These models typically rely on either static or kinematic theorems of Limit Analysis, although the inclusion of friction in the calculations is often non-conservative in relation to the Limit Analysis theorems. These approaches will be further discussed in Section 4.8.
- *Extended finite element approaches*: in recent years, block-based models have been developed using the extended finite element method (XFEM). One such model proposed by Abdulla et al. [64] is a 3D model that utilizes surface-based cohesive behavior and a Drucker-Prager plasticity model to simulate the crushing of masonry under compression. Another study [65] implemented XFEM to model the compressive failure and cracking of masonry in infill panels, using the discrete interface element to simulate the behavior of the masonry mortar joints and the joints at the frame-to-infill interface.

In *continuum models*, masonry material is modelled as a continuum deformable body, without distinction between blocks and mortar and hence the mesh discretization does not have to correspond to the real arrangement of masonry. Therefore, the computational effort is lower than *block-based* approaches. However, given the heterogeneity of masonry and its complex mechanical behavior, the definition of suitable constitutive laws is crucial. The constitutive law adopted for the material can be defined either through direct approaches or through

homogenization procedures and multiscale approaches that relates the structural-scale model to a material scale model of a representative volume element (RVE) of the structure [66] [67]
Macro-element models approach idealizes the structure into panel-scale structural components (macro-elements) through a phenomenological or mechanical-based response. The subdivision of the structure into panel-scale portions, piers, and spandrels, is an operation depending on the interpretation of the structural behaviour of a structure.
In *geometry-based models*, the structure is modeled as a rigid body without discretizing the masonry block-by-block. For this reason, the global geometry of the structure represents the main input of these type of modeling approaches. The structural behavior is investigated through different methods implementing limit analysis approaches, which can be based on either static or kinematic theorems. A comprehensive review of the various proposed solutions for *geometry-based models* with limit analysis approaches can be found in Sections 4.6, 4.7 and 4.8.

3.3. Analysis approaches

As mentioned above, the collapse response of masonry construction can be described trough two analysis approaches: *incremental-iterative analyses* and *limit analysis-based solutions*.
The *incremental-iterative analyses* allow to achieve a reliable assessment of the collapse behavior, since both mechanical nonlinearities and large displacements can be considered.
This type of analysis approach is defined as "incremental" because the structural equilibrium of a masonry construction withstanding a certain loading condition is studied step-by-step, in other terms the structural response is analyzed with a proper number of iterations where loads are incrementally varied within each step. Incremental-iterative analysis can be classified into two categories: *nonlinear static analysis* and *nonlinear dynamic analysis*. Nonlinear static analysis involves the sequential description of the structural behavior of a masonry construction until the peak-load by solving nonlinear differential equations using either load control or displacement control (an example is here [68] reported). This type of analysis is commonly used for simulating quasi-static experimental tests on masonry constructions and for performing pushover analysis. On the other hand, nonlinear dynamic analysis allows for the step-by-step analysis of the structural response of masonry constructions under time-dependent actions such as earthquakes or impacts. In this approach, the equations governing motion at each time step are solved using time integration methods. For further details, the reader is referred to [69].
The second analysis method consist in *limit analysis-based solutions*. Heyman, with his work [14] was a pioneer in applying the principles of Plasticity Theory to masonry structures and

introduced the concept of the rigid no-tension material, which is widely used to analyze the stability of masonry systems [49]. This model allowed for simple graphic statics solutions to assess the stability analysis of masonry vaults [70], and for kinematic analysis of common seismic failure modes [71]. The hypotheses by Heyman formed the basis for the development of modern computational limit analysis-based methods. These methods, which will be discussed in later chapters, are based on either the static theorem [72] [or the kinematic theorem [73], and the problem can be formulated with different approaches (optimization problem, nonlinear differential equations, of linear or sequential linear programming). A major limitation of limit analysis-based solutions is that they only provide information on the collapse multiplier and the collapse mechanism, and do not provide information on the ultimate displacement or post-peak response.

Chapter 4
Limit Analysis: state of the art

Formulated half a century ago, Limit Analysis has proven to be a powerful tool for providing a clear understanding of physical phenomena through the use of straightforward theorems yielding remarkable results. By the latter half of the 20th century, the theorems of Limit Analysis had been generalized through the concurrent development of Plasticity Theory. Originally derived from experimental observations of metallic materials and later extended to model soil behavior, the formalization of plasticity theorems was essential in overcoming the limitations of the classical Elasticity Theory, which assumes a linear relationship between stress and strain based on Hooke's law and has limitations in accurately predicting the behavior of materials under certain conditions. Specifically, the mechanical behavior of metals or soils is linear only for small-intensity stresses, and once a certain critical stress value, known as the *yield value*, is exceeded, the material leaves the elastic range and enters the plastic flow range, deforming plastically at a constant state of stress. These concepts played a crucial role in formulating the fundamental principles of Limit Analysis.

Limit Analysis methods have been adopted in various fields, ranging from metal deformation processes to the design of reinforced structures, owing to their effectiveness and accuracy in predicting the load capacity of structures. The versatility of Limit Analysis has garnered the interest of numerous researchers who have made significant contributions to the formulation of basic theorems and the development of efficient methods for determining the collapse load. Some noteworthy examples include the pioneering works by Hill [74], Prager [75], and Drucker [76]. In [77] Drucker made significant contributions to the formulation of plastic

limit theorems that can be used to obtain upper and lower bounds of the collapse load for stability problems. In the following decades, other researchers Chen [78], Lubliner et al. [79], Lemaître et al. [80] have contributed to the development and dissemination of the Limit Analysis theory within the scientific community.

As the fundamental principles of Limit Analysis were being developed, some researchers reformulated the Limit Analysis theorems for rigid body systems. This approach interprets a material that can deform plastically as a *perfectly rigid material* that exhibits cracking with constant displacements. The analogy between plastic deformation and cracking phenomena was a key insight that enabled the introduction of the *unilateral material model* and the application of Limit Analysis to rigid bodies. These advancements in Limit Analysis have significantly broadened the range of problems that can be addressed involving rigid body systems.

In the second half of the 20th century, Kooharian [81] first applied Plastic Analysis to study masonry arches. This marked the beginning of the formalization of Limit Analysis for perfectly rigid solids. Heyman [14] accomplished a significant reformulation of the Limit Analysis theories for masonry in 1966, based on two fundamental theorems of Plasticity and sound assumptions about the masonry materials. His work represented a major milestone in the field and has had a significant influence on the understanding and analysis of masonry structures. The insights provided by Heyman's work have contributed to the development of more effective methods for forecasting the behavior of masonry structures. Livesley [82] [83] applied Limit Analysis to investigate the behavior of three-dimensional structures composed of rigid block assemblies by considering the forces acting at the interface between each of the blocks. The insights developed from these works were subsequently formalized by the Italian School of Structural Engineering. Notable contributions in this regard include the work by Del Piero [84] [85], Como [86] [87], and Di Pasquale [88].

Accurately predicting the collapse load of a structure is of crucial importance in ensuring the safety of masonry structures, as their behavior is a matter of stability and equilibrium rather than strength, being stresses typically quite low in these structures. It is noteworthy that the effectiveness of these methods can be considerably impacted by various aspects, such as the assumptions made about material properties and loading conditions. As a result, it is essential to meticulously evaluate these assumptions and thoroughly validate the outcomes attained.

4.1. Fundamental concepts of Classical Plasticity: basic assumptions

The validity and accuracy of the Limit Analysis theory are strictly dependent on the assumptions made about the mechanical properties of the material under investigation. These assumptions may result in differences between the actual behavior of the material and its idealized behavior. Therefore, it is essential to carefully consider the assumptions made when using the Plasticity Theory. In this regard, a brief overview of the assumptions used in the Plasticity Theory will be presented.

The theory assumes infinitesimal deformations and requires three conditions to formulate a constitutive law that is consistent with the physical phenomena [89]:

- Partition hypothesis and elastic-perfectly plastic assumption
- Yield function
- Flow rule and Drucker stability notion

Based on the assumptions of Plasticity theory, the fundamental theorems of Limit Analysis will be presented in the following section:

- Kinematic theorem
- Static theorem

The fundamental theorems of Limit Analysis are known for their conceptual simplicity and computational efficiency, often providing a closed-form solution to many problems, based on the governing parameters and geometry of the specific problem being analyzed [78].

4.1.1. Partition hypothesis and elastic-perfectly plastic assumption

Strain (and stress) partitioning into elastic and plastic part allow defining of a mathematical model for the *elasto-plastic* constitutive law consistent with experimental evidence and physical phenomena. In fact, when a material, subjected to loads, reaches its plastic limit, it deforms while generating plastic and elastic deformations. Deformations are related to stress increments by the generalized Hooke's law:

$$\sigma_{ij} = \mathbf{D}_{ijkl}\varepsilon^{e}_{kl}\,, \tag{4.1}$$

being σ_{ij} and $\mathbf{D}_{ijkl}$ the stress vector and elastic tensor.

The internal variable for total deformation ε_{ij} is decoupled into an *elastic* or *reversible strain rate* ε^{e}_{kl}, which is related linearly to the stress by the Hooke's law, and a *plastic* or *permanent strain rate* ε^{p}_{ij}.

Based on the nature of the physical phenomena and by the hypothesis of small deformations and small displacements, total strain is defined by the decoupling:

$$\varepsilon_{ij} = \varepsilon_{ij}^{e} + \varepsilon_{ij}^{p} . \tag{4.2}$$

In loading processes with explicit time dependence, total strain can be defined in terms of increment $\dot{\varepsilon}_{ij}^{e}$ and $\dot{\varepsilon}_{ij}^{p}$, with dt the infinitesimal time increment:

$$\dot{\varepsilon}_{ij} = \dot{\varepsilon}_{ij}^{e} + \dot{\varepsilon}_{ij}^{p} = \frac{d\varepsilon_{ij}^{e}}{dt} + \frac{d\varepsilon_{ij}^{p}}{dt} . \tag{4.3}$$

As we can see in Figure 28, the stress-strain diagram for soils shows how elastic-plastic materials exhibit distinct behaviors at different stages of loading, and that their behavior is highly dependent on the level of stress applied. Outside the initial linear section corresponding to a low level of stress, the stress-strain curve changes reaching a peak or failure stress followed by *softening*.

Experimental evidence has shown that ductile structural materials typically exhibit plastic deformations, which can be accurately analyzed using the theory of Limit Analysis. In such materials, the attainment of a certain stress level σ_{ij}, along with certain stress increments $\dot{\sigma}_{ij}$, marks the onset of plastic deformation. In the stress space this means that the representative point of the stress state is on the yield surface, which will be defined in the next section.

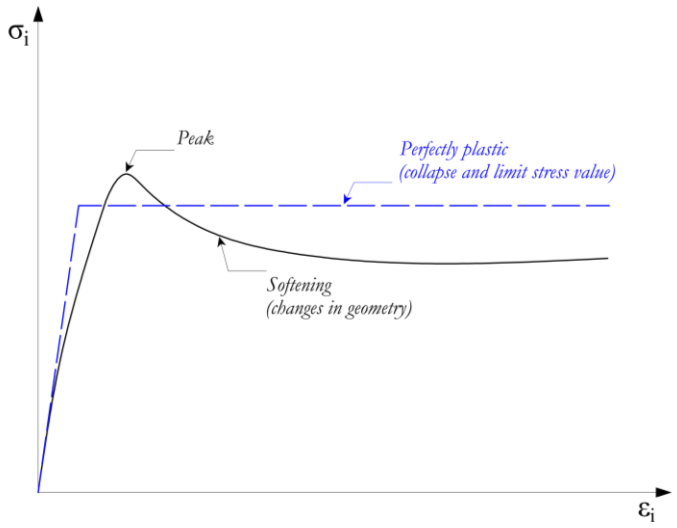

Figure 28: Stress-strain diagram for elasto-plastic material with softening and perfectly plastic material

In the context of Limit Analysis, it is often necessary to simplify the stress-strain diagram of the real material into two straight lines, as depicted by the dashed lines in Figure 28. This simplified diagram represents the behavior of a hypothetical material known as *ideally plastic* or *elastic-perfectly plastic*, which undergoes continuous plastic flow at constant stress. It should

be noted that this assumption is justified for stability problems, and specifically for rigid-body masonry systems.

4.1.2. Yield function

This section summarizes the basic properties of a *yield function* required in Limit Analysis. It is generally observed that the onset of plastic deformations depends on reaching a certain limiting level of stress σ_{ij} with specific increments of stress $\dot{\sigma}_{ij}$, as defined by a *yield criterion*. In the six-dimensional stress space, a *yield surface*, delimiting a yield domain, represents the threshold corresponding to the beginning of a plastic phenomenon whose variations are governed by history dependent material parameters. For a perfectly plastic material in particular, a yield function f is strictly dependent on stress $\sigma_{ij} = \left(\sigma_x \ \sigma_y \ \sigma_z \ \tau_{xy} \ \tau_{yz} \ \tau_{zx}\right)$ and not on strain components $\varepsilon_{ij} = \left(\varepsilon_x \ \varepsilon_y \ \varepsilon_z \ \varepsilon_{xy} \ \varepsilon_{yz} \ \varepsilon_{zx}\right)$. Plastic deformation in a perfectly plastic material occurs when the following two conditions are satisfied:

$$f(\sigma_{ij}) = 0 \tag{4.4}$$

$$df(\sigma_{ij}) = \left(\frac{df(\sigma_{ij})}{d\sigma_i}\right)_{\sigma} d\sigma_i = \nabla f(\sigma_{ij}) \cdot \dot{\sigma}_{ij} = 0 \tag{4.5}$$

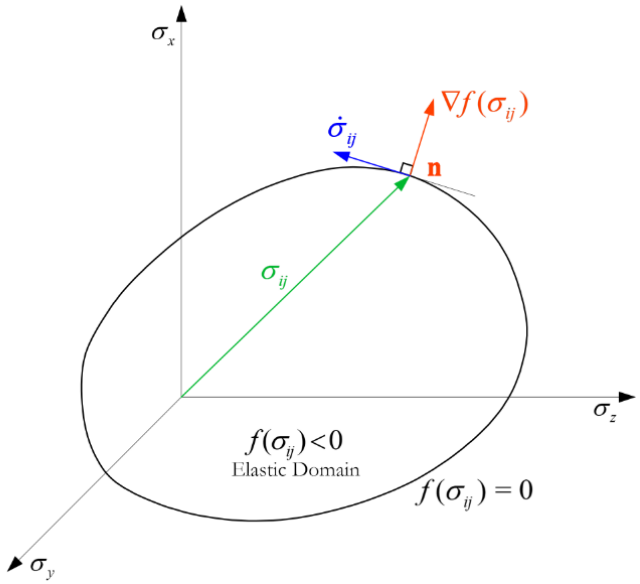

Figure 29: Yield domain and plastic flow in a perfectly plastic material

In other terms, *plastic flow* occurs when the current stress σ_{ij} belongs to the yield surface and the stress increment $\dot{\sigma}_{ij}$ is orthogonal to the normal **n** to the yield surface and belongs to

its tangent plane. Stress states for which $f(\sigma_{ij}) < 0$ corresponds to elastic behaviour, although stress states lying outside the yield surface $f(\sigma_{ij}) > 0$ are excluded.

4.1.3. Flow rule and Drucker stability notion

When the stress state reaches the yield surface, the material starts to deform plastically meaning that the current stress vector is located on the yield surface and is oriented in a direction that exceeds the boundaries of the yield surface. The following equation states that $\dot{\varepsilon}_{ij}^{p}$ is aligned with the outward normal to the yield surface at the current stress state point σ_{ij}. For this reason, it is known as the *normality flow rule:*

$$\dot{\varepsilon}_{ij}^{p} = \lambda \frac{\partial f(\sigma_{ij})}{\partial \sigma_{ij}} \tag{4.6}$$

where $\lambda > 0$ is a scalar factor denoting the plastic strain magnitude, while $\frac{\partial f}{\partial \sigma_{ij}}$ defines the direction. With:

$$\begin{array}{ll} (\dot{\varepsilon}_{ij}^{p} \neq 0) \text{ loading} & (\dot{\varepsilon}_{ij}^{p} = 0) \text{ unloading} \\ \begin{cases} f(\sigma_{ij}) = 0 \\ \text{and} \\ \dfrac{\partial f}{\partial \sigma_{ij}} \dot{\sigma}_{ij} \geq 0 \end{cases} & \begin{cases} f(\sigma_{ij}) = 0 \\ \text{and} \\ \dfrac{\partial f}{\partial \sigma_{ij}} \dot{\sigma}_{ij} < 0 \quad \text{or} \quad f(\sigma_{ij}) < 0 \end{cases} \end{array} \tag{4.7}$$

From these considerations derives the definition of the *Drucker's postulate* or *Drucker's inequality*. Regarding the experimental response shown in Figure 30 concerning a one-dimensional stress test experiment, Drucker provides a definition for a *work-hardening* or *stable* material and a *perfectly plastic* or *neutrally stable* material. A work-hardening material is a plastic material that exhibits positive work during incremental loading and nonnegative work during the loading-unloading cycle.

$$\dot{\sigma}_i \dot{\varepsilon}_i^{p} \geq 0, \tag{4.8}$$

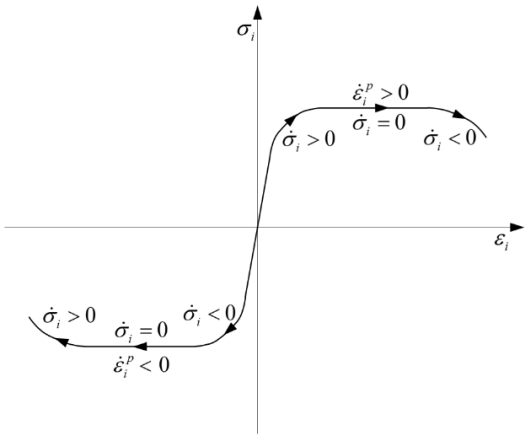

Figure 30: One-dimensional stress test experiment and definition of hardening, perfectly plastic and softening material according to Drucker's postulate

It is evident from the figure that the plastic strain rate, $\dot{\varepsilon}_i^p$, conjugate to a single stress component, σ_i, satisfies the given equation and the following definition can be derived:

$$\dot{\sigma}_i \dot{\varepsilon}_i^p \begin{cases} \geq 0 & \text{hardening material} \\ = 0 & \text{perfectly plastic material} \\ \leq 0 & \text{softening material} \end{cases} \tag{4.9}$$

In Figure 31 a possible loading path is illustrated, where the initial stress σ_{ij}^* remains within the elastic region and gradually increases to a stress σ_{ij} on the current yield surface. This results in a small stress increment $\dot{\sigma}_{ij}$ that is associated with an incremental plastic strain $\dot{\varepsilon}_{ij}$ followed by elastic unloading back to stress level σ_{ij}^*.

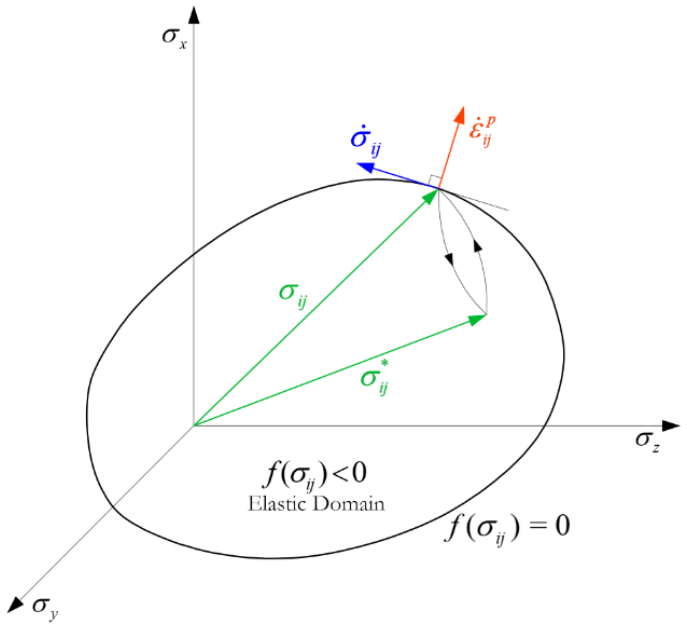

Figure 31: One possible loading path from the initial stress σ_{ij}^* within the elastic region to a stress σ_{ij} on the current yield surface.

The work done by the external loads is $\left(\sigma_{ij}-\sigma_{ij}^{*}\right)\dot{\varepsilon}_{ij}^{p}$. Drucker's postulate implies:

$$\left(\sigma_{ij}-\sigma_{ij}^{*}\right)\dot{\varepsilon}_{ij}^{p}\geq 0 \tag{4.10}$$

This inequality constitutes a postulate in its own right, called *the postulate of maximum plastic dissipation*. The validity of the postulate implies that:

- the yield surface is convex or smooth,
- $\dot{\varepsilon}_{ij}^{p}$ must be directed along the outward normal to the yield surface.

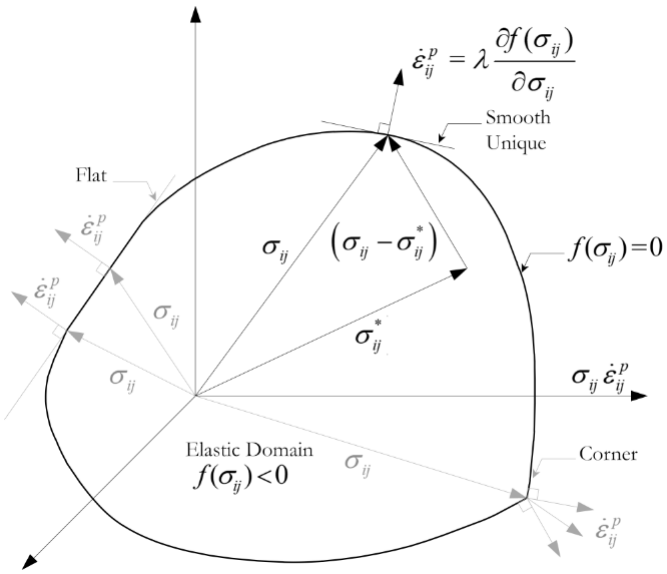

Figure 32: Yield surface

In cases where multiple sections of the yield surface intersect at a vertex point, the strain $\dot{\varepsilon}_{ij}^{p}$ vector cannot lie outside the cone formed by the normal to the planes that are tangent to the individual sections. As a result, a single stress σ_{ij} corresponds to multiple plastic strain increment $\dot{\varepsilon}_{ij}^{p}$. While, if the yield surface has flat sections, which means it is not strictly convex, the equation 2.1 is verified with an equal sign. As a result, a single $\dot{\varepsilon}_{ij}^{p}$ corresponds to multiple σ_{ij}, as illustrated in Figure 32.

Therefore, for the correspondence between $\dot{\varepsilon}_{ij}^{p}$ and σ_{ij} to be biunivocal, the yield surface must be regular and strictly convex.

4.2. Limit Analysis theorems

In this section, the general theorems of Limit Analysis for elastic-perfectly plastic material are introduced. The theorems of Limit Analysis give upper and lower bounds on the loads under which a body, modeled as a perfectly plastic material, reaches a critical state. At this critical state, significant plastic deformation can occur with minimal increase in load. In the case of perfectly plastic bodies this state is called unrestricted plastic flow, and the loading state at which it becomes possible is called limit or collapse load.

Being the Limit Analysis theorems based on the principle of maximum plastic dissipation, they are valid only for materials that are referred to in the literature as normal or standard material. Some extensions of the limit analysis theorems valid for non-associated material, or non-standard material, will be shown in Section 4.2.4.

4.2.1. Static theorem

As reported in [89] and [90] the *collapse load multiplier* λ^c is determined as the maximum among the *static admissible multipliers* λ^s. It follows:

$$\lambda^s \leq \lambda^c \tag{4.11}$$

According to equation (4.11), it can be shown that any statically admissible stress distribution, as determined by the equilibrium equations, corresponds to a static admissible multiplier λ^s that is lower than or equal to the collapse multiplier λ^c of the actual loads $\left(\mathbf{b}_i, \mathbf{f}_i\right)$ which represent external forces on the volume and surface of a body. Assume that the loads $\left(\mathbf{b}_i, \mathbf{f}_i\right)$ change proportionally, meaning that the loading process can be expressed as:

$$\mathbf{b}_i = k\mathbf{b}_i^c \quad \mathbf{f}_i = k\mathbf{f}_i^c, k \geq 1, \tag{4.12}$$

with $\left(\mathbf{b}_i^c, \mathbf{f}_i^c\right)$ actual loads. The objective of the Limit Analysis is to determine the value λ^c of the load multiplier k below which the collapse occurs. With reference to the collapse loads $\left(\mathbf{b}_i, \mathbf{f}_i\right)$ and the statically admissible $\left(\mathbf{b}_a, \mathbf{f}_a\right)$, follows that:

$$\mathbf{b}_i = \lambda^c\mathbf{b}_i^c \quad \mathbf{f}_i = \lambda^c\mathbf{f}_i^c \quad \mathbf{b}_a = \lambda^s\mathbf{b}_i^c \quad \mathbf{f}_a = \lambda^s\mathbf{f}_i^c \tag{4.13}$$

By considering the principle of virtual works, which involves two separate and unrelated sets, namely the *equilibrium set* including a generalized static admissible stress state σ_{ij}^s and the collapse stress state σ_{ij}^c related to the strain rate $\dot{\varepsilon}_{ij}^c$ and the *compatible set* including the displacement field $\dot{\mathbf{u}}_i^c$ combined in the equation with (4.13), it can be observed that:

Equilibrium set

$$\begin{aligned}\int_v \sigma_{ij}^s \dot{\varepsilon}_{ij}^c dv &= \lambda^s \left\{ \int_v \mathbf{b}_i^c \dot{\mathbf{u}}_i^c dv + \int_s \mathbf{f}_i^c \dot{\mathbf{u}}_i^c ds \right\} \\ \int_v \sigma_{ij}^c \dot{\varepsilon}_{ij}^c dv &= \lambda^c \left\{ \int_v \mathbf{b}_i^c \dot{\mathbf{u}}_i^c dv + \int_s \mathbf{f}_i^c \dot{\mathbf{u}}_i^c ds \right\}\end{aligned} \tag{4.14}$$

Compatible set

From this it can be deduced that:

$$\lambda^c - \lambda^s = \frac{\int_v \left(\sigma_{ij}^c - \sigma_{ij}^s \right) \dot{\varepsilon}_{ij}^c dv}{\int_v \mathbf{f}_i^c \dot{\mathbf{u}}_i^c dv + \int_s \mathbf{b}_i^c \dot{\mathbf{u}}_i^c ds} \tag{4.15}$$

Since:

$$\int_v \sigma_{ij}^c \dot{\varepsilon}_{ij}^c dv > 0 \tag{4.16}$$

After equation (4.10), the numerator is positive or zero, while the denominator of the second term is positive.

4.2.2. Kinematic theorem

The *collapse multiplier* λ^c is determined as the minimum among the *kinematically admissible multipliers* λ^k. It follows:

$$\lambda^c \leq \lambda^k \tag{4.17}$$

By considering the principle of virtual works it can be observed that:

$$\begin{aligned}\int_v \sigma_{ij}^c \dot{\varepsilon}_{ij}^k dv &= \lambda^c \left\{ \int_v \mathbf{b}_i^k \dot{\mathbf{u}}_i^k dv + \int_s \mathbf{f}_i^k \dot{\mathbf{u}}_i^k ds \right\} \\ \int_v \sigma_{ij}^k \dot{\varepsilon}_{ij}^k dv &= \lambda^k \left\{ \int_v \mathbf{b}_i^k \dot{\mathbf{u}}_i^k dv + \int_s \mathbf{f}_i^k \dot{\mathbf{u}}_i^k ds \right\}\end{aligned} \tag{4.18}$$

By integrating over the entire surface S or volume V of the body, the first term of the expression representing the power dissipated by the considered mechanism is always positive. From these two equations, we can derive the following:

$$\lambda^k - \lambda^c = \frac{\int_v \left(\sigma_{ij}^k - \sigma_{ij}^c \right) \dot{\varepsilon}_{ij}^k dv}{\int_v \mathbf{f}_i^k \dot{\mathbf{u}}_i^k dv + \int_s \mathbf{b}_i^k \dot{\mathbf{u}}_i^k ds} \tag{4.19}$$

It can be noted that the denominator of the second term is positive. For equation (4.10), the numerator is non-negative and the yield stress state σ_{ij}^k corresponds to $\dot{\varepsilon}_{ij}^k$, while σ_{ij}^c is a generic admissible stress state.

4.2.3. Determination of the plastic collapse multiplier

The collapse multiplier, as defined, belongs to both the statically and kinematically admissible classes of multipliers. The former class refers to the last incremental step of a loading path, while the latter class corresponds to the formation of a collapse mechanism at the end of the last step. Therefore, two adjacent classes consist of statically admissible and kinematically admissible multipliers, with λ^c serving as the dividing element, leading to:

$$\lambda^s \leq \lambda^c \leq \lambda^k \tag{4.20}$$

4.2.4. Limit Analysis theorems for materials with non-associative flow rule

According to Lubliner [79], the theorems of Limit Analysis can be expressed in as follows:

A body will not collapse under a given loading if a possible stress field can be found that is in equilibrium with a loading greater than the given loading.

A body will collapse under a given loading if a velocity field obeying the constraints (or a mechanism) can be found that so that the internal dissipation is less than the rate of work of the given loading.

While the theorems of Limit Analysis can be stated in a simplified form that does not directly reference concepts from Plasticity Theory, it should be noted that the postulate of maximum plastic dissipation, and therefore the normality of the flow rule, is a crucial component of the proof. In fact, the proof of the limit theorems relies on the inequality (4.10), which is a direct consequence of the *normality* relation between a yield surface and its associated plastic strain rate $\dot{\varepsilon}_{ij}^p$. The normality condition, also known as the *associated flow rule*, is crucial and without it, the theorems cannot be generally proven.

Although the theorems of Limit Analysis have been proven to be effective in analysing *plastic* materials, some researchers have attempted to find counterexamples that demonstrate their limitations in analysing *non-standard* or *frictional* materials. For instance, Drucker [91] and Salenco [92] presented a model in which plasticity is combined with Coulomb friction.

Frictional materials, in general, are not analogous to *plastic* materials. Therefore, the inequality (4.10) does not hold for them, and as a result, the limit theorems of plastic bodies cannot be applied to bodies with frictional interfaces.

For perfectly plastic materials, the plastic strain rate $\dot{\varepsilon}_{ij}^p$ is normal to the yield surface, whereas for frictional materials, it is parallel to the γ-axis. To provide a clearer demonstration of this concept, a straightforward physical model from [78] depicted in Figure 33 can be useful.

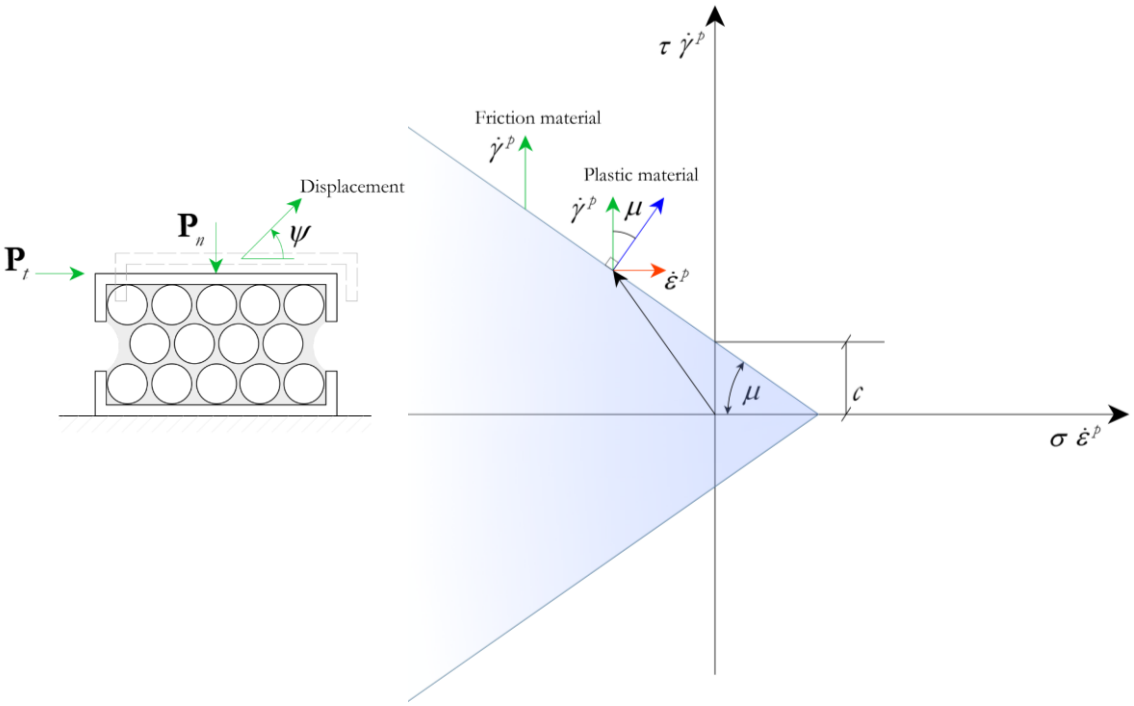

Figure 33: A simple plastic model (left), Flow rule (right)

The figure depicts a layer of densely packed granular material under two forces: a normal force, denoted as $\mathbf{P}_n$, and a tangential force, denoted as $\mathbf{P}_t$. It is assumed that the normal force $\mathbf{P}_n$ remains constant throughout the experiment, while the horizontal force $\mathbf{P}_t$ gradually increases from zero until it reaches the value that causes sliding. When sliding occurs, the horizontal force $\mathbf{P}_t$ must not only overcome cohesion c but also exceed the resistance provided by friction. This type of friction, known as *interlocking friction*, results from the interference between the particles, which makes it difficult to change their relative position. Due to interlocking friction, both upward and horizontal displacement are required. Therefore, the displacement vector must form an angle ψ with the slip plane, the so-called angle of *dilatancy*. Moreover, the soil is modelled as a perfectly plastic material following Coulomb's rule of yielding, shown in Figure 33. As the stress state vector increases from zero, yield will occur when the stress vector reaches the curve consisting of two straight lines. A convenient way to obtain a geometric interpretation of the flow rule is to plot the values of plastic normal strain rate $\dot{\varepsilon}^p$ and plastic shear strain rate $\dot{\gamma}^p$ in a set of coordinates that correspond to the stress coordinates σ and τ. This allows to associate each strain rate vector with the corresponding stress vector. Figure 33 illustrates this combined stress and strain rate plot where the stresses and plastic strain rates are set out parallel and in the same direction. The flow rule implies that the plastic strain rate vector should be normal to the yield curve when their

corresponding axes are overlaid. Figure 33 shows that this is equivalent to setting ψ equal to μ, the *friction coefficient*.

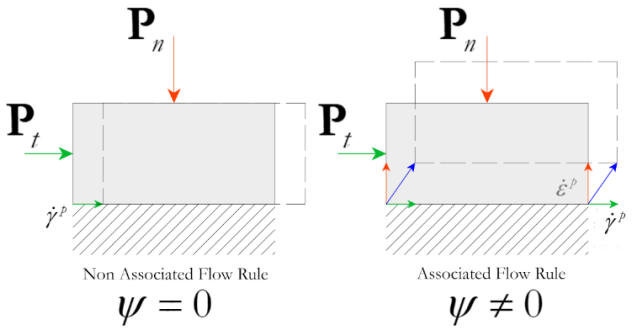

Figure 34: Difference between non associated flow rule and associated flow rule.

The Limit Analysis for *non-standard materials*, that is, for those materials that do not comply with the normality law of plastic flow, was essentially formulated by Radenkovic [15]in relation to problems concerning soils, which, as is well known, usually exhibit dilatancy effects, leading to non-associated flow laws.

After its initial formulation by Radenkovic in 1960, the theory of Limit Analysis for non-standard materials was modified and reformulated by several researchers, including Palmer [93], Sacchi and Save [94] and Salencon[95]. Radenkovic's first theorem can be stated as follows:

The limit loading for a body made of a nonstandard material is bounded from above by the limit loading for the standard material obeying the same yield criterion.

For a deeper insight into Radencovick's theorems for non-standard materials, refer to [79].

4.3. Heyman's model for masonry materials

Heyman's model, proposed in 1966 [14], represents a simple yet comprehensive approach to understanding the behavior of masonry materials. This model conceives of masonry as a *no-tension material* that is rigid under compression. The Heyman's model provides a mechanically rational reinterpretation of classical approaches, such as graphical statics methods, enabling their integration into a theoretically rigorous framework of Limit Analysis. In [96] Heyman applied Limit Analysis to investigate the mechanical behavior of a model consisting of a system of rigid blocks connected through joints and subjected to self-weight.

La Hire, Couplet, and Coulomb's contributions were significant in the definition of Heyman's model. In the 18th century, they studied masonry arches as a system of rigid bodies capable of undergoing relative displacements. According to Couplet, arch collapse occurs when enough hinges develop to trigger a mechanism[97]. Coulomb's essay [98] was the first general theory on the stability of arches, which provided a mathematical description of the various modes of collapse, considering relative rotations and sliding between blocks. Coulomb suggested that, for practical purposes, only overturning rotational failures should be considered, since sliding rarely occur.

Therefore, as previously noted by Couplet and Coulomb, in nearly all cases, friction is sufficient to prevent mutual sliding between ashlars and compressive stresses are considerably lower than the material strength. Therefore, the only admissible mechanism is the formation of a hinge with the rotation of two rigid adjacent blocks around the contact point at the intrados or extrados.

Heyman's formulation for Limit Analysis of masonry structures combines these insights to provide a robust and theoretically sound approach for studying this type of structures. Therefore, Heyman's hypotheses were formalized in [99] and [100] and introduced in [87] with the aim to define the domain of material admissibility as follows:

- masonry is incapable of withstanding tensions,
- masonry has infinite compressive strength,
- elastic strains are negligible,
- masonry has infinite shear strength.

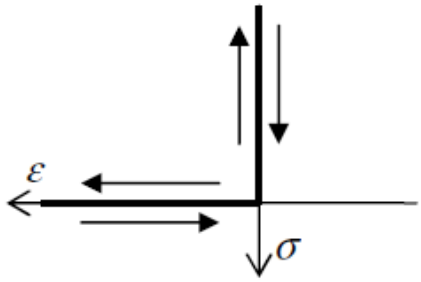

Figure 35: Uniaxial stress-strain relation of rigid no-tension masonry material [87]

By assuming the above hypotheses, and considering that elastic strains can be neglected, it became possible to formulate the static theorem (lower-bound limit analysis) and the kinematic theorem (upper-bound limit analysis) for masonry structures.

The uniaxial stress-strain relationship depicted in Figure 35 is an essential element in understanding the mechanical behavior of the material under Heyman's hypothesis. The hypothesis of the absence of tensile strength in masonry materials is supported by the observation that arches built with dry-assembled blocks or using low-strength mortars have no tensile strength. As mentioned above, the compressive strength of masonry can be considered effectively infinite due to the low compressive stresses. Instead of collapse due to crushing of ashlars, failure occurs due to the formation of hinges caused by rigid rotation of adjacent blocks. Therefore, it is typically the development of rocking mechanisms that leads to the collapse of the structure. The presence of friction between the ashlars is also crucial, as the transmitted compressive force must activate the frictional resistance to prevent sliding between the blocks.

These conditions are sufficient to enable the application of limit analysis methods to study the stability of masonry structures. In fact, masonry structures can be considered as a rigid body system in which the collapse condition is due to loss of equilibrium and thus without any material failure. This is because masonry exhibits lower tensile strength than compressive strength, allowing it to displace without experiencing material failure.

As defined in [87], the elementary resistant element of a masonry structure is defined as rigid masonry bricks that are compressed against each other by an eccentric axial load and potentially subjected to a shear force. This elementary cell represents the basic unit of resistance within a masonry structure. The structural response of the entire construction can be understood by examining the behavior of these individual cells and the interactions between them. It is important to consider the effects of both the axial load and shear force on the behavior of the cell, as they can have significant impacts on the overall stability of the masonry structure.

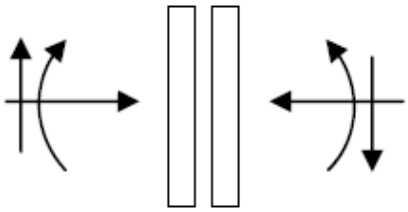

Figure 36: The unit resistant masonry cell [87],

Two generic rigid blocks of height h that constitute the elementary resistant cell of a masonry structure. These blocks are assumed to not deform internally but can detach from each other. Based on the first hypothesis, which assumes that the tensile strength is negligible, only compressive stresses and displacement fields resulting from hinge formation at the ends of the joint connecting the two bricks are allowed. Therefore, the eccentricity of the normal stress N is equal to:

$$e = \frac{M}{N} \tag{4.21}$$

have to satisfy the inequality:

$$-\frac{h}{2} \leq e \leq \frac{h}{2} \tag{4.22}$$

This condition defines the area representing admissible stress states. In other words, if the eccentricity reaches the limit value, a crack forms in the cell. As the hinge opens, the law of plastic flow is observed, ensuring that the plastic displacement is orthogonal to the boundary domain. This relation is critical for predicting the behavior of masonry structures.

4.4. The Limit Analysis theorems for masonry

The hypothesis of Heyman's model allows for the formulation of the *lower-bound* (or *safe*) *theorem* for masonry structures:

The structure is safe, meaning that the collapse will not occur, if a statically admissible state of equilibrium can be found.

The lower-bound theorem in Heyman's model is based on the hypothesis that if a thrust line can be defined, in equilibrium with external loads, which falls within the boundaries of the masonry structure, then the load applied is a lower-bound of the actual ultimate load that would cause failure. This theorem is used to support the static approach, also known as *static limit analysis*, for the safety assessment of masonry structures. By establishing a thrust line that is in equilibrium with the external loads, Heyman's model provides an approach to determine a lower-bound for the load that a masonry structure can withstand before collapsing. This approach can be used to assess the safety of historical masonry structures, which often lack complete and reliable information about their material properties.

As an example, when analyzing an arch subjected to specific loads, a funicular curve representing the load distribution is first defined and then evaluated to determine if it is entirely comprised within the arch. If this is the case, it can be inferred that the imposed loads do not exceed the collapse load and that the structure is in a state of equilibrium.

The *upper-bound theorem* states that:

If a kinematically admissible mechanism can be found, for which the work developed by external forces is positive or zero, then the arch will collapse.

In other words, assuming the presence of hinges, the load at which the work done by external forces becomes zero is an upper bound of the actual load that will cause collapse. This approach is known as the *kinematic approach* or *kinematic limit analysis*.

Assuming Heyman's hypotheses, the *uniqueness theorem* states that:

A limit condition will be reached (i.e., the structure will be about to collapse) if a both statically and kinematically admissible collapsing mechanism can be found.

This means that if a thrust line can be found forming enough hinges to develop a mechanism, the structure will collapse. Hinges occur when the thrust line becomes tangent to the boundaries of the structure. At this point, the load is the true collapse load, the mechanism is the true collapse mechanism, and the current thrust line is the only possible one.

When Heyman's assumptions are not satisfied and sliding arises, the behavior of masonry cannot be described by classical limit analysis theory. The normality law is not applicable, and the collapse multiplier is not unique. The reformulation of the limit analysis problem for non-standard materials is required as discussed in Section 4.2.4.

4.5. Structural analysis in ancient masonry structures: before Heyman's model

Robert Hooke discovered that the inverted catenary curve is the ideal shape for a masonry arch in equilibrium, as it is subjected to the same weight distribution as a chain. He presented his solution as an anagram, which reads "*Ut pendet continuum flexile, sic stabit contiguum rigidum inversum*" [101]. David Gregory later extended Hooke's assertion to the case of arches with finite thickness and found that stability is achieved when a catenary can be contained within the arch's thickness.

The analogy between the equilibrium of compressed block elements and funicular models was commonly used for analyzing masonry arches in the 18th, 19th, and early 20th centuries. Poleni's study of the dome of St. Peter, depicted in Figure 37, used Robert Hooke's concept of a hanging chain to evaluate the stability of the dome. To do this, he hung a rope with weights proportional to the sections of a radial slice of the dome. This technique allowed him to examine the dome's stability, but it was only suitable for two-dimensional structures and could be challenging and time-consuming for complex structures.

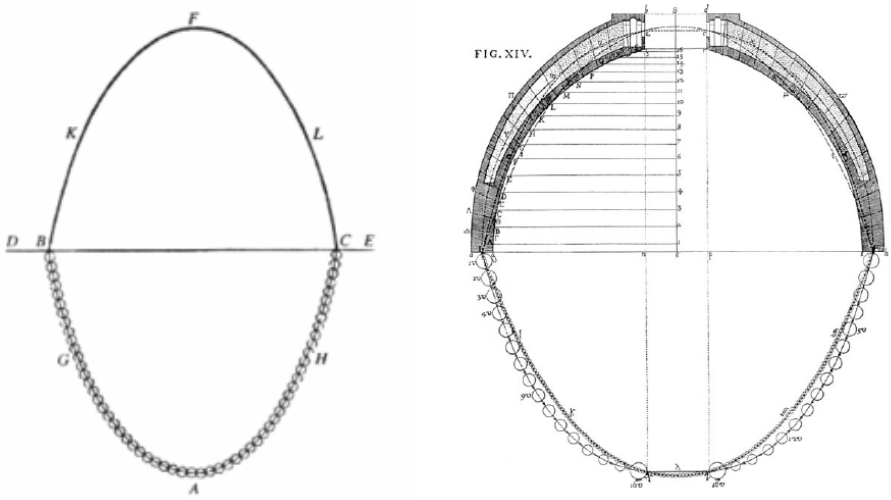

Figure 37: Poleni's illustration of Hooke's analogy between an arch and a hanging chain model (left), his analysis of the Dome of St. Peter's in Rome [101] .

During the 19th century, the thrust line theory and graphic statics brought further advancements in the analysis of masonry arches. Graphic statics is a useful technique for analyzing historical unreinforced masonry structures by utilizing force polygon and force diagram [102] [103].

This method was widely used for the evaluation of masonry bridges and large buildings until the early 20th century. Huerta [70] conducted a comprehensive review of the application of the thrust line theory to the analysis of vaults and domes. However, this method is limited to two-dimensional systems.

4.6. Static theorem-based approaches: equilibrium analysis

Heyman's hypothesis [14], as discussed in Section 4.3 , allows for the formulation of a lower-bound theorem for masonry structures, which states that a structure is stable if a thrust line within the boundaries of the structure can be determined. This lower-bound theorem forms the basis for the *static approach*, also known as *static limit analysis*, for the safety assessment of masonry structures.

In 1993, O'Dwyer [104] proposed a first example of three-dimensional equilibrium method based on force networks, which extends beyond the traditional two-dimensional thrust line analysis. This approach implements optimization methods to analyze masonry compression-only force networks. However, a limitation of O'Dwyer's approach is its ineffectiveness in handling the high degree of indeterminacy of three-dimensional force networks. Additionally, another approach for the assessment of vaulted masonry was introduced by Andreu et al. [105], which is based on the analogy between the equilibrium of arches and hanging strings and implemented within an optimization framework that finds a virtual funicular shape in equilibrium constrained within the limits of a vault.

Oppenheim et al. [106] proposed the static equilibrium analysis of unreinforced masonry structures of rigid material with no tensile strength based on a variant to the membrane shell theory.

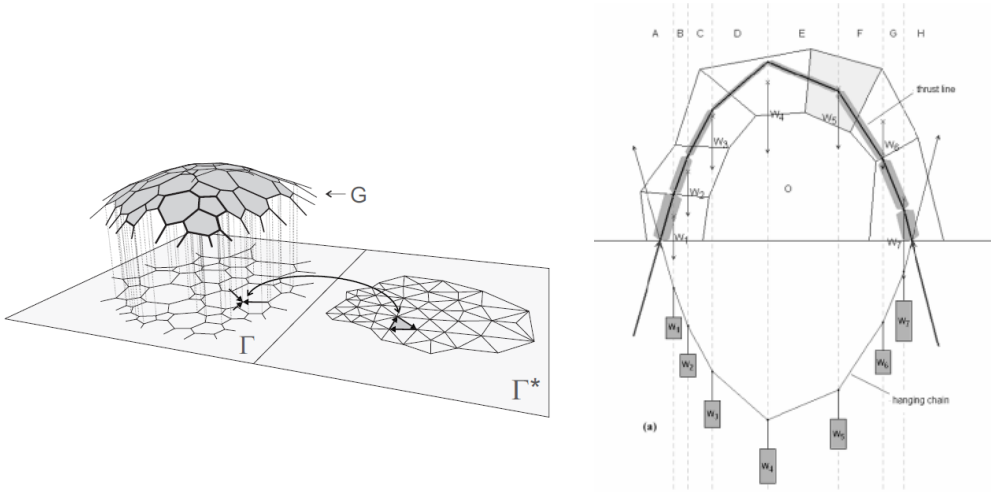

Figure 38 : Relationship between the compression equilibrium shape the reciprocal force diagram [107].*(left), analogy between thrust line and hanging chain* [108] *(right).*

Block and Ochsendorf in [108] introduced a real-time limit analysis tool for the assessment of masonry structures. Some years later, they proposed a new method for analyzing vaulted masonry structures called Thrust Network Analysis (TNA) [107]. Based on O'Dwyer's Force Network Method, this approach enables three-dimensional analysis using duality between geometry and internal forces in networks to find funicular solutions under gravitational

loading and exploring equilibrium shapes. This makes it a valuable tool for safety assessment of historic vaults with complex geometries in unreinforced masonry, as well as for design exploration of funicular shapes for assessment and design purposes.

The TNA method has been reformulated by Marmo and Rosati [72] to improve computational performance and has also been extended to include horizontal forces and holes or free edges in the vault, as well as applied to masonry helical staircases [109].

Fraternali and Rocchetta [110], introduced a new approach for analyzing masonry vaults using piecewise-linearly approximated thrust surfaces. Their force equilibrium is related to discrete Airy stress functions, and this approach extends the *Lumped Stress Method* to three-dimensional applications [111]. Treating the vault as a no-tension membrane, polyhedral stress functions are utilized to study the equilibrium problem and determine the optimal shape of the discretized thrust surface that fits within the vault section [112].

Another approach for analyzing masonry vaulted structures by treating them as unilateral membranes is proposed in Angelillo et al. [113] and Angelillo [114]. In [115] a discrete network of singular stresses based on Airy's stress formulation is defined. However, the solving algorithm used in this approach may not allow for the incorporation of structural discontinuities.

Smars [116] applied limit analysis to the safety assessment of block masonry structures taking into account the influence of friction on masonry structure stability when sliding mechanisms occur and Heyman's hypothesis are neglected.

In [117], Nodargi presented a revisited approach based on the thrust line analysis for the optimization of masonry arches.

To summarize, static theorem-based methods are effective for assessing the safety of masonry structures by identifying compression-only thrust line or networks within the masonry's boundaries. However, most of the approaches mentioned earlier do not consider some aspects that are crucial in describing the structural behavior of masonry.

4.7. Kinematic theorem-based approaches

Kinematic theorem-based limit analysis methods have been widely used in recent years to assess the seismic vulnerability of masonry buildings. Giuffrè [16] introduced a kinematic limit analysis approach for decomposing masonry structures into rigid blocks based on the failure mechanisms observed in Italian masonry constructions. This approach has been incorporated into the Italian code [118] [29]and is commonly used in professional practice for safety assessments of existing masonry structures. Kinematic linear and nonlinear methods are used to evaluate the displacement capacity of the structure before collapse.

Advanced computational kinematic theorem-based approaches have been developed to accurately evaluate the collapse multiplier and collapse mechanism of masonry structures. For example, Milani [119] introduced a simple discontinuous upper bound limit analysis approach with sequential linear programming mesh adaptation to analyze the actual failure mechanisms of masonry structures with double curvature. Chiozzi et al.[73] recently proposed a genetic algorithm for the limit analysis of masonry vaults based on an upper bound formulation, using a non-uniform rational B-spline (NURBS) parametric surface representation of the vault geometry. This approach has also been validated for the out-of-plane collapse behavior of masonry walls [120]. Additionally, an automatic upper bound adaptive limit analysis program for masonry churches, has been proposed in [121]. While these methods may not be able to determine the displacement capacity of a masonry structure, they are highly effective in rapidly assessing their safety level.

4.8. Limit Analysis: numerical approaches

Advanced numerical methods and modern computers have greatly enhanced the analysis of masonry constructions when combined with limit analysis theorems.

Livesley [82] made a significant contribution to the development of a computational method for masonry structures by providing an approach where masonry is studied as a discrete system of rigid blocks. This was achieved through the reformulation of the static theorem of limit analysis as a linear programming (LP) problem, where Coulomb friction law was assumed at block interfaces. However, limit analysis theorems require an associative flow law, which leads to the occurrence of dilatancy resulting in an overestimation of the collapse multiplier, as demonstrated by Drucker [76] and Radenkovic [15].

The earliest block-based limit analysis method applied to masonry structures is the one defined by Baggio and Trovalusci [122]. Their approach involves solving a linearized limit analysis problem with dilatancy at interfaces as a preliminary step to obtain the solution to the nonlinear programming problem with friction [123].

Ferris and Tin Loi [124] proposed a different approach to compute the collapse loads of rigid block systems with non-associative friction and tensionless contact interfaces. They formulated and solved the problem as a constrained optimization problem with equilibrium constraints.

Melbourne and Gilbert [125] (see also Gilbert and Melbourne [126], and Gilbert [127]) proposed a method to determine the collapse load of masonry structures composed of a system of masonry blocks. The method is both conceptually simple and computationally efficient, utilizing the upper-bound theory of plasticity along with geometrical compatibility criteria.

Casapulla in [128] studies the influence of Coulomb friction in dry rigid masonry block systems. Moreover, to analyze masonry block structures with non-associative frictional joints, Gilbert and Casapulla proposed in [129] a formulation using linear programming has been, which has been further extended to 3D structures accounting for torsional effects in [130] by Portioli et al. and optimized using cone programming in [131]. In these approaches, the rigid blocks interact through no-tension contact surfaces with Coulomb friction.

Sutcliffe et al. [132] implemented a method for calculating lower bound limit loads in unreinforced masonry shear walls subjected to plane strain conditions. They used a Mohr-Coulomb approximation of yield surfaces to compute a statically admissible stress field using linear programming and finite elements. By imposing equilibrium, they obtained an expression for the collapse load, which is a rigorous lower bound on the actual collapse load. This technique allows for the computation of lower bounds on the collapse loads of unreinforced masonry shear walls in a theoretically sound and computationally efficient manner.

The authors Orduña and Lourenço [133] proposed a Cap Model for the non-associated limit analysis of rigid block masonry assemblages, which includes non-associated flow rules and limited compressive strength of masonry. A formulation of the limit analysis problem for three-dimensional rigid blocks with frictional interfaces was proposed in [134] [135]

Milani proposed an approach for upper bound limit analysis of in- and out-of-plane loaded masonry walls using 3D finite element analysis [136]. This approach uses interfaces with a Mohr-Coulomb failure criterion and accounts for mortar joint cohesion and masonry crushing. Direct applications of this model can be found in other studies [137] [138].

Nodargi et al. [139] implemented a variational-based fixed-point algorithm to solve the limit analysis problem for dry-masonry block structures with frictional behavior at the interface.

Bertolesi et al. [47] analyze with a FE lower bound limit analysis code the failure mechanism in presence of FRP reinforcement.

PART III STRUCTURAL ANALYSIS APPROACHES FOR SUPPORTING OPTIMAL REINFORCEMENT DESIGN

Chapter 5
Limit analysis problem for two-dimensional block dry reinforced masonry

In this part of the thesis, the formulation of the limit analysis problem for two-dimensional dry reinforced masonry is proposed.

In Section 5.6.1 and 5.6.2, with the assumption of associated plastic flow rule, both the kinematic and static limit analysis problem are formulated as a LP problem to find the collapse multiplier.

In Section 5.7, the dilatancy effect associated to friction at the interface is considered. The limit analysis problem is formulated with a non-associated flow rule and the nonlinear programming (NLP) optimization problem is solved with an iterative procedure of linear programming (LP) optimization.

In Section 5.10, the algorithm solving the non-standard limit analysis problem will be enhanced with the introduction of constraint equations to take into account the introduction of the reinforcement. Two types of reinforcement will be considered: elastic reinforcement and elastic-perfectly plastic reinforcement.

5.1. Kinematics of the rigid block

In this section, the limit analysis problem for dry masonry block structures is illustrated. In particular, dry masonry is assumed to be made of a proper number N_b of two-dimensional rigid blocks, mutually connected through N_3 rough interfaces, capable of transmitting also attritive forces.

Introducing a global coordinate Cartesian system $\{O;x,y\}$, the centroid $\mathbf{G}_k$ of the k-th rigid block b_k of the dry masonry is identified by the position vector $\mathbf{x}_k = \{x_k \quad y_k\}^T$. The Lagrangian parameters defining the kinematics of b_k, and referred to $\mathbf{G}_k$, are denoted as:

$$\mathbf{U}_k = \{U_k \; V_k \; \Phi_k\}^T, \tag{5.1}$$

where U_k and V_k represent the x- and y- components of the displacement of the centroid $\mathbf{G}_k$, while Φ_k is the rotation angle of the block b_k.

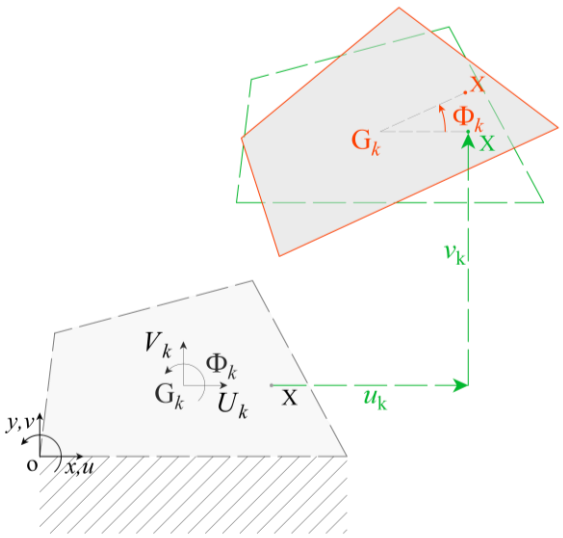

Figure 39: Generalized rigid displacement field of the block b_k expressed in terms of Lagrangian parameters at the $\mathbf{G}_k$ centroid.

From here on vectors are intended not as absolute entities, but as arrays of components depending on the choice of the reference system.

The displacement vector of the typical point of the block, denoted as $\mathbf{u}_k(\mathbf{x}) = \{u_k \quad v_k\}^T$ with $\mathbf{x} = \{x \quad y\}^T$, can be determined as a function of the Lagrangian parameters through the classical representation formula for infinitesimal plane rigid displacements:

$$\mathbf{u}_k(\mathbf{x}) = \begin{Bmatrix} U_k \\ V_k \end{Bmatrix} + \Phi_k \mathbf{e} \wedge (\mathbf{x} - \mathbf{x}_k), \tag{5.2}$$

where $\mathbf{e}$ is the unit vector orthogonal to the $x-y$ plane. In matrix form, equation (5.2) can be written as:

$$\mathbf{u}_k(\mathbf{x}) = \mathbf{B}_k(\mathbf{x})\mathbf{U}_k\,, \tag{5.3}$$

with $\mathbf{B}_k(\mathbf{x})$ the kinematic matrix:

$$\mathbf{B}_k = \begin{bmatrix} 1 & 0 & -(y-y_k) \\ 0 & 1 & x-x_k \end{bmatrix}. \tag{5.4}$$

5.2. Kinematics of the interface

The relative displacement field for the zero thickness interfaces $N_\Im$ joining the N_b rigid blocks constituting the dry masonry system can be determined as a function of the Lagrangian parameters of the blocks. In fact, let be b_j and b_k two rigid blocks interacting each other through the i-th interface as shown in Figure 40.

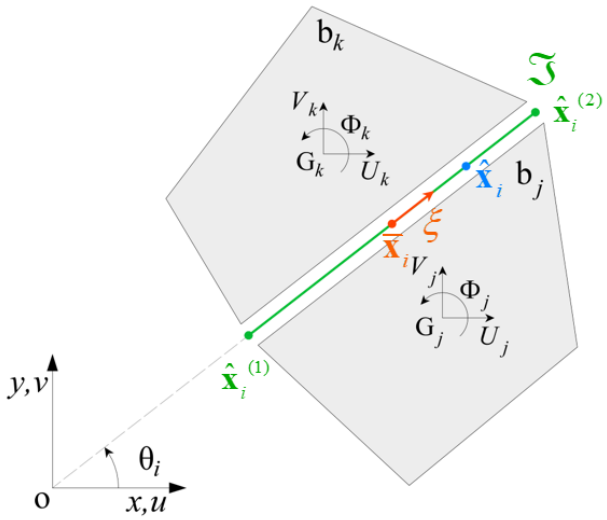

Figure 40: Block model for dry masonry discretized into N_b blocks and $N_\Im$ interfaces, with displacement at centroid representing the Lagrangian parameters.

Introducing the midpoint of the interface, defined by the position vector $\bar{\mathbf{x}}_i = \left(\hat{\mathbf{x}}_i^{(1)} + \hat{\mathbf{x}}_i^{(2)}\right)/2$, with $\hat{\mathbf{x}}_i^{(1)}$ and $\hat{\mathbf{x}}_i^{(2)}$ the position vectors of the initial and final points of the interface, the generalized kinematic parameters describing the interfacial relative displacement field can be referred to the interface midpoint, and identified by the relative displacement components at $\bar{\mathbf{x}}_i$ and the relative rotation of the joined blocks:

$$\bar{\mathbf{s}}_i = \begin{Bmatrix} u_k(\bar{\mathbf{x}}_i) - u_j(\bar{\mathbf{x}}_i) \\ v_k(\bar{\mathbf{x}}_i) - v_j(\bar{\mathbf{x}}_i) \\ \Phi_k - \Phi_j \end{Bmatrix} = \bar{\mathbf{B}}_i \mathbf{d}_i, \tag{5.5}$$

where the interface compatibility matrix $\bar{\mathbf{B}}_i$ results:

$$\bar{\mathbf{B}}_i = \begin{bmatrix} -1 & 0 & \bar{y}_i - y_j & 1 & 0 & -(\bar{y}_i - y_k) \\ 0 & -1 & -(\bar{x}_i - x_j) & 0 & 1 & \bar{x}_i - x_k \\ 0 & 0 & -1 & 0 & 0 & 1 \end{bmatrix}, \tag{5.6}$$

and the vector $\mathbf{d}_i = \{\mathbf{U}_j^T \quad \mathbf{U}_k^T\}^T$ collects the Lagrangian parameters of the two joined blocks.

The kinematically admissible relative displacement $\boldsymbol{\eta}_i$, evaluated at the typical point of the i-th interface, with position vector $\hat{\mathbf{x}}_i = \{\hat{x}_i \quad \hat{y}_i\}^T$, can be computed as:

$$\boldsymbol{\eta}_i = \mathbf{u}_k(\hat{\mathbf{x}}_i) - \mathbf{u}_j(\hat{\mathbf{x}}_i) = \begin{bmatrix} -1 & 0 & \hat{y}_i - y_j & 1 & 0 & -(\hat{y}_i - y_k) \\ 0 & -1 & -(\hat{x}_i - x_j) & 0 & 1 & \hat{x}_i - x_k \end{bmatrix} \begin{Bmatrix} U_j \\ V_j \\ \Phi_j \\ U_k \\ V_k \\ \Phi_k \end{Bmatrix}. \tag{5.7}$$

It is easy to show that in term of the relative displacement at the interface midpoint $\boldsymbol{\eta}_i$ can be written as:

$$\boldsymbol{\eta}_i = \begin{bmatrix} 1 & 0 & -(\hat{y}_i - \bar{y}_i) \\ 0 & 1 & \hat{x}_i - \bar{x}_i \end{bmatrix} \bar{\mathbf{s}}_i. \tag{5.8}$$

A local system is introduced, considering the tangent and the leftward normal direction at the i-th interface, defined by the unit vectors $\mathbf{t}_i$ and $\mathbf{n}_i$, respectively:

$$\begin{aligned} \mathbf{t}_i &= \begin{Bmatrix} t_x \\ t_y \end{Bmatrix} = \frac{1}{\ell_i} \begin{Bmatrix} \hat{x}_i^{(2)} - \hat{x}_i^{(1)} \\ \hat{y}_i^{(2)} - \hat{y}_i^{(1)} \end{Bmatrix} = \begin{Bmatrix} \cos\theta_i \\ \sin\theta_i \end{Bmatrix} \\ \mathbf{n}_i &= \begin{Bmatrix} n_x \\ n_y \end{Bmatrix} = \begin{Bmatrix} -t_y \\ t_x \end{Bmatrix} = \begin{Bmatrix} -\sin\theta_i \\ \cos\theta_i \end{Bmatrix} \end{aligned} \tag{5.9}$$

where ℓ_i is the interface length and θ_i is the inclination angle of the interface with respect to the global x-axis, and having origin in the middle point $\bar{\mathbf{x}}_i$. The orientation of local axis is chosen such that the normal unit vector $\mathbf{n}_i$ is oriented from b_j to b_k. The generalized

interface kinematic parameters can be represented in the local system by a rotation of the reference coordinates:

$$\hat{\mathbf{s}}_i = \mathbf{R}_i \bar{\mathbf{s}}_i = \hat{\mathbf{B}}_i \mathbf{d}_i \,, \tag{5.10}$$

with $\mathbf{R}_i$ the rotation matrix from the global to the local coordinate system:

$$\mathbf{R}_i = \begin{bmatrix} t_x & t_y & 0 \\ n_x & n_y & 0 \\ 0 & 0 & 1 \end{bmatrix} \quad \text{and} \quad \hat{\mathbf{B}}_i = \mathbf{R}_i \bar{\mathbf{B}}_i \,. \tag{5.11}$$

In equation (5.10) $\hat{\mathbf{s}}_i$ is a vector whose components $\hat{s}_{i|t} = \mathbf{t}_i^T \hat{\mathbf{s}}_i$ and $\hat{s}_{i|n} = \mathbf{n}_i^T \hat{\mathbf{s}}_i$ represent the tangent and normal components of the relative displacement at the interface midpoint $\bar{\mathbf{x}}_i$, and $\Theta_i = \Phi_k - \Phi_j$ is the relative rotation between the blocks $\mathbf{b}_k$ and $\mathbf{b}_j$.

The components in the local coordinate system of the relative displacement at the typical point $\hat{\mathbf{x}}_i$ of the interface can be collected in a vector $\hat{\boldsymbol{\eta}}_i$. It is straightforward to see that the latter can be evaluated as function of the vector of generalized kinematic parameters $\hat{\mathbf{s}}_i$ as:

$$\hat{\boldsymbol{\eta}}_i = \begin{bmatrix} 1 & 0 & 0 \\ 0 & 1 & \xi_i \end{bmatrix} \hat{\mathbf{s}}_i \,, \tag{5.12}$$

ξ_i being the abscissa of $\hat{\mathbf{x}}_i$ evaluated starting from $\bar{\mathbf{x}}_i$ along the tangent direction (see Figure 40).

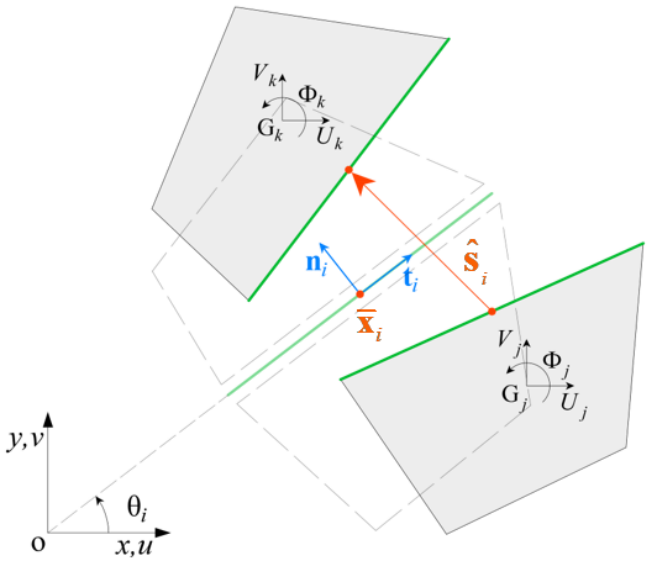

Figure 41: Relative displacement $\hat{\mathbf{s}}_i$ at the midpoint $\bar{\mathbf{x}}_i$ on the shared interface; local reference system.

5.3. Interface forces

From the static point of view, the interaction forces arising at the i- th interface are organized in the vector of the interface generalized forces $\hat{\mathbf{X}}_i = \{T_i \quad N_i \quad M_i\}^T$ collecting the components of the contact forces in the local coordinate system. The shear force T_i, the normal force N_i, and the bending moment M_i are dual entities of the generalized interface kinematic parameters in the same reference system. In particular, the shear force T_i, the normal force N_i and the bending moment M_i are assumed positive if having the same verse of the local coordinate system on the side of the interface belonging to the j- th block. As consequence, the normal force N_i turns out to be positive when tensile interaction occurs between the blocks.

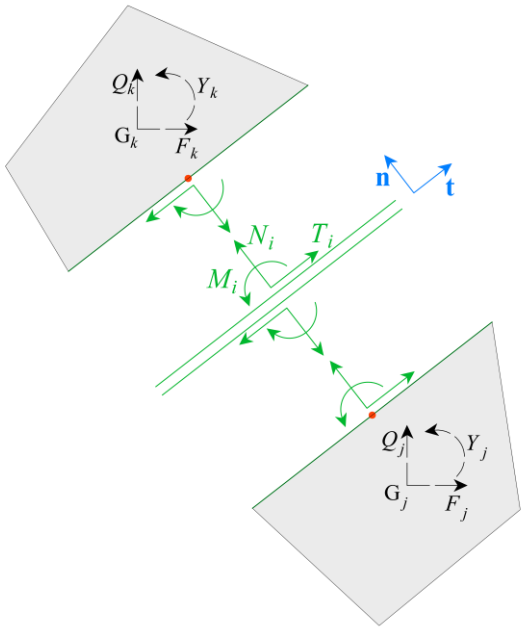

Figure 42: Contact forces at the interface.

The contribution of the interface generalized forces to the equilibrium equations of the b_j and b_k joined blocks can be accounted for by the force vectors $\mathbf{F}_j^{(i)} = \{F_j^{(i)} \; Q_j^{(i)} \; Y_j^{(i)}\}^T$ and $\mathbf{F}_k^{(i)} = \{F_k^{(i)} \; Q_k^{(i)} \; Y_k^{(i)}\}^T$, respectively, where the first two components of $\mathbf{F}_j^{(i)}$ and $\mathbf{F}_k^{(i)}$ are the components of the interface forces along the $x-$ and $y-$directions, and the third component is the moment of the interface forces computed around the centroid of each block. Note that the force vectors $\mathbf{F}_j^{(i)}$ and $\mathbf{F}_k^{(i)}$ are dual to the displacement vectors $\mathbf{U}_j$ and $\mathbf{U}_k$. Collecting the two forces vectors $\mathbf{F}_j^{(i)}$ and $\mathbf{F}_k^{(i)}$ in a unique vector of

components of the interface forces in the global reference system $\mathbf{D}_i = \left\{ \left(\mathbf{F}_j^{(i)} \right)^T \quad \left(\mathbf{F}_k^{(i)} \right)^T \right\}^T$, dual of the kinematic vector $\mathbf{d}_i$, and taking into account equation (5.10), it results:

$$\hat{\mathbf{s}}_i^T \hat{\mathbf{X}}_i = \mathbf{d}_i^T \hat{\mathbf{B}}_i^T \hat{\mathbf{X}}_i = \mathbf{d}_i^T \mathbf{D}_i . \tag{5.13}$$

Thus, it holds:

$$\mathbf{D}_i = \hat{\mathbf{B}}_i^T \hat{\mathbf{X}}_i , \tag{5.14}$$

resulting $\hat{\mathbf{B}}_i^T$ the equilibrium operator for the $i-$th interface, relating interface forces evaluated with respect to the local reference system and to the centroids of the two joined blocks. It is underlined the duality with the compatibility operator defined in equation (5.11).

5.4. Stress limit conditions

According to the almost classical hypotheses adopted in the mechanics of masonry structures, it is assumed that no-tensile forces can be transmitted between the blocks at the joining interface, and that the amount of shear force and bending moment between two joined blocks is limited by the classical dry friction Coulomb law and by the rocking relationship, respectively. The latter condition requires that the application point of the resulting normal force associated to bending moment, i.e., the eccentricity M_i / N_i of the normal force, must fall into the interface. The above assumptions imply that the components of the vector $\hat{\mathbf{X}}_i$ have to satisfy the following inequalities:

$$\begin{aligned} N_i &\le 0 \\ |T_i| + \mu N_i &\le 0 , \\ |M_i| + \rho_i N_i &\le 0 \end{aligned} \tag{5.15}$$

where μ is the friction coefficient and ρ_i is the half of the interface length, i.e., $\rho_i = \ell_i / 2$. Notice that equation (5.15) has been obtained from the condition imposed by the rocking relationship, i.e., $|M_i| \le \rho_i |N_i|$, taking into account the restriction on the values of the normal interface force N_i imposed by equation (5.15).

Equations (5.15) can be written in the equivalent form:

$$\begin{aligned}
\alpha_i^1\left(\hat{\mathbf{X}}_i\right) &= N_i \le 0 \\
\alpha_i^2\left(\hat{\mathbf{X}}_i\right) &= T_i + \mu N_i \le 0 \\
\alpha_i^3\left(\hat{\mathbf{X}}_i\right) &= -T_i + \mu N_i \le 0 \quad , \\
\alpha_i^4\left(\hat{\mathbf{X}}_i\right) &= M_i + \rho_i N_i \le 0 \\
\alpha_i^5\left(\hat{\mathbf{X}}_i\right) &= -M_i + \rho_i N_i \le 0
\end{aligned} \tag{5.16}$$

or, in matrix form:

$$\boldsymbol{\alpha}_i = \mathbf{N}_i^T \hat{\mathbf{X}}_i \le \mathbf{0} \qquad \text{with } \mathbf{N}_i = \begin{bmatrix} 0 & 1 & -1 & 0 & 0 \\ 1 & \mu & \mu & \rho_i & \rho_i \\ 0 & 0 & 0 & 1 & -1 \end{bmatrix}. \tag{5.17}$$

$\boldsymbol{\alpha}_i$ being the interface limit forces vector, and $\mathbf{0}$ the null vector of dimension 5. In the framework of the plasticity theory, the inequality conditions (5.16) or (5.17) can be interpreted as the admissibility condition for the interface forces, defining a multisurface yield domain for $\hat{\mathbf{X}}_i$ described by the five yield functions $\alpha_i^k\left(\hat{\mathbf{X}}_i\right)$, k=1,2,...,5 in equations (5.16)

5.5. Associative kinematic evolution law

In the classical limit analysis setting, the assumption of associated plastic flow rule is required. This allows for relating evolution law of the interface kinematic parameters to the yield domain defined in Section 5.4.

By following standard formalisms of the theory of the plasticity, and adopting the Koiter's generalization for multisurface yield domain plasticity the kinematic quantities expressing the plastic flow, i.e. the kinematic vectors describing displacements conjugated to the interface stress $\hat{\mathbf{X}}_i$ when limit conditions are achieved, can be computed as:

$$\boldsymbol{\eta}_i = \sum_{k=1}^{5} \boldsymbol{\eta}_{i|k} = \sum_{k=1}^{5} \dot{\lambda}_k \frac{\partial\left(\alpha_i^k\left(\hat{\mathbf{X}}_i\right)\right)}{\partial \hat{\mathbf{X}}_i}, \tag{5.18}$$

where $\dot{\lambda}_k \ge 0,\ k = 1,2,...,5$ are non-negative plastic multiplier. For better enlightening the mechanical meanings of the quantities in equation (5.18), it is possible to employ the following formalism:

$$\boldsymbol{\eta}_{i|1} = \boldsymbol{\eta}_{i|n} = \tilde{s}_{i|n} \frac{\partial\left(\alpha_i^1\left(\hat{\mathbf{X}}_i\right)\right)}{\partial\hat{\mathbf{X}}_i} = \tilde{s}_{i|n} \frac{\partial(N_i)}{\partial\hat{\mathbf{X}}_i} = \tilde{s}_{i|n} \begin{Bmatrix} 0 \\ 1 \\ 0 \end{Bmatrix}$$

$$\boldsymbol{\eta}_{i|2} = \boldsymbol{\eta}_{i|t}{}^{+} = \tilde{s}_{i|t}{}^{+} \frac{\partial\left(\alpha_i^2\left(\hat{\mathbf{X}}_i\right)\right)}{\partial\hat{\mathbf{X}}_i} = \tilde{s}_{i|t}{}^{+} \frac{\partial(T_i + \mu N_i)}{\partial\hat{\mathbf{X}}_i} = \tilde{s}_{i|t}{}^{+} \begin{Bmatrix} 1 \\ \mu \\ 0 \end{Bmatrix}$$

$$\boldsymbol{\eta}_{i|3} = \boldsymbol{\eta}_{i|t}{}^{-} = \tilde{s}_{i|t}{}^{-} \frac{\partial\left(\alpha_i^3\left(\hat{\mathbf{X}}_i\right)\right)}{\partial\hat{\mathbf{X}}_i} = \tilde{s}_{i|t}{}^{-} \frac{\partial(-T_i + \mu N_i)}{\partial\hat{\mathbf{X}}_i} = \tilde{s}_{i|t}{}^{-} \begin{Bmatrix} -1 \\ \mu \\ 0 \end{Bmatrix}$$

$$\boldsymbol{\eta}_{i|4} = \boldsymbol{\eta}_{i|\Theta}{}^{+} = \Theta_i^{+} \frac{\partial\left(\alpha_i^4\left(\hat{\mathbf{X}}_i\right)\right)}{\partial\hat{\mathbf{X}}_i} = \Theta_i^{+} \frac{\partial(M_i + \rho_i N_i)}{\partial\hat{\mathbf{X}}_i} = \Theta_i^{+} \begin{Bmatrix} 0 \\ \rho \\ 1 \end{Bmatrix}$$

$$\boldsymbol{\eta}_{i|5} = \boldsymbol{\eta}_{i|\Theta}{}^{-} = \Theta_i^{-} \frac{\partial\left(\alpha_i^5\left(\hat{\mathbf{X}}_i\right)\right)}{\partial\hat{\mathbf{X}}_i} = \Theta_i^{-} \frac{\partial(-M_i + \rho_i N_i)}{\partial\hat{\mathbf{X}}_i} = \Theta_i^{-} \begin{Bmatrix} 0 \\ \rho \\ -1 \end{Bmatrix}, \qquad (5.19)$$

where $\dot{\lambda}_1 = \tilde{s}_{i|n} \geq 0,\ \dot{\lambda}_2 = \tilde{s}_{i|t}{}^{+} \geq 0,\ \dot{\lambda}_3 = \tilde{s}_{i|t}{}^{-} \geq 0,\ \dot{\lambda}_4 = \Theta_i^{+} \geq 0,\ \dot{\lambda}_5 = \Theta_i^{-} \geq 0$ are the plastic multipliers, expressing the amplitude of the relative displacement normal to the interface ($\tilde{s}_{i|n}$), of the relative displacement parallel to the interface in both directions ($\tilde{s}_{i|t}{}^{+}$ and $\tilde{s}_{i|t}{}^{-}$), and of relative clockwise and counterclockwise rotations (Θ_i^{+} and Θ_i^{-}), respectively. Figure 43 allows for better understanding the symbols employed in equation (5.19). In particular, in Figure 43 (left) are schematically illustrated possible sliding mechanisms that, for the assumption of associated flow rule, are accompanied by an interface opening, called interface dilatancy. In Figure 43 (right) are illustrated possible rocking mechanisms, involving again the opening of the interface between the two joined blocks. Notice that the "+" superscript refers to mechanisms related to the edge of the yield locus in the positive T or M semi planes, conversely for the "-" superscript.

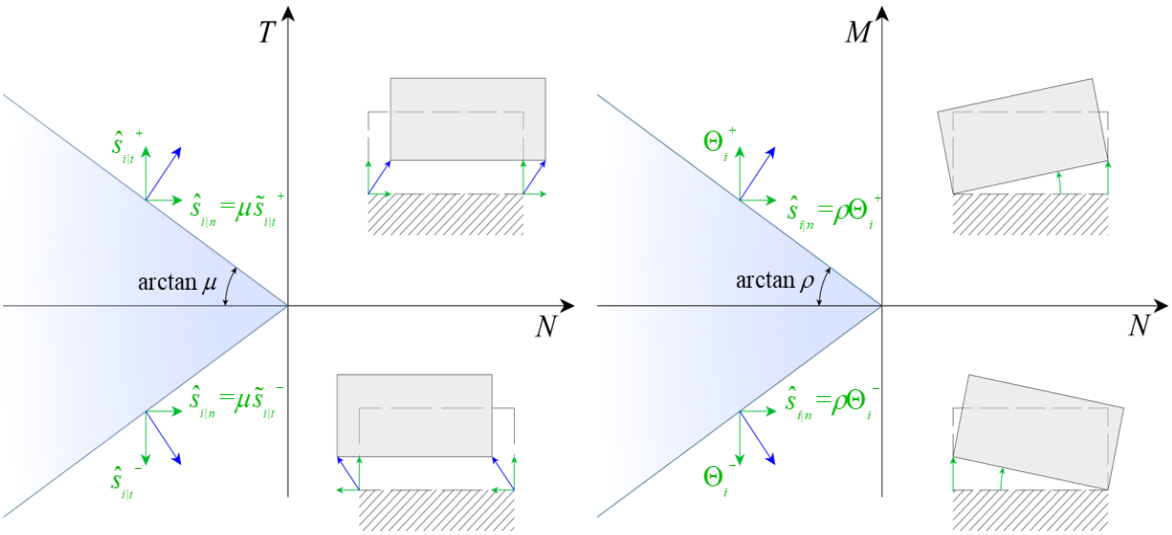

Figure 43: Flow rule corresponding to friction and unilateral constraints.

Therefore, by equation (5.19) the global kinematic vector describing the interface evolution is computed as:

$$\begin{aligned}\boldsymbol{\eta}_i &= \boldsymbol{\eta}_{i|n} + \boldsymbol{\eta}_{i|t}^{+} + \boldsymbol{\eta}_{i|t}^{-} + \boldsymbol{\eta}_{i|\Theta}^{+} + \boldsymbol{\eta}_{i|\Theta}^{-} \\ &= \tilde{s}_{i|n} \begin{Bmatrix} 0 \\ 1 \\ 0 \end{Bmatrix} + \tilde{s}_{i|t}^{+} \begin{Bmatrix} 1 \\ \mu \\ 0 \end{Bmatrix} + \tilde{s}_{i|t}^{-} \begin{Bmatrix} -1 \\ \mu \\ 0 \end{Bmatrix} + \Theta_i^{+} \begin{Bmatrix} 0 \\ \rho \\ 1 \end{Bmatrix} + \Theta_i^{-} \begin{Bmatrix} 0 \\ \rho \\ -1 \end{Bmatrix}.\end{aligned} \tag{5.20}$$

Notice that by following the approach introduced in [140] this evolution law can be rewritten by using the following non-negative kinematic quantities expressing the total interface relative displacements, and thus allowing a clearer mechanical interpretation of the interface evolution from the kinematic point of view:

$$\begin{aligned}\hat{s}_{i|t} &= \tilde{s}_{i|t}^{+} - \tilde{s}_{i|t}^{-} \\ \hat{s}_{i|n} &= \tilde{s}_{i|n} + \mu\left(\tilde{s}_{i|t}^{+} + \tilde{s}_{i|t}^{-}\right) + \rho\left(\Theta_i^{+} + \Theta_i^{-}\right) \\ \Theta_i &= \Theta_i^{+} - \Theta_i^{-}\end{aligned} \tag{5.21}$$

where it results $\left|\hat{s}_{i|t}\right| = \tilde{s}_{i|t}^{+} + \tilde{s}_{i|t}^{-}$ and $\left|\Theta_i\right| = \Theta_i^{+} + \Theta_i^{-}$ as it is shown in Figure 44.

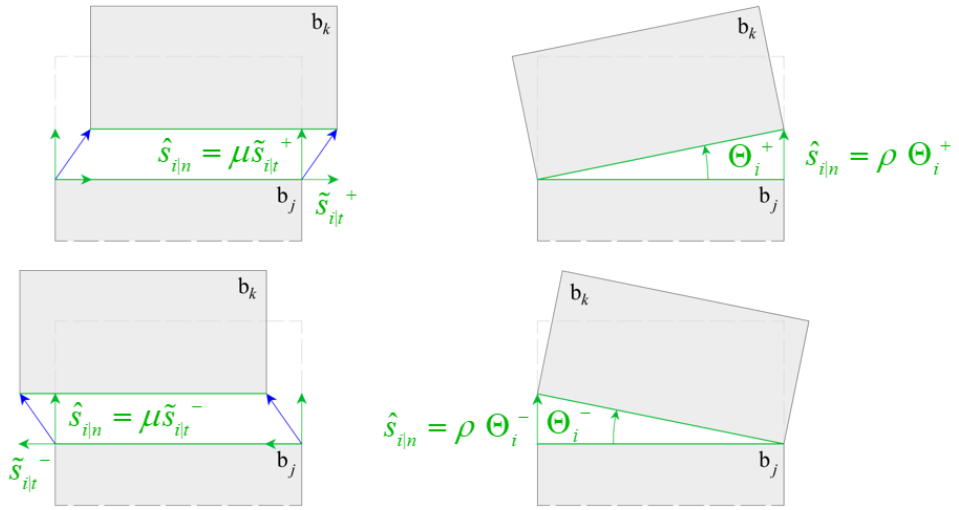

Figure 44: The interface kinematic parameters.

Figure 43 clarifies also why in equation (5.21) the total normal relative displacement of the interface mid-point $\hat{s}_{i|n}$ is obtained by adding to the normal opening $\tilde{s}_{i|n}$ associated to the yield condition (5.16) also the dilatancy and relative rotation effects.

In matrix form, equations (5.20) become:

$$\hat{\mathbf{s}}_i = \mathbf{N}_i \boldsymbol{\beta}_i \qquad \text{with } \boldsymbol{\beta}_i = \begin{Bmatrix} \tilde{s}_{i|n} \\ \tilde{s}_{i|t}^{+} \\ \tilde{s}_{i|t}^{-} \\ \Theta_i^{+} \\ \Theta_i^{-} \end{Bmatrix} \geq \mathbf{0}, \tag{5.22}$$

where $\mathbf{N}_i$ already defined in equation (5.17) is named as the interface evolution law matrix, and $\boldsymbol{\beta}_i$ is named as the contact vector.

As the kinematic evolution of the interface becomes possible only when the stress state is in a yield condition, the following further condition must hold (see also Figure 45):

$$\begin{aligned} \boldsymbol{\beta}_i > \mathbf{0} \quad & \text{if } \boldsymbol{\alpha}_i = \mathbf{0} \\ \boldsymbol{\beta}_i = \mathbf{0} \quad & \text{if } \boldsymbol{\alpha}_i < \mathbf{0} \end{aligned} \qquad \Rightarrow \qquad \boldsymbol{\beta}_i^T \boldsymbol{\alpha}_i = 0 \tag{5.23}$$

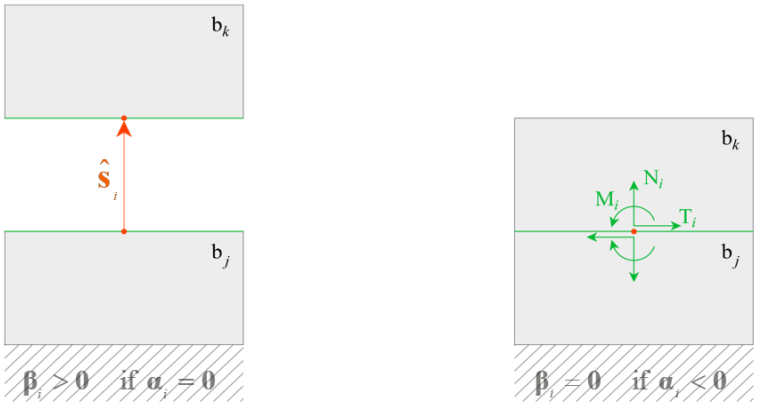

Figure 45: Relation between static and kinematic interface parameters.

In short, equations (5.17), (5.19) and (5.20) can be grouped as follows:

$$\boldsymbol{\alpha}_i \leq \mathbf{0} \qquad \boldsymbol{\beta}_i \geq \mathbf{0} \qquad \boldsymbol{\beta}_i^T \boldsymbol{\alpha}_i = 0 \tag{5.24}$$

having the form of the classical Kuhn-Tucker conditions.

5.6. Limit analysis problem of the structural system

The structural problem of the whole masonry system is recovered by standard assemblage of the equations written for the blocks and for the interfaces. Taking into account local equations (5.10) and (5.22), the kinematic compatibility equation of mechanisms for the whole structure is written as:

$$\hat{\mathbf{B}}\mathbf{U} - \mathbf{N}\boldsymbol{\beta} = \mathbf{0}, \tag{5.25}$$

where the lack of subscript indices denotes that the assemblage operation has been performed. Note that the assemblage of the vectors $\mathbf{d}_i = \left\{ \mathbf{U}_j^T \quad \mathbf{U}_k^T \right\}^T$ results in the global displacement vector $\mathbf{U}$ with dimension $N_{DOF} \times 1$, where $N_{DOF} = 3N_b - N_0$ is the number of degrees of freedom of the system obtained as the difference between the total degrees of freedom of the N_b blocks and the N_0 conditions describing the external constraints applied to the masonry system. In equation (5.25), $\hat{\mathbf{B}}$ is the $3N_\Im \times N_{DOF}$ compatibility matrix of the system, $\mathbf{N}$ is the $3N_\Im \times 5N_\Im$ evolution law matrix and $\boldsymbol{\beta}$ is the $5N_\Im \times 1$ contact vector.

In the analysis, it is assumed the presence of dead and live loads defined by two $N_{DOF} \times 1$ vectors of forces applied in the centroid of each block at the non-constrained degrees of freedom, i.e., $\mathbf{P}_d$ and $\lambda \mathbf{P}_l$, respectively, where λ is a load multiplier and $\mathbf{P}_l$ is a vector

collecting the base values of the live loads. Taking into account equation (5.14), the global equilibrium condition becomes:

$$\hat{\mathbf{B}}^T \hat{\mathbf{X}} - \mathbf{P}_d - \lambda \mathbf{P}_l = \mathbf{0}, \tag{5.26}$$

where $\hat{\mathbf{X}}$ is the $3N_\Im \times 1$ vector of the assembled interface forces.

Moreover, the following Kuhn-Tucker conditions (5.24) for the whole structure have to be satisfied:

$$\boldsymbol{\alpha} \le \mathbf{0} \qquad \boldsymbol{\beta} \ge \mathbf{0} \qquad \boldsymbol{\beta}^T \boldsymbol{\alpha} = 0, \tag{5.27}$$

with

$$\boldsymbol{\alpha} = \mathbf{N}^T \hat{\mathbf{X}}, \tag{5.28}$$

the $5N_\Im \times 1$ interface limit forces vector.

Summarizing, the governing equations of the limit analysis problem, consisting in evaluating the load multiplier λ_c (collapse multiplier) that leads the structure to the collapse, are:

$$\begin{array}{rlr} \hat{\mathbf{B}}\mathbf{U} - \mathbf{N}\boldsymbol{\beta} = \mathbf{0} & \text{kinematics} & 3N_\Im \text{ eqs.} \\ \hat{\mathbf{B}}^T \hat{\mathbf{X}} - \mathbf{P}_d - \lambda \mathbf{P}_l = \mathbf{0} & \text{equilibrium} & N_{DOF} \text{ eqs.} \\ \mathbf{N}^T \hat{\mathbf{X}} \le \mathbf{0} & \text{static admissibility} & 5N_\Im \text{ ineqs.} \\ \boldsymbol{\beta} \ge \mathbf{0} & \text{kinematic evolution} & 5N_\Im \text{ ineqs.} \\ \boldsymbol{\beta}^T \mathbf{N}^T \hat{\mathbf{X}} = 0 & \text{orthogonality condition} & 1 \text{ eq.} \end{array} \tag{5.29}$$

Equations (5.29) represent a linear programming (LP) optimization problem.

Notice that in view of equation (5.17) the conditions (5.27) can be rewritten as:

$$\mathbf{N}^T \hat{\mathbf{X}} \le \mathbf{0} \qquad \boldsymbol{\beta} \ge \mathbf{0} \qquad (\mathbf{N}\boldsymbol{\beta})^T \hat{\mathbf{X}} = 0, \tag{5.30}$$

and, because of equation (5.22), equation (5.29) takes the form:

$$\hat{\mathbf{s}}^T \hat{\mathbf{X}} = 0, \tag{5.31}$$

where $\hat{\mathbf{s}}^T$ is the vector assembling all the interface relative displacements. Moreover, taking into account equations (5.10) and (5.25), condition (5.31) can be rewritten as:

$$\mathbf{U}^T \hat{\mathbf{B}}^T \hat{\mathbf{X}} = 0 \tag{5.32}$$

Generally, two approaches are adopted to solve the limit analysis problem: the kinematic and the static approach.

5.6.1. Kinematic limit analysis

For setting the kinematic limit analysis problem, equation (5.26) can be pre-multiplied by $\mathbf{U}^T$ and reformulated in terms of virtual works as an equilibrium condition between the internal work at the interfaces and the total work done by external forces:

$$\mathbf{U}^T \left(\hat{\mathbf{B}}^T \hat{\mathbf{X}} - \mathbf{P}_d - \lambda \mathbf{P}_l \right) = 0. \tag{5.33}$$

Taking into account equation (5.32), it results that the virtual work of the internal forces must be equal to zero, and therefore equation (5.33) gives:

$$\mathbf{U}^T \left(\mathbf{P}_d + \lambda \mathbf{P}_l \right) = 0. \tag{5.34}$$

Moreover, possible mechanisms of the structure must be associated to positive work produced by the live loads; this requirement can be enforced by introducing the following condition, conveniently normalized since the arbitrariness of the amplitude of possible mechanisms.:

$$\mathbf{U}^T \mathbf{P}_l = 1. \tag{5.35}$$

At this point, the kinematic LP problem can be formulated to find the collapse multiplier as the minimum value for the load multiplier, that is the objective function, expressed in terms of the resisting work of the dead loads subjected to kinematic compatibility, normalized dissipation and admissibility of the interface kinematic conditions, as indicated in equation (5.25) and (5.35):

$$\begin{aligned} &\min_{\mathbf{U},\boldsymbol{\beta}} \; -\mathbf{U}^T \mathbf{P}_d, \\ &\text{s.t.} \quad \hat{\mathbf{B}}\mathbf{U} - \mathbf{N}\boldsymbol{\beta} = \mathbf{0} \\ &\qquad \mathbf{U}^T \mathbf{P}_l - 1 = 0 \\ &\qquad \boldsymbol{\beta} \geq 0 \end{aligned} \tag{5.36}$$

Therefore, the linear programming problem consists in minimizing the objective function $-\mathbf{U}^T \mathbf{P}_d$ with respect to the displacement vector $\mathbf{U}$ and the interface contact kinematic parameters assembled in the vector $\boldsymbol{\beta}$.

5.6.2. Static limit analysis

On the other hand, the static limit analysis problem can be formulated as a LP problem that finds the collapse multiplier as the maximum for the load multiplier with constraints expressing the equilibrium and admissibility of interface local forces as defined in (5.26) and (5.27). This problem may be stated as follows:

$$\begin{aligned} &\max_{\lambda,\hat{\mathbf{X}}} \ \lambda, \\ &\text{s.t.} \quad \hat{\mathbf{B}}^T \hat{\mathbf{X}} - \mathbf{P}_d - \lambda \mathbf{P}_l = \mathbf{0} \\ &\qquad \mathbf{N}^T \hat{\mathbf{X}} \le \mathbf{0} \end{aligned} \tag{5.37}$$

Therefore, the linear programming problem consists in maximizing the objective function, i.e., the load multiplier λ, with respect to the interface forces assembled in the vector $\hat{\mathbf{X}}$. Since a (frictional) associative flow law is assumed, static LP problem formulation is dual to the kinematic LP problem formulation, and the collapse multiplier obtained by solving the two problems is unique.

5.7. Limit analysis problem with non-associative Coulomb friction law

The dilatancy effect associated to the frictional law, consisting in accompanying opening normal relative displacements at the interface related to sliding displacements, whit the relation expressed by means of the friction coefficient μ since the associative flow law assumption, is often considered physically implausible. Indeed, in a masonry structure the interfacial sliding generally occurs without significant opening displacements or at least with opening displacements of small amount.

Thus, for representing this behavior a dilatancy coefficient $\tilde{\mu} \le \mu$ is assumed to rule the normal interface opening as function of the sliding. In particular, it is set $\tilde{\mu} = 0$ when the classical Coulomb friction is considered (no opening displacements accompanying sliding).

The assumption of a value of the dilatancy coefficient $\tilde{\mu}$ different to the frictional one μ leads to the loss of associativity of the evolution law for interface kinematic parameters, which at interface level now takes the form:

$$\hat{\mathbf{s}}_i = \tilde{\mathbf{N}}_i \boldsymbol{\beta}_i \qquad \text{with } \tilde{\mathbf{N}}_i = \begin{bmatrix} 0 & 1 & -1 & 0 & 0 \\ 1 & \tilde{\mu} & \tilde{\mu} & \rho_i & \rho_i \\ 0 & 0 & 0 & 1 & -1 \end{bmatrix}. \tag{5.38}$$

In this case, the governing equations of the limit analysis problem for the masonry system, consisting in evaluating the load multiplier λ_c that leads the structure to the collapse, are:

$$\begin{aligned} \hat{\mathbf{B}}\mathbf{U} - \tilde{\mathbf{N}}\boldsymbol{\beta} &= \mathbf{0} && \text{kinematics} \\ \hat{\mathbf{B}}^T \hat{\mathbf{X}} - \mathbf{P}_d - \lambda \mathbf{P}_l &= \mathbf{0} && \text{equilibrium} \\ \mathbf{N}^T \hat{\mathbf{X}} &\le \mathbf{0} && \text{static admissibility} \\ \boldsymbol{\beta} &\ge \mathbf{0} && \text{kinematic admissibility} \\ \boldsymbol{\beta}^T \mathbf{N}^T \hat{\mathbf{X}} &= 0 && \text{orthogonality condition} \end{aligned} \tag{5.39}$$

along with the normalized dissipation condition (5.35).

Equations (5.39) represent a nonlinear programming (NLP) optimization problem. The determination of the solution of the nonlinear programming problem is significantly more complex than for the linear programming ones. Several procedures have been developed in literature for solving this kind of problem. An interesting approach is the possibility to transform the nonlinear programming in a sequence of linear programming problems.

5.8. Kinematic limit analysis

The kinematic limit analysis formulation in case of non-associative evolution law is recovered pre-multiplying the equilibrium equation (5.39) by $\mathbf{U}^T$ leading to:

$$\mathbf{U}^T \left(\hat{\mathbf{B}}^T \hat{\mathbf{X}} - \mathbf{P}_d - \lambda \mathbf{P}_l \right) = 0. \tag{5.40}$$

It can be remarked that, differently from the associative case, the term $\mathbf{U}^T \hat{\mathbf{B}}^T \hat{\mathbf{X}}$ is no longer equal to zero and, hence, it cannot be eliminated from the equation. Because of equation (5.39), it results:

$$\mathbf{U}^T \hat{\mathbf{B}}^T \hat{\mathbf{X}} = \left(\tilde{\mathbf{N}} \boldsymbol{\beta} \right)^T \hat{\mathbf{X}}, \tag{5.41}$$

which is modified subtracting to the right side of the equation the null quantity $\left(\mathbf{N} \boldsymbol{\beta} \right)^T \hat{\mathbf{X}}$ thus obtaining, in view of (5.39):

$$\mathbf{U}^T \hat{\mathbf{B}}^T \hat{\mathbf{X}} = \boldsymbol{\beta}^T \left(\tilde{\mathbf{N}} - \mathbf{N} \right)^T \hat{\mathbf{X}}, \tag{5.42}$$

so that the objective function to minimize becomes:

$$-\left(\mathbf{U}^T \mathbf{P}_d - \boldsymbol{\beta}^T \left(\tilde{\mathbf{N}} - \mathbf{N} \right)^T \hat{\mathbf{X}} \right). \tag{5.43}$$

Analogously, the kinematic equation $(5.39)_1$ can be written as

$$\hat{\mathbf{B}} \mathbf{U} - \mathbf{N} \boldsymbol{\beta} - \left(\tilde{\mathbf{N}} - \mathbf{N} \right) \boldsymbol{\beta} = \mathbf{0}. \tag{5.44}$$

An iterative procedure is herein proposed to solve the NLP problem as sequence of LP problems. In fact, taking into account equations (5.43) and (5.44), at the typical iteration the kinematic limit analysis problem can be set in the form:

$$\begin{aligned} \min_{\mathbf{U},\boldsymbol{\beta}} \quad & -\left(\mathbf{U}^T \mathbf{P}_d - \left(\boldsymbol{\beta}^* \right)^T \left(\tilde{\mathbf{N}} - \mathbf{N} \right)^T \hat{\mathbf{X}}^* \right), \\ \text{s.t.} \quad & \hat{\mathbf{B}} \mathbf{U} - \mathbf{N} \boldsymbol{\beta} - \left(\tilde{\mathbf{N}} - \mathbf{N} \right) \boldsymbol{\beta}^* = \mathbf{0} \\ & \mathbf{U}^T \mathbf{P}_l - 1 = 0 \\ & \boldsymbol{\beta} \geq 0 \end{aligned} \tag{5.45}$$

where $\hat{\mathbf{X}}^*$ and $\boldsymbol{\beta}^*$ are intended as known quantities computed at the end of previous iteration. In particular, at the typical iteration, as $\hat{\mathbf{X}}^*$ and $\boldsymbol{\beta}^*$ are known, the minimization problem can be written as:

$$\begin{aligned}
&\lambda = \lambda_1 + \lambda_2 \\
&\lambda_2 = \left(\boldsymbol{\beta}^*\right)^T \left(\tilde{\mathbf{N}} - \mathbf{N}\right)^T \hat{\mathbf{X}}^* \\
&\lambda_1 = \min_{\mathbf{U},\boldsymbol{\beta}} \; -\mathbf{U}^T \mathbf{P}_d, \\
&\text{s.t.} \quad \hat{\mathbf{B}}\mathbf{U} - \mathbf{N}\boldsymbol{\beta} - \left(\tilde{\mathbf{N}} - \mathbf{N}\right)\boldsymbol{\beta}^* = \mathbf{0} \\
&\qquad \mathbf{U}^T \mathbf{P}_l - 1 = 0 \\
&\qquad \boldsymbol{\beta} \geq 0
\end{aligned} \tag{5.46}$$

At the first iteration, the linear programming problem is solved to find solution values for $\mathbf{U}$ and $\boldsymbol{\beta}$, setting $\boldsymbol{\beta}^* = \mathbf{0}$ and $\hat{\mathbf{X}}^* = \mathbf{0}$, thus reducing the problem to the form (5.36) characterizing the associative case. Then, at each iteration, for computing λ_1 the vector $\boldsymbol{\beta}^*$ is replaced by quantities determined at the previous iteration, with the iterations stop when the condition:

$$\frac{\left\|\boldsymbol{\beta}^* - \boldsymbol{\beta}\right\|}{\left\|\boldsymbol{\beta}\right\|} + \frac{\left\|\mathbf{U}^* - \mathbf{U}\right\|}{\left\|\mathbf{U}\right\|} \leq t \tag{5.47}$$

is verified, with $\mathbf{U}^*$ the displacement vector determined at the previous iteration and t a prefixed tolerance. At the end of each iteration, the interface stress $\hat{\mathbf{X}}$ is evaluated as the Lagrange multiplier of the kinematic compatibility condition (5.39), written as $\left(\mathbf{U}^T\hat{\mathbf{B}}^T - \left(\boldsymbol{\beta}^*\right)^T \left(\tilde{\mathbf{N}} - \mathbf{N}\right)^T\right)\hat{\mathbf{X}}^* = \mathbf{0}$ and thus regarded as a constraint, and λ_2 is simply computed by (5.46). Finally, the value of λ is determined by (5.46).

5.9. Static limit analysis

Starting from the NLP limit analysis formulation governed by equations (5.39), the static limit analysis problem can be solved by the following iterative procedure of LP optimization:

$$\begin{aligned}
&\max_{\lambda,\hat{\mathbf{X}}} \; \lambda, \\
&\text{s.t.} \quad \hat{\mathbf{B}}^T\hat{\mathbf{X}} - \mathbf{P}_d - \lambda\mathbf{P}_l = \mathbf{0} \\
&\qquad \tilde{\mathbf{N}}^T\hat{\mathbf{X}} - \left(\tilde{\mathbf{N}}^T - \mathbf{N}^T\right)\hat{\mathbf{X}}^* \leq \mathbf{0}
\end{aligned} \tag{5.48}$$

where (5.48) is obtained from (5.39) by adding and subtracting $\tilde{\mathbf{N}}^T\hat{\mathbf{X}}$ and by considering that in the typical iteration $\hat{\mathbf{X}}^*$ is a known interface force vector, equal to the interface force

vector evaluated from the previous iteration. In particular, at the first iteration, the classical associated limit analysis problem of the form (5.37) is solved. Then, the evaluated interface force vector is assumed as $\hat{\mathbf{X}}^*$ for solving the second iteration of the problem in the form (5.48), and so on, the condition:

$$\frac{\left\|\hat{\mathbf{X}}^* - \hat{\mathbf{X}}\right\|}{\left\|\hat{\mathbf{X}}\right\|} \leq t \tag{5.49}$$

is satisfied, being t a prefixed tolerance.

5.10. Limit analysis for reinforced masonry

The safety of masonry structures is mainly related to its geometry and to the loading disposition. In fact, for a given geometrical shape, the masonry structure can be able to carry a certain load in a safe way, even indefinitely increasing the amount of the load. On the other hand, a slight change of the loading distribution may lead the structure to an unsafe state, and also to the collapse. For instance, masonry structures are generally designed to carry vertical loads, but they are significantly vulnerable to horizontal loadings, like that associated to seismic inertia forces. For reducing this vulnerability, masonries are often reinforced introducing suitable measures for increasing their strength.

One of the most adopted strengthening procedures is the application of tensile reinforcements able to constraint the kinematics of the masonry structure, reducing in some way the degrees of freedom of the system, and hence increasing the collapse load. Reinforcements are mainly able to limit the relative displacements of couples of points along one direction, or to constraint the interface opening at one of its two extremities, while generally are incapable of significantly constraining the sliding of interfaces. For this reason, in the following only limitation of the normal relative displacements at the extremities of the interfaces are considered as constraint representing the effect of the reinforcements.

As discussed before, a key purpose of the thesis is to develop a design procedure for appropriate reinforcement interventions capable of suitably increasing the value of the collapse multiplier, without completely constraint the structural system, so that the reinforced masonry construction still may undergo mechanisms. Indeed, this way not only it is possible to limit the extension of the strengthening interventions, but, above all, the typical mechanical behavior of masonry is not violated, and the forces transmitted by the reinforced part of the structure to the remaining part are controlled and substantially reduced.

One possible option consists in using elastic reinforcements able to limit the opening at the extremity of the interface where the reinforcement is applied (see Figure 46a), inhibiting the free formation of a hinge on opposite side of the interface. In this case, the opening of the latter hinge is related to the tensile force exerted in the reinforcement by its elastic stiffness, and the extent of the opening is not relevant for the computation of the collapse load in the framework of limit analysis. Of course, a hinge possibly can be formed on the side where the reinforcement is affixed. An alternative option could be employing elastic-perfectly plastic reinforcements, that give the structure some degree of ductility, since after the yielding force

the reinforcement is able to freely deform, while still allowing the hinge to open without further limitations (see Figure 46b).

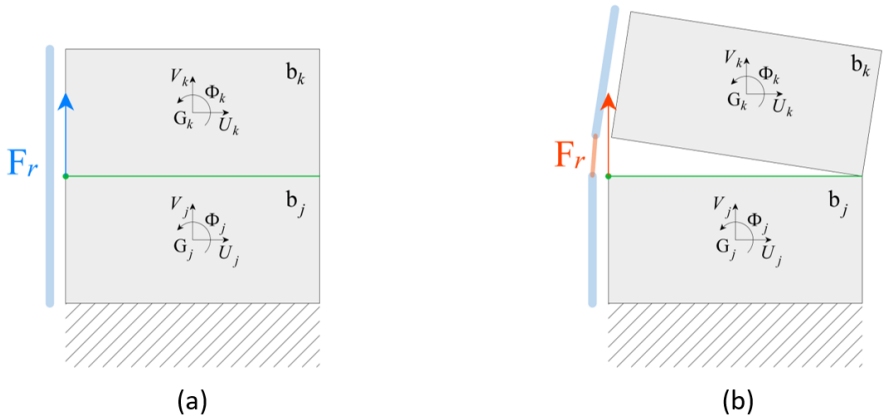

Figure 46: (a) Elastic reinforcement, (b) Plastic reinforcement.

In the framework of limit analysis, the introduction of elastic reinforcements leads a full constraint for the relative displacement, reducing in such a way the degrees of freedom of the structural system. The introduction of elastic-perfectly plastic reinforcement does not limit possible mechanisms, but for mechanisms involving the yielding of the reinforcement the yielding forces correspond to reactive forces that dissipate energy and have to be accounted for in the equilibrium equation.

In the following, the equations ruling the limit analysis problems for the two possible behaviors of the reinforcement are detailed, considering the case of associative evolution law for masonry. The extension to the non-associative case can be developed in a similar way of 5.7.

5.11. Elastic reinforcements

Let the $i-$th interface be considered, joining the blocks b_j and b_k; it is characterized by two extremities, the initial and the final points individuated by the position vectors $\hat{\mathbf{x}}_i^{(1)}$ and $\hat{\mathbf{x}}_i^{(2)}$, respectively.

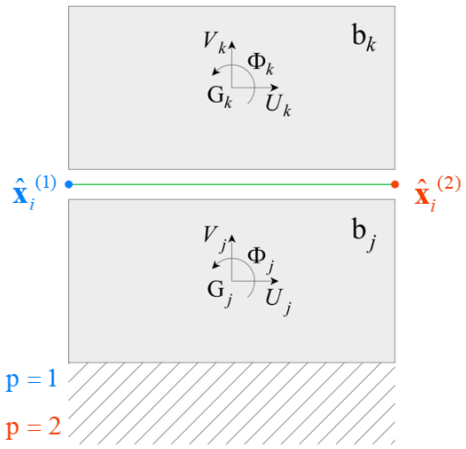

Figure 47: The initial and the final points of the interface to be reinforced.

Taking into account equation (5.7), a reinforcement linking the two blocks along the direction normal to the $i-$th interface at the point $\hat{\mathbf{x}}_i^{(p)}$, with p equal to 1 or 2, introduces a kinematic constraint ruled by the equation:

$$\mathbf{n}_i^T\left[\mathbf{u}_k\left(\hat{\mathbf{x}}_i^{(p)}\right)-\mathbf{u}_j\left(\hat{\mathbf{x}}_i^{(p)}\right)\right]=0, \tag{5.50}$$

or, explicitly, in view of (5.9).

$$\frac{1}{\ell_i}\begin{Bmatrix}-\hat{y}_i^{(2)}+\hat{y}_i^{(1)}\\ \hat{x}_i^{(2)}-\hat{x}_i^{(1)}\end{Bmatrix}^T\begin{bmatrix}-1 & 0 & \hat{y}_i^{(p)}-y_j & 1 & 0 & -\left(\hat{y}_i^{(p)}-y_k\right)\\ 0 & -1 & -\left(\hat{x}_i^{(p)}-x_j\right) & 0 & 1 & \hat{x}_i^{(p)}-x_k\end{bmatrix}\begin{Bmatrix}U_j\\ V_j\\ \Phi_j\\ U_k\\ V_k\\ \Phi_k\end{Bmatrix}=0. \tag{5.51}$$

The presence of a kinematic constraint of type (5.50) is associated to a reactive force at the point $\hat{\mathbf{x}}_i^{(p)}$ in the direction orthogonal to the interface.

Introducing N_R reinforcements, N_R constraint equations of type (5.51) have to be imposed, that can be written as:

$$\mathbf{C}\,\mathbf{U}=\mathbf{0} \tag{5.52}$$

where $\mathbf{C}$ is the constraints $N_R \times N_{DOF}$ matrix. The N_R reactive forces associated to the introduced reinforcements can be organized in a vector $\mathbf{F}_r$ satisfying the classical frictionless bilateral condition:

$$\left(\mathbf{C}\,\mathbf{U}\right)^T \mathbf{F}_r = 0 \tag{5.53}$$

To enforce the equilibrium, the force vector $\mathbf{F}_r$ has to be suitably accounted for. In particular, for referring the reactive forces to the centroid of the blocks, (5.53) shows that the work-conjugated entity to the centroid displacement vector $\mathbf{U}$ is $\mathbf{C}^T\mathbf{F}_r$. Therefore, the limit analysis problem (5.29), in presence of elastic reinforcements, takes the form:

$$\begin{aligned}
\hat{\mathbf{B}}\mathbf{U} - \mathbf{N}\boldsymbol{\beta} &= \mathbf{0} && \text{kinematics} && 3N_{\mathfrak{Z}} \text{ eqs.} \\
\mathbf{C}\,\mathbf{U} &= \mathbf{0} && \text{reinforcements constraints} && N_R \text{ eqs.} \\
\hat{\mathbf{B}}^T\hat{\mathbf{X}} - \mathbf{P}_d - \lambda\mathbf{P}_l + \mathbf{C}^T\mathbf{F}_r &= \mathbf{0} && \text{equilibrium} && N_{DOF} \text{ eqs.} \\
\mathbf{N}^T\hat{\mathbf{X}} &\le \mathbf{0} && \text{static admissibility} && 5N_{\mathfrak{Z}} \text{ ineqs..} \\
\boldsymbol{\beta} &\ge \mathbf{0} && \text{kinematic evolution} && 5N_{\mathfrak{Z}} \text{ ineqs.} \\
\boldsymbol{\beta}^T\mathbf{N}^T\hat{\mathbf{X}} &= 0 && \text{orthogonality condition} && 1 \text{ eq.} \\
\left(\mathbf{C}\,\mathbf{U}\right)^T \mathbf{F}_r &= 0 && \text{frictionless and bilateral constraint} && 1 \text{ eq.}
\end{aligned} \tag{5.54}$$

5.11.1. Kinematic limit analysis

In view of limit analysis equations (5.54), the formulation of the kinematic limit analysis for the elastically reinforced system can be formulated as the following LP problem:

$$\begin{aligned}
\min_{\mathbf{U},\boldsymbol{\beta}} \quad & -\mathbf{U}^T\mathbf{P}_d, \\
\text{s.t.} \quad & \hat{\mathbf{B}}\mathbf{U} - \mathbf{N}\boldsymbol{\beta} = \mathbf{0} \\
& \mathbf{C}\,\mathbf{U} = \mathbf{0} \\
& \mathbf{U}^T\mathbf{P}_l - 1 = 0 \\
& \boldsymbol{\beta} \ge 0
\end{aligned} \tag{5.55}$$

The linear programming problem consists in minimizing the objective function with respect to the displacement vector $\mathbf{U}$ and the interface contact kinematic parameters assembled in the vector $\boldsymbol{\beta}$.

5.11.2. Static limit analysis

Analogously, the static limit analysis for the elastically reinforced system takes the form of the following LP problem:

$$\begin{aligned} &\max_{\lambda,\hat{\mathbf{X}},\mathbf{F}_r} \ \lambda, \\ &\text{s.t.} \quad \hat{\mathbf{B}}^T \hat{\mathbf{X}} - \mathbf{P}_d - \lambda \mathbf{P}_l + \mathbf{C}^T \mathbf{F}_r = \mathbf{0} \\ &\qquad \mathbf{N}^T \hat{\mathbf{X}} \le \mathbf{0} \end{aligned} \tag{5.56}$$

The linear programming problem consists in maximizing the objective function, i.e. the loading multiplier λ, with respect to the interface forces assembled in the vector $\hat{\mathbf{X}}$ and the reactive force vector $\mathbf{F}_r$.

5.12. Elastic-perfectly plastic reinforcements

It is now assumed that the reinforcement is characterized by an elastic-perfectly plastic response. In such a case, the kinematics of the interface point where the reinforcement is placed, is no more constrained in limit conditions (yielding of the reinforcement), as the opening of a plastic hinge at the reinforced interface is possible, but reactive force arise whose value F_y represents the yield force for the reinforcement. The latter forces have to be considered in the equilibrium equation.

Thus, taking into account what discussed in Section 5.11 about the expression of reaction forces exerted by the reinforcement, the equations governing the limit analysis problem become:

$$\begin{array}{rll} \hat{\mathbf{B}}\mathbf{U} - \mathbf{N}\boldsymbol{\beta} = \mathbf{0} & \text{kinematics} & 3N_{\mathfrak{Z}} \text{ eqs.} \\ \hat{\mathbf{B}}^T \hat{\mathbf{X}} - \mathbf{P}_d - \lambda \mathbf{P}_l + \mathbf{C}^T \mathbf{F}_r = \mathbf{0} & \text{equilibrium} & N_{DOF} \text{ eqs.} \\ \mathbf{F}_r - F_y \mathbf{1} = \mathbf{0} & \text{plastic yield condition} & N_R \text{ eqs.} \\ \mathbf{N}^T \hat{\mathbf{X}} \le \mathbf{0} & \text{static admissibility} & 5N_{\mathfrak{Z}} \text{ ineqs.} \\ \boldsymbol{\beta} \ge \mathbf{0} & \text{kinematic evolution} & 5N_{\mathfrak{Z}} \text{ ineqs.} \\ \boldsymbol{\beta}^T \mathbf{N}^T \hat{\mathbf{X}} = 0 & \text{orthogonality condition} & 1 \text{ eq.} \end{array} \tag{5.57}$$

5.12.1. Kinematic limit analysis

Starting from the limit analysis formulation (5.57), the kinematic limit analysis for the system reinforced with elastic-perfectly plastic reinforcements can be set in view of (5.32) and (5.35) as the following LP problem:

$$\begin{aligned} \min_{\mathbf{U},\boldsymbol{\beta}} \quad & -\mathbf{U}^T\left(\mathbf{P}_d - \mathbf{C}^T\mathbf{F}_R\right), \\ \text{s.t.} \quad & \hat{\mathbf{B}}\mathbf{U} - \mathbf{N}\boldsymbol{\beta} = \mathbf{0} \\ & \mathbf{U}^T\mathbf{P}_l - 1 = 0 \\ & \mathbf{F}_r - F_y\mathbf{1} = \mathbf{0} \\ & \boldsymbol{\beta} \geq 0 \end{aligned} \tag{5.58}$$

The linear programming problem consists in minimizing the objective function with respect to the displacement vector $\mathbf{U}$ and the interface contact kinematic parameters assembled in the vector $\boldsymbol{\beta}$.

Notice that according to mechanism found as the solution found by the optimization process, it is possible that the reinforcement applied to some interfaces does not yield: the reinforced interfaces activated in the mechanism are only that where work is dissipated.

5.12.2. Static limit analysis

Analogously, the static limit analysis problem for the reinforced system takes the form:

$$\begin{aligned} \max_{\lambda,\hat{\mathbf{X}}} \quad & \lambda, \\ \text{s.t.} \quad & \hat{\mathbf{B}}^T\hat{\mathbf{X}} - \mathbf{P}_d - \lambda\mathbf{P}_l + \mathbf{C}^T\mathbf{F}_r = \mathbf{0} \\ & \mathbf{N}^T\hat{\mathbf{X}} \leq \mathbf{0} \\ & \mathbf{F}_r - F_y\mathbf{1} = \mathbf{0} \end{aligned} \tag{5.59}$$

The linear programming problem consists in maximizing the objective function, i.e., the load multiplier λ, with respect to the interface forces assembled in the vector $\hat{\mathbf{X}}$.

5.13. Notation

This chapter presents a comprehensive summary of the notation used in the analytical development to aid in the understanding and interpretation of the meanings and definitions associated with the symbols introduced in the previous section.

N_b	total number of two-dimensional rigid blocks of the system,
$N_\Im$	total number of rough interfaces mutually connecting the rigid blocks,
G_k	centroid of the k- th block,
$\mathbf{x}_k$	centroid position vector of the k- th rigid block b_k,
b_k	k- th rigid block,
$\mathbf{U}_k$	Lagrangian parameters vector defined at G_k,
U_k	x- component of the displacement of the centroid G_k,
V_k	y- component of the displacement of the centroid G_k,
Φ_k	rotation angle of b_k around the centroid G_k,
$\mathbf{x}$	position vector of the typical point of b_k,
$\mathbf{u}_k(\mathbf{x})$	displacement vector of the typical point of b_k,
$\mathbf{e}$	unit vector orthogonal to the $x-y$ plane,
$\mathbf{B}_k$	kinematic matrix of b_k,
$\overline{\mathbf{x}}_i$	position vector of the midpoint of the i- th interface,
$\hat{\mathbf{x}}_i$	position vector of the typical point on the i- th interface,
$\overline{\mathbf{s}}_i$	interfacial relative displacement referred to the interface midpoint $\overline{\mathbf{x}}_i$,
$\overline{\mathbf{B}}_i$	interface compatibility matrix,
$\mathbf{d}_i$	Lagrangian parameters of the two joined blocks,
$\boldsymbol{\eta}_i$	kinematically admissible relative displacement at the i- th interface
θ_i	inclination angle of the i- th interface,
$\mathbf{t}_i$	tangent unit vector at the i- th interface,
$\mathbf{n}_i$	leftward normal unit vector at the i- th interface,
$\mathbf{R}_i$	rotation matrix from global to local coordinate system,
ℓ_i	length the i- th interface,
$\hat{\mathbf{s}}_i$	relative displacement jumps at the i- th interface in the local coordinate system,
$\hat{s}_{i\|t}$	tangent component of the relative displacement at the interface midpoint $\overline{\mathbf{x}}_i$,
$\hat{s}_{i\|n}$	normal component of the relative displacement at the interface midpoint $\overline{\mathbf{x}}_i$,
Θ_i	relative rotation between the blocks $\mathbf{b}_k$ and $\mathbf{b}_j$,
$\hat{\boldsymbol{\eta}}_i$	relative displacement vector in the local reference system at the i- th interface,
ξ_i	abscissa of $\hat{\mathbf{x}}_i$ starting from $\overline{\mathbf{x}}_i$ along the tangent direction,

$\hat{\mathbf{X}}_i$ vector of the i- th interface generalized forces in the local coordinate system,

T_i shear contact force of the i- th interface,

N_i normal contact force of the i- th interface,

M_i bending moment of the i- th interface,

$\mathbf{F}_k^{(i)}$ vector of the i- th interface generalized forces in the global coordinate system,

$F_k^{(i)}$ component of the interface forces along the x- direction,

$Q_k^{(i)}$ component of the interface forces along the y- direction,

$Y_k^{(i)}$ moment of the interface forces around the centroid at G_k ,

$\mathbf{D}_i$ vector collecting the interface forces in the global reference system,

$\hat{\mathbf{B}}_i^T$ equilibrium operator for the i- th interface,

μ friction coefficient,

ρ_i half of the interface length,

$\boldsymbol{\alpha}_i$ interface limit forces vector,

$\tilde{s}_{i|n}$ normal opening associated to the yield condition,

$\tilde{s}_{i|t}^{+}$ non-negative kinematic quantity for sliding related to the positive semi plane,

$\tilde{s}_{i|t}^{-}$ non-negative kinematic quantity for sliding related to the negative semi plane,

Θ_i^{+} non-negative kinematic quantity for rotation related to the positive semi plane,

Θ_i^{-} non-negative kinematic quantity for rotation related to the negative semi plane,

$\boldsymbol{\beta}_i$ contact vector,

$\mathbf{N}_i$ interface evolution law matrix,

$\boldsymbol{\beta}$ contact vector,

$\mathbf{U}$ global displacement vector,

$\hat{\mathbf{B}}$ compatibility matrix of the system,

$\mathbf{N}$ evolution law matrix,

$\mathbf{P}_d$ vector of dead loads applied in the centroid of each block,

$\mathbf{P}_l$ vector of live loads applied in the centroid of each block,

λ load multiplier,

$\hat{\mathbf{X}}$ vector of the assembled interface forces,

$\boldsymbol{\alpha}$ interface limit forces vector,

λ_c collapse multiplier,

$\tilde{\mu}$ dilatancy coefficient,

$\tilde{\mathbf{N}}_i$ non-associative evolution law matrix,

$\hat{\mathbf{X}}^*$ vector of the assembled interface forces of the previous iteration,

$\boldsymbol{\beta}^*$ contact vector of the previous iteration,

λ_1 load multiplier component depending on the external work done by $\mathbf{P}_d$,

λ_2 load multiplier component depending on the internal work,

$\mathbf{U}^*$ displacement vector of the previous iteration,

t prefixed tolerance,

$\hat{\mathbf{x}}_i^{(1)}$ position vector of the initial interface point,

$\hat{\mathbf{x}}_i^{(2)}$ position vector of the final interface point,

$\hat{\mathbf{x}}_i^{(p)}$ position vector of the point where the reinforcement is applied,

N_R total number of constraint equations for reinforcements,

$\mathbf{C}$ constraints matrix,

$\mathbf{F}_r$ vector of the reactive forces associated to the reinforcements,

F_y yield force for the reinforcement.

Chapter 6
Numerical simulations

In the upcoming sections, a comprehensive evaluation of the effectiveness of the proposed optimization algorithm is performed through numerical simulations for both unreinforced and reinforced masonry block systems.

The initial focus will be on unreinforced masonry block systems, with small-scale problems discussed in Sections 6.1 and 6.2 to assess the approach. The efficiency of the algorithm is then further tested by analyzing more complex structures in Sections 6.3 and 6.4 .

After this validation, the optimization algorithm implemented in Section 5.10 will be employed to define the optimal reinforcement for a masonry arches. The aim is to enhance the overall safety of a masonry arch while preserving the original four-hinge collapse mechanism through the exploration of appropriate reinforcement configurations.

In Section 6.5.1, an ideal "elastic" reinforcement, with indefinitely elastic behavior and no possible failure, will be considered as strengthening material for the arch. This way, an initial assessment of the response of the reinforced arch is performed, identifying the optimal location for partial reinforcements. In Section 6.5.2 an elastic-perfectly plastic reinforcement will be introduced to preserve the four-hinge collapse mechanism. By considering "plastic behavior", the design will account for the possibility of localized reinforcement failure to occur and force redistribution, ensuring the structural integrity of the arch.

6.1. Numerical validation: single dry masonry rigid block

In the present section, the validation of the MATLAB code implementing the optimization algorithm to address the kinematic limit analysis problem will be discussed.

To this aim, a basic 2D model consisting of a single masonry block, modeled as a rigid body, and characterized by regular geometry (rectangle) and a density $\gamma = 2000$ kg/m^3 is considered. The block is connected at the base to a fixed plane through a unilateral and frictional interface with a variable friction coefficient μ (0.5, 0.75 or 1). For the subsequent analysis, as the failure criterium for the interface both the Coulomb criterium with associative flow rule (and, therefore, with the resulting dilatancy associated to the sliding) and a non-associative Coulomb criterium (sliding without dilatancy) have been considered. The block is subjected to a load condition consisting in the self-weight $\mathbf{P}_d$ and in a horizontal load $\mathbf{P}_l$ proportional to the load multiplier λ, applied at the centroid. As depicted in Figure 48, the horizontal load $\mathbf{P}_l$ is set equal to the self-weight $\mathbf{P}_d$ to investigate the effect of the friction coefficient increment on the collapse load multiplier value and related mechanism.

The obtained collapse load multiplier values exhibit no difference between the associative and non-associative cases. Moreover, in the non-associative case, the collapse mechanism closely resembles the one expected in the absence of dilatancy. Thus, given the observed negligible difference in the collapse load multiplier values, only the non-associative case will be considered in the following analyses.

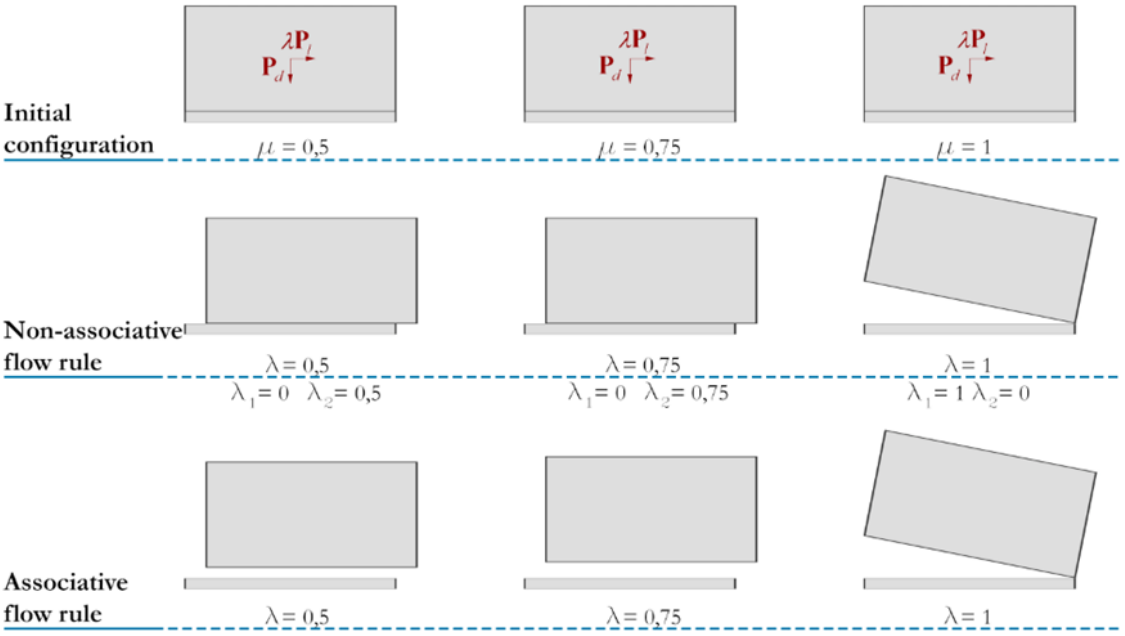

Figure 48: Sliding mechanism with associative and non-associative flow rule with horizontal load equal to the self-weight.

The next part of this section aims to assess the influence of the height-to-base ratio of the block on both the collapse mechanism and the related collapse load multiplier values. To validate the proposed numerical approach, the obtained results are compared to the results analytically determined by De Felice [141]. As depicted in Figure 49, the block is subjected to a load condition consisting in the self-weight $\mathbf{P}_d$, applied at the centroid, and in a horizontal load $\mathbf{P}_l$ at the right top vertex, proportional to the load multiplier λ. Additionally, an overload $\mathbf{P}_q$ is applied at the top of the block, such that $\mathbf{P}_q$ passes through the centroid. For this purpose, the friction value $\mu = 0.5$ and the base width $b = 1$ m have been fixed, while the height h is varied, thus obtaining different height-to-base ratios.

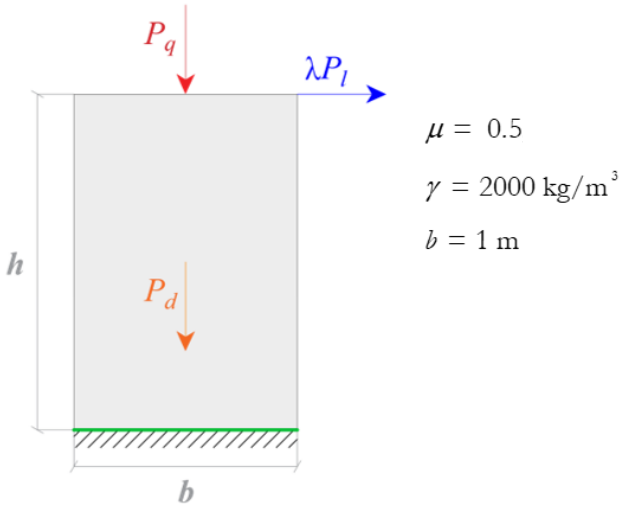

Figure 49: Single dry masonry rigid block model with loading and constraint conditions.

When the height-to-base ratio is less than a certain value, the block is classified as *squat*, and the collapse takes place through a sliding mechanism. Conversely, when the height-to-base ratio is greater, the wall can be classified as *slender*, and collapse by overturning occurs. It is useful to plot the collapse load force $\mathbf{P}_l$ as a function of the height-to-base ratio. More specifically, as depicted in Figure 50, it is found that when the height-to-base ratio is less than 1, sliding is the collapse mechanism, whereas when the height-to-base ratio exceeds 1, the blocks collapses through overturning.

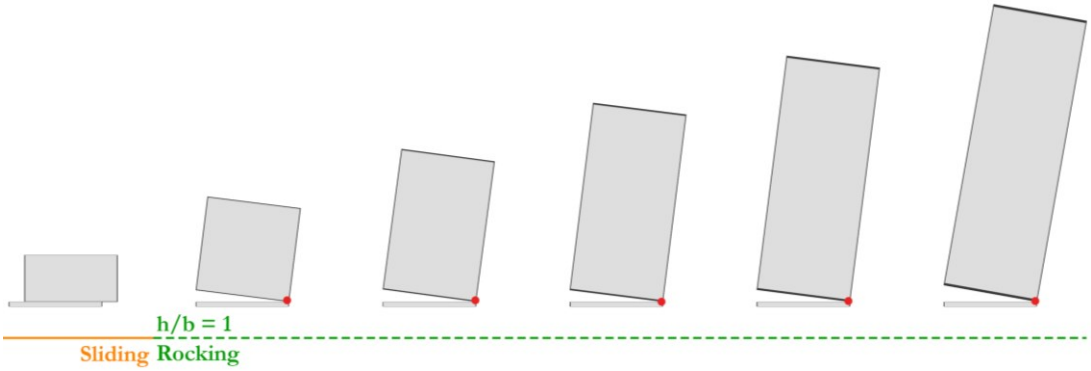

Figure 50: Relation between height-to-base ratio and the collapse mechanism.

Moreover, when the height-to-base ratio is less than 1 an increasing force is necessary to induce sliding as h increases, because the mass of the object to be displaced increases with the height. On the other hand, as shown in Figure 51, with an increasing value of the overload $\mathbf{P}_q$ from zero to 2000 kg, the load collapse multiplier that activates an overturning mechanism increases. In particular, when the block is slender, the force required to trigger overturning remains constant if the overload $\mathbf{P}_q$ is zero or decreases as the height increases for $\mathbf{P}_q$ different from zero.

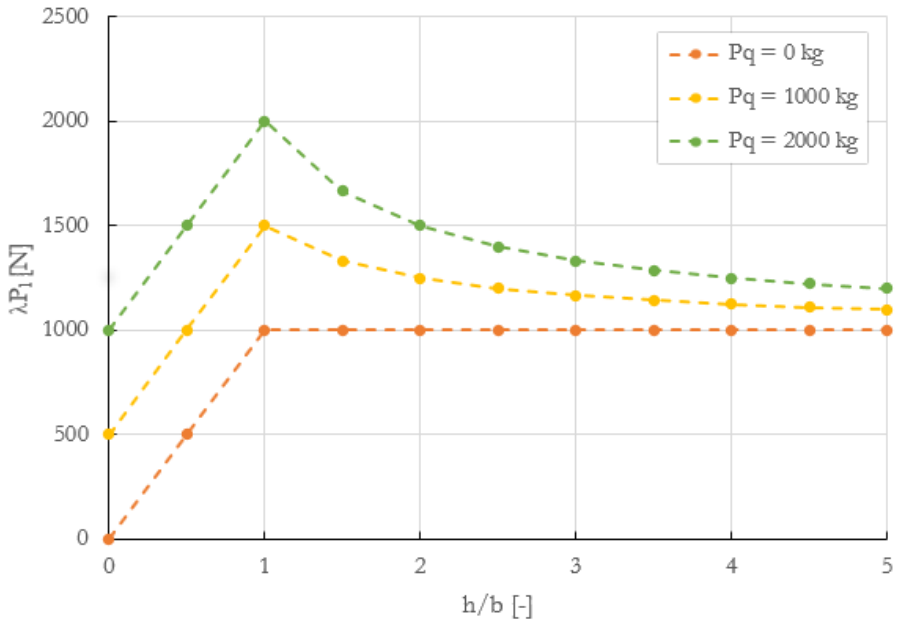

Figure 51: Relation between the height-to-base ration and the collapse load in presence of an overload with different values.

In this latter case, the force required for overturning the block is always greater than that required in the absence of overload. Therefore, is possible to claim that the overload increases the stability of the block.

6.2. A second small-scale problem: three blocks mutually connected through rough interfaces.

In this section, the effectiveness of the optimization approach formulated to address the kinematic limit analysis problem is evaluated with reference to a second small-scale model. As depicted in Figure 52, a dry masonry system is composed of three two-dimensional rigid blocks identical in size and shape, and mutually connected through unilateral and zero-thickness rough interfaces. The base of the first block is fixed to the plane. In particular, the shear failure of the interfaces is modeled by a Coulomb criterium with non-associative flow rule (no dilatancy is assumed). The blocks are made of stone with density $\gamma = 1700$ kg/m^3, while friction coefficient at interface is equal to 1. The load condition on the structure includes self-weight $\mathbf{P}_d$ and a horizontal load $\mathbf{P}_l$, both applied at the centroid of each block. The horizontal load $\mathbf{P}_l$ is proportional to the load multiplier λ.

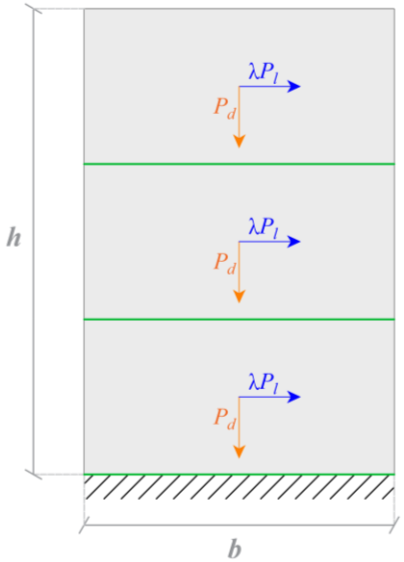

Figure 52: geometrical and material features of the three two-dimensional rigid blocks

In order to assess the effectiveness of the optimization algorithm adopted for addressing the kinematic limit analysis problem with a non-associative flow rule, the influence of the geometric features of the model is studied by varying the height-to-base ratio of the blocks. This affect both the collapse mechanism and the magnitude of the collapse load multiplier λ.

As depicted in Figure 53, an increase in the height-to-base ratio results in a change in the collapse mechanism, with a reduction in the magnitude of the collapse load multiplier. In particular, when the collapse mechanism is of sliding type, the collapse load multiplier is also influenced by the value of the friction coefficient. On the other hand, when the collapse mechanism is of rocking type, it turns out that the collapse load multiplier depends only on the base-to-height ratio.

In the following two cases, shown in Figure 54 and Figure 55, additional loading conditions are introduced by varying the value of the horizontal force with the height. The horizontal load $\mathbf{P}_l$ is decreasing (Figure 54) or increasing (Figure 55) with the height for each block.

As evidenced in Figure 54, when the horizontal load $\mathbf{P}_l$ decreases with the height and the friction coefficient is sufficiently low ($\mu = 0.5$), the collapse mechanism is characterized by sliding for higher values of the height-to-base ratio, as evident when comparing Figure 53 and Figure 54. In fact, under this loading condition, the load collapse multiplier, both in presence of sliding and rocking mechanism, is greater than the previous case where the horizontal load $\mathbf{P}_l$ was uniformly applied to each block.

In the case where the horizontal load increases with height (Figure 55), the collapse mechanism involves sliding of the top block, and the load multiplier is determined by the height of the single block rather than the height-to-base ratio, if the friction coefficient is not sufficiently high, as demonstrated in Figure 53 and Figure 55. Essentially, in this scenario, the trend of the collapse multiplier value for the case with decreasing load and the uniform load remains comparable.

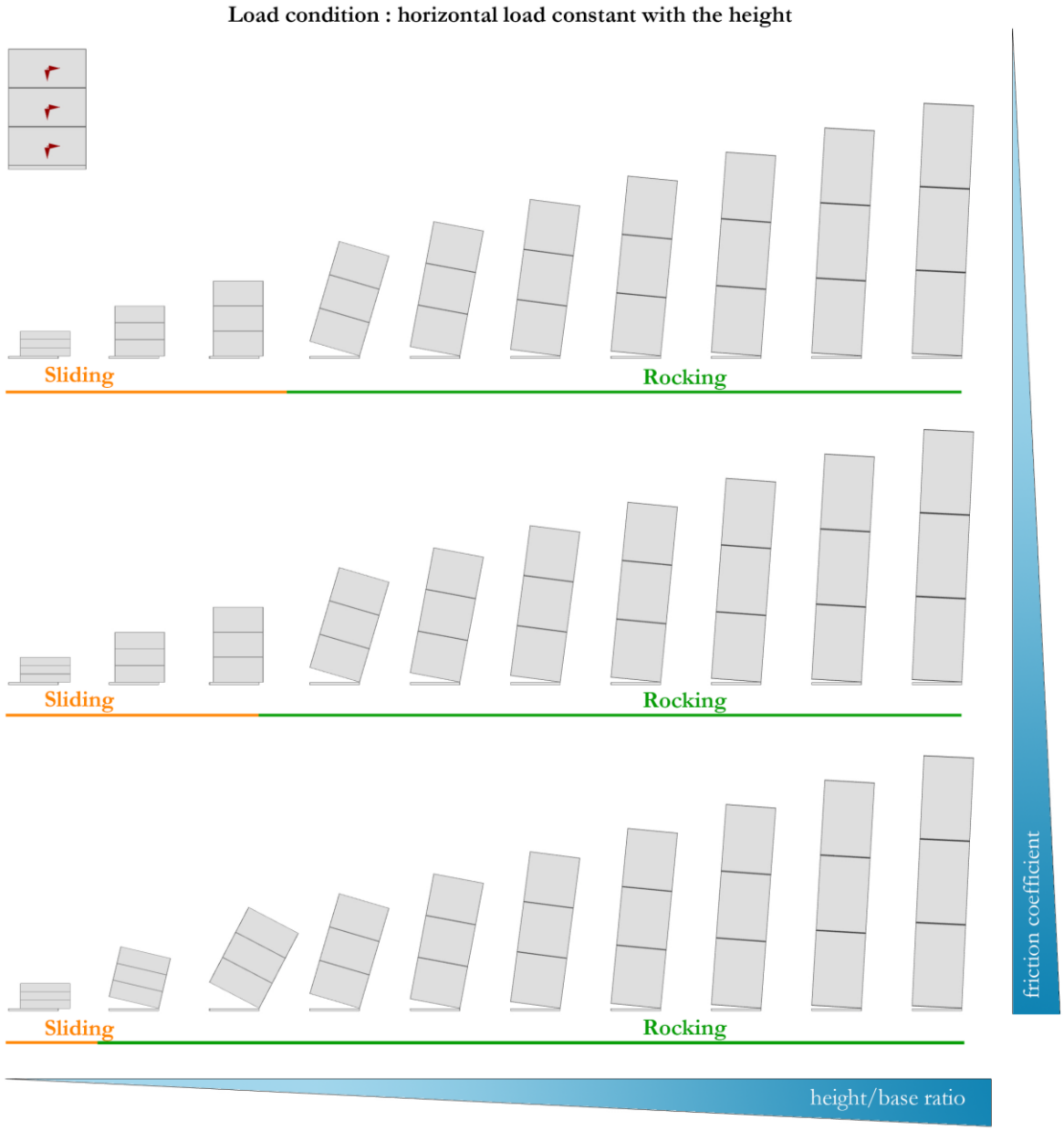

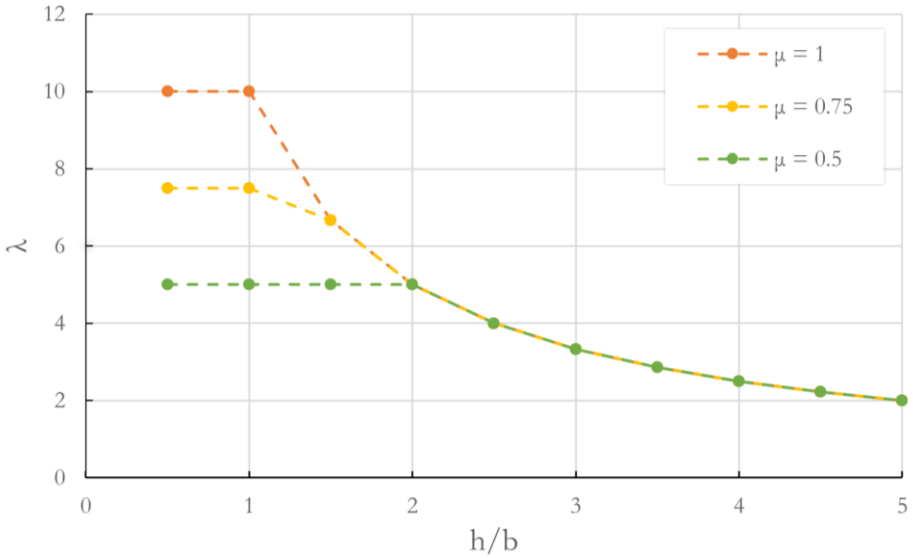

Figure 53: Collapse mechanism modes (up) and load multiplier trend (down) by varying the heigh-to-base ratio in the case of horizontal load constant with height.

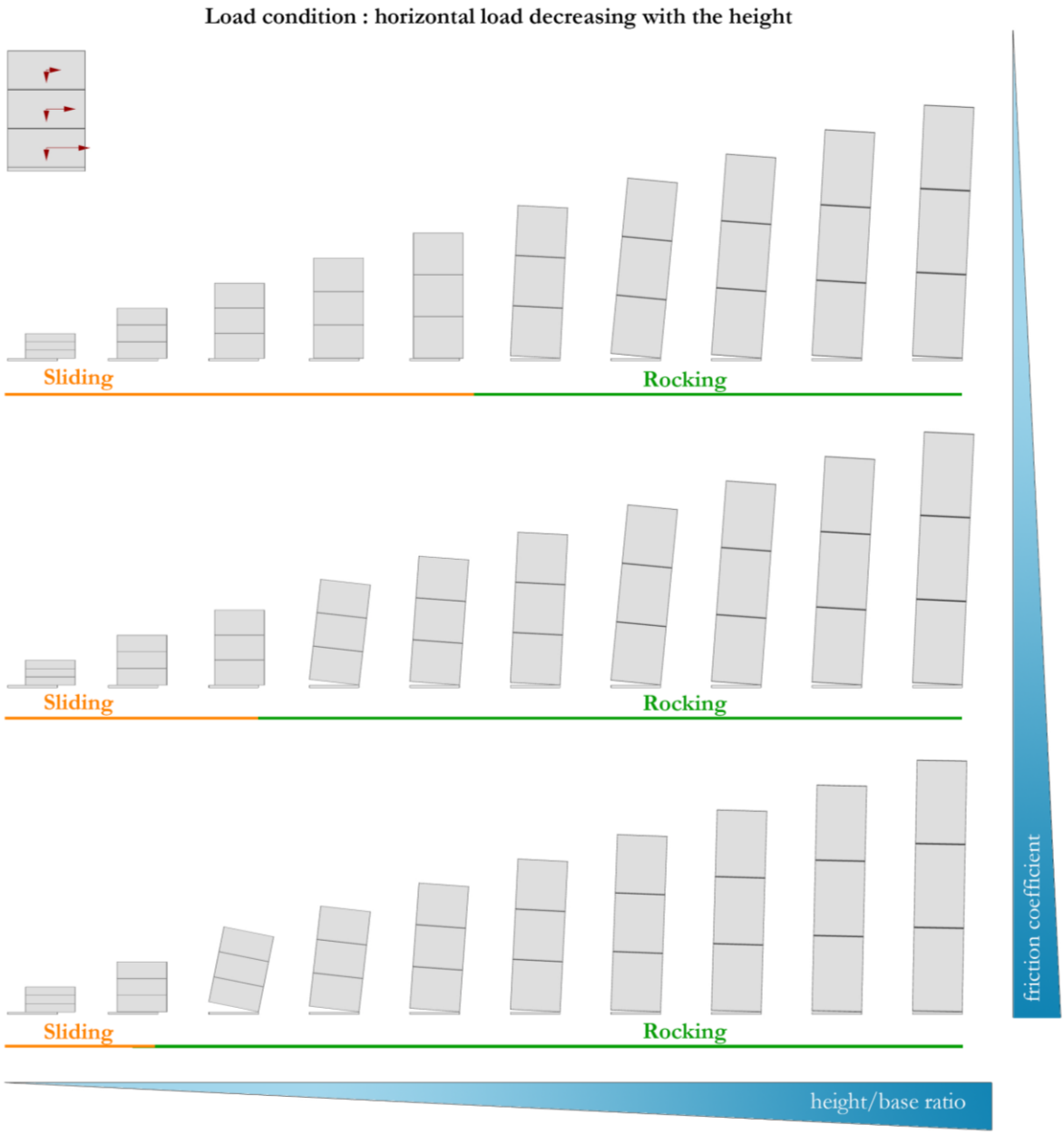

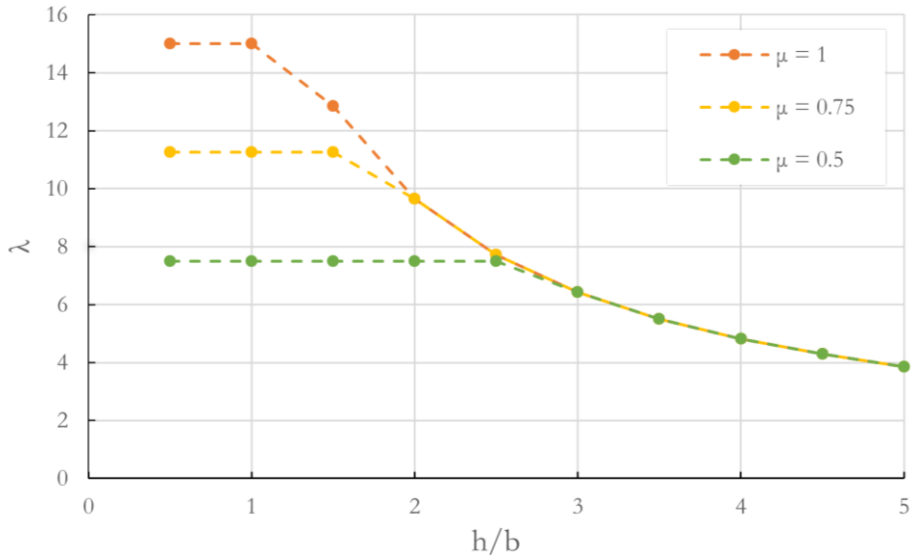

Figure 54: Collapse mechanism modes (up) and load multiplier trend (down) by varying the heigh-to-base ratio in the case of horizontal load decreasing with height.

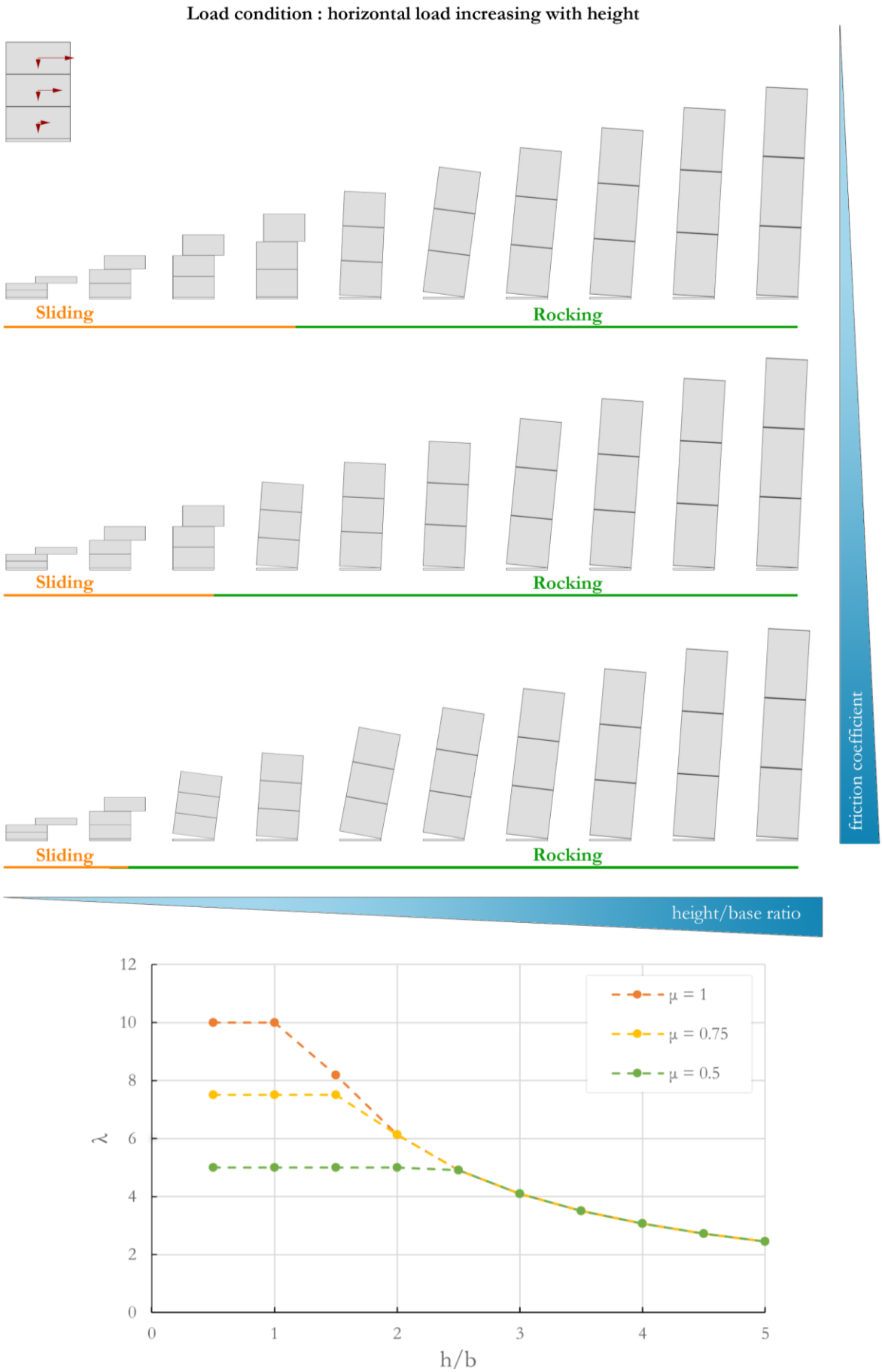

Figure 55: *Collapse mechanism modes (up) and load multiplier trend (down) by varying the heigh-to-base ratio in the case of horizontal load increasing with height.*

6.3. Trilite

As observed in previous sections, the collapse mode of small-scale models changes from a sliding to overturning mechanism at a certain value of the height-to-base ratio. In this section, the influence of both the height-to-base ratio and the friction coefficient on the collapse mode is analyzed in the case of a *trilite* by varying the geometrical proportions of the piers.

The *trilite* is discretized into two-dimensional rigid block made of stone with density of $\gamma = 2000$ kg/m^3, connected through zero-thickness rough interfaces. In particular, the piers are connected at the base and with the lintel through unilateral and frictional interfaces with a variable friction coefficient μ (0.5, 0.75 or 1.2). Geometrical features are indicated in Figure 56. The load conditions consist of the self-weight $\mathbf{P}_d$ and a horizontal load $\mathbf{P}_l$ proportional to the load multiplier λ.

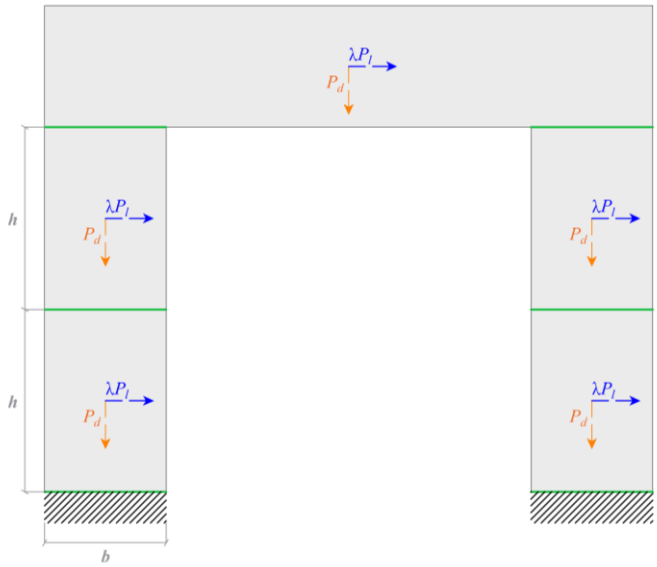

Figure 56: Geometrical properties of the trilite model.

Assuming the same load condition, friction and height-to-base ratio are varied in order to evaluate their effect on the load multiplier value and collapse mode mechanism. Outcomes are reported in the following Figure 57. As it is possible to observe, if the value of both the friction coefficient and the height-to-base ratio is high, the *trilite* collapses with the overturning of the piers. On the other hand, if the friction coefficient or the height-to-base ratio is not sufficiently high, the mechanism occurring is characterized by the coexistence of sliding and rocking. As depicted in Figure 57, the horizontal force applied at the centroid of the lintel generates a bending moment. A consequence of this is that the compression stress on the left pier is reduced by the combination with the normal force due to the bending moment and a mixed mechanism of sliding and rocking occurs. For the same reason, the normal force on the right pier increases leading to the overturning of the pier.

Moreover, in the cases with a lower friction coefficient (μ equal to 0.5 or 0.75), a sliding mechanism occurs even if the height-to-base ratio is high when compared to the same cases where friction coefficient is higher. Further evidence of this can be observed in the graph in Figure 58, where the values of the load multiplier are higher as the value of the friction coefficient and the height-to-base ratio grow, considering that an increment in the height-to-base ratio results in an increase in the weight of the piers and thus in the stability of the *trilite*.

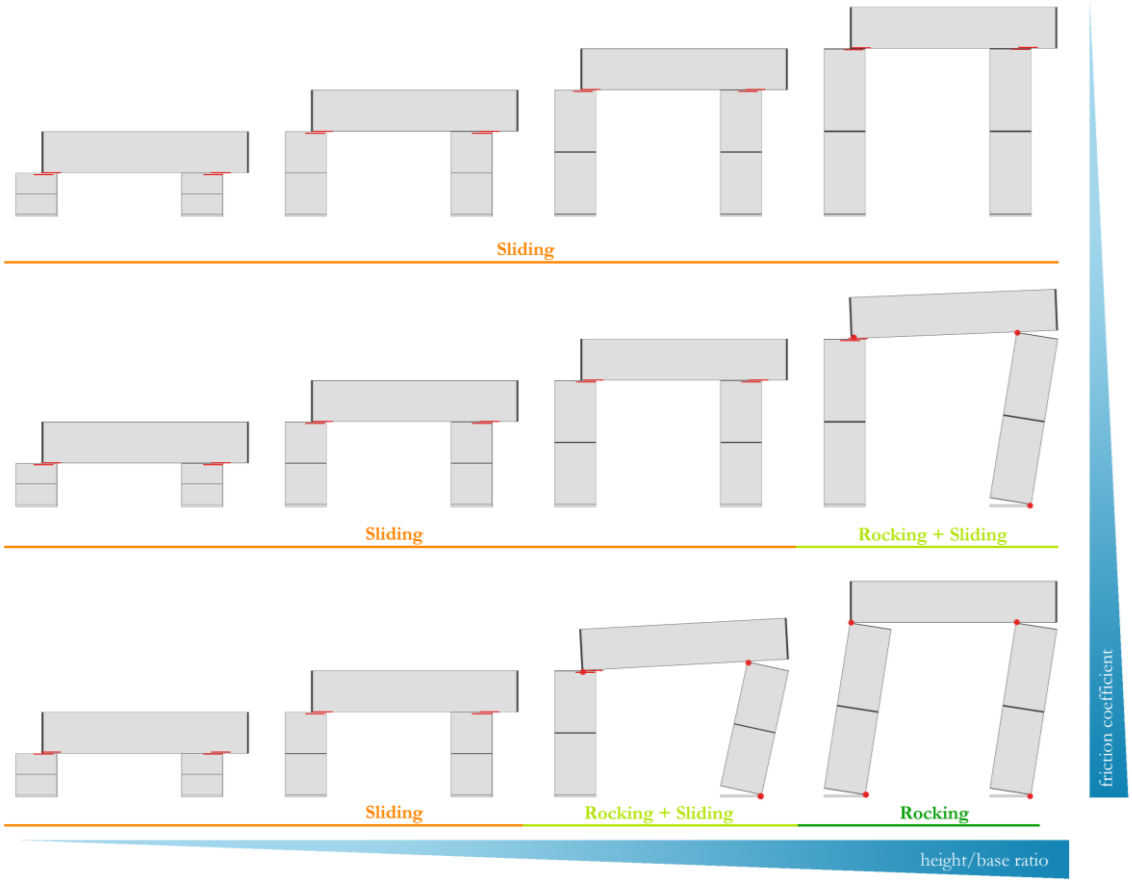

Figure 57: Collapse mechanism by varying the height-to-base ratio and the friction coefficient.

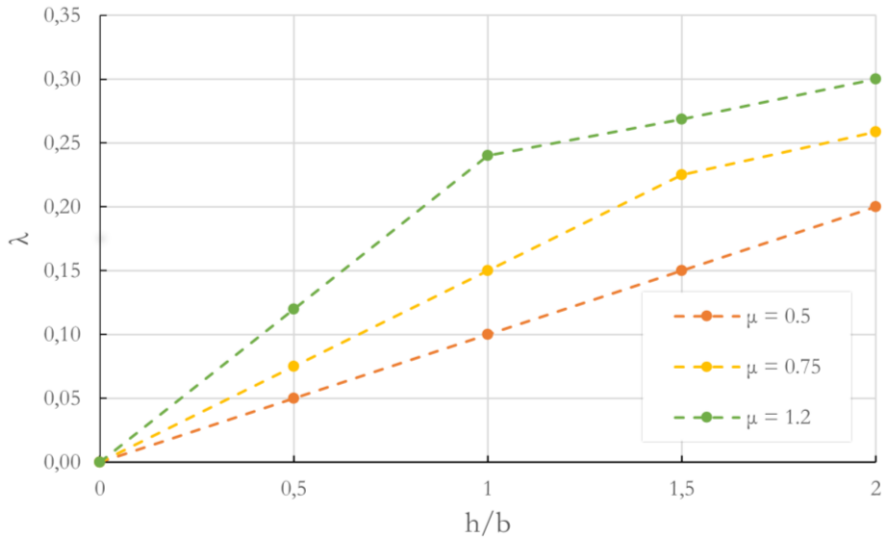

Figure 58: Collapse load multiplier trend with increasing height-to-base ratio and friction coefficient.

6.4. Masonry arch

In the case of masonry arches, the failure mechanism is generally dependent on geometric factors rather than material strength issues. As stated in [96], the stability of a masonry arch is strictly related to its geometrical factor of safety, specifically the thickness ratio t/r where t is the arch thickness and r is its midline radius. This factor along with other geometrical features, such as the span-to-rise ratio and the embrace angle α, determining the overall shape of the arch significantly affect its structural behavior. In particular, the geometrical factor is adequate to determine the safety level of a specific arch shape if there is only dead load, that is the self-weight load. As reported in [142], if a live load is present, the geometrical factor alone cannot guarantee a sufficient level of safety. This is because the thrust line, or funicular polygon, may diverge, and if the live loads are significant, the thrust line may shift, leading to the collapse of the arch.

This section focuses on this aspect of the structural behavior of unreinforced masonry arches examining the safety level based on their geometry. Starting from considering the optimization problem with non-associative flow rule, the aim is to assess the influence of geometric factors on safety under specific constraints and loading conditions.

An arch with variable geometry will be considered. As shown in Figure 59, a masonry arch made of stone with $\gamma = 1700$ kg/m^3 is discretized into 20 rigid blocks mutually connected through rough interfaces. As for the load and constraints conditions, the arch is fixed at the springer and subjected to self-weight $\mathbf{P}_d$ and horizontal load $\mathbf{P}_l$, equal in magnitude to the self-weight and proportional to λ, both applied at the centroid of each voussoir. To evaluate their influence in the collapse mechanism and load multiplier λ, the thickness ratio t/r, (from 0.1 to 0.5) and the embrace angle α (from 25 to 85 degrees), will be varied.

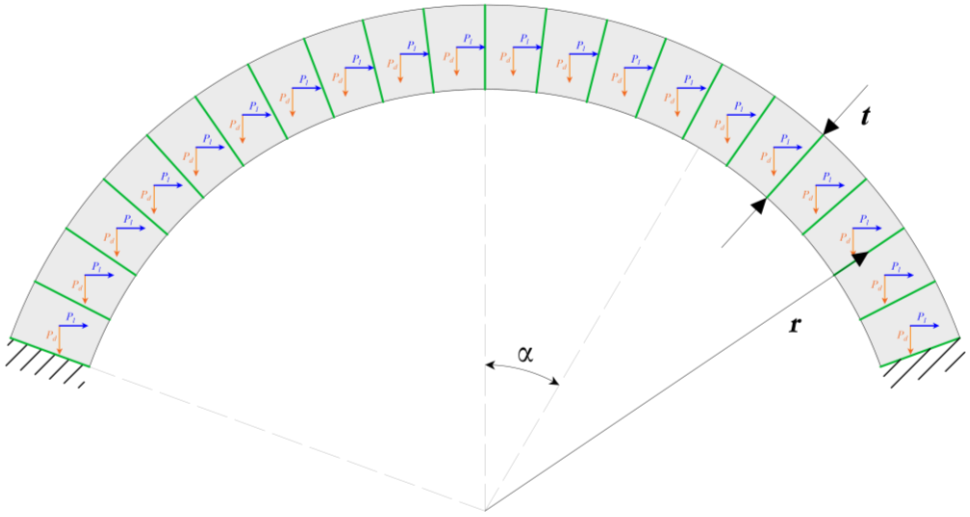

Figure 59: Geometrical properties of the masonry arch.

In Figure 60, the thrust line and collapse mechanism of an arch with variable thickness ratio are reported. As it is possible to observe, arches with a high value of the t/r ratio collapse with a mixed mechanism with the coexistence of sliding and rocking while arches with a lower value of the t/r ratio collapse with a four-hinge mechanism.

In Figure 61, the embrace angle α is varied. It is possible to see that with an increasing value of α, the load collapse multiplier increases significantly and both rocking and sliding mechanism occurs. In particular, arches with a lower value of the embrace angle α behave as a flat arch. As illustrated in Figure 61, when α is equal to 30 and 27, the four-hinge mechanism does not occur and only three hinges can form. Moreover, the magnitude of the collapse load multiplier is consistently higer if compared with the arches having lower values of α. When the embrace angle α becomes very low, even a small reduction in the angle value can result in ever increasing increments of the load multiplier λ.

Since the value of the collapse load multiplier is influenced by the geometric characteristics of the masonry arch, in Figure 62 the three most widespread geometric configurations are compared to figure out which one show the best response to the live loads. For this purpose, a pointed, circular, and flat arch with the same span and t/r ratio is compared.

As illustrated in Figure 62, the pointed arch has the low value of the load multiplier λ, while the flat arch can withstand a live load with a higher load multiplier. This is essentially due to geometrical aspects. In fact, the flat arch can accommodate a thrust line entirely comprised into the thickness of the arch whose resultant at the support has a horizontal component greater in magnitude if compare with the resultant at the support of the pointed and circular arch. In fact, the circular and, in particular, the pointed arch, have a reduced capacity to withstand horizontal load as demonstrated by the low value of the load multiplier λ.

On the other hand, in the case of the flat arch sliding mechanisms are most easily triggered, and a mixed collapse mode of sliding and rocking occurs. This is due to a geometrical configuration where the tangential component of the resultant acting on the interface at the springer can overcome the Coulomb yield condition on friction. For the same reason, as indicated in Figure 62, the pointed and circular arch, having the same span and t/r ratio of the flat arch, collapse with a four-hinge mechanism. The tangential component of the resultant is not sufficiently high to trigger sliding mechanism.

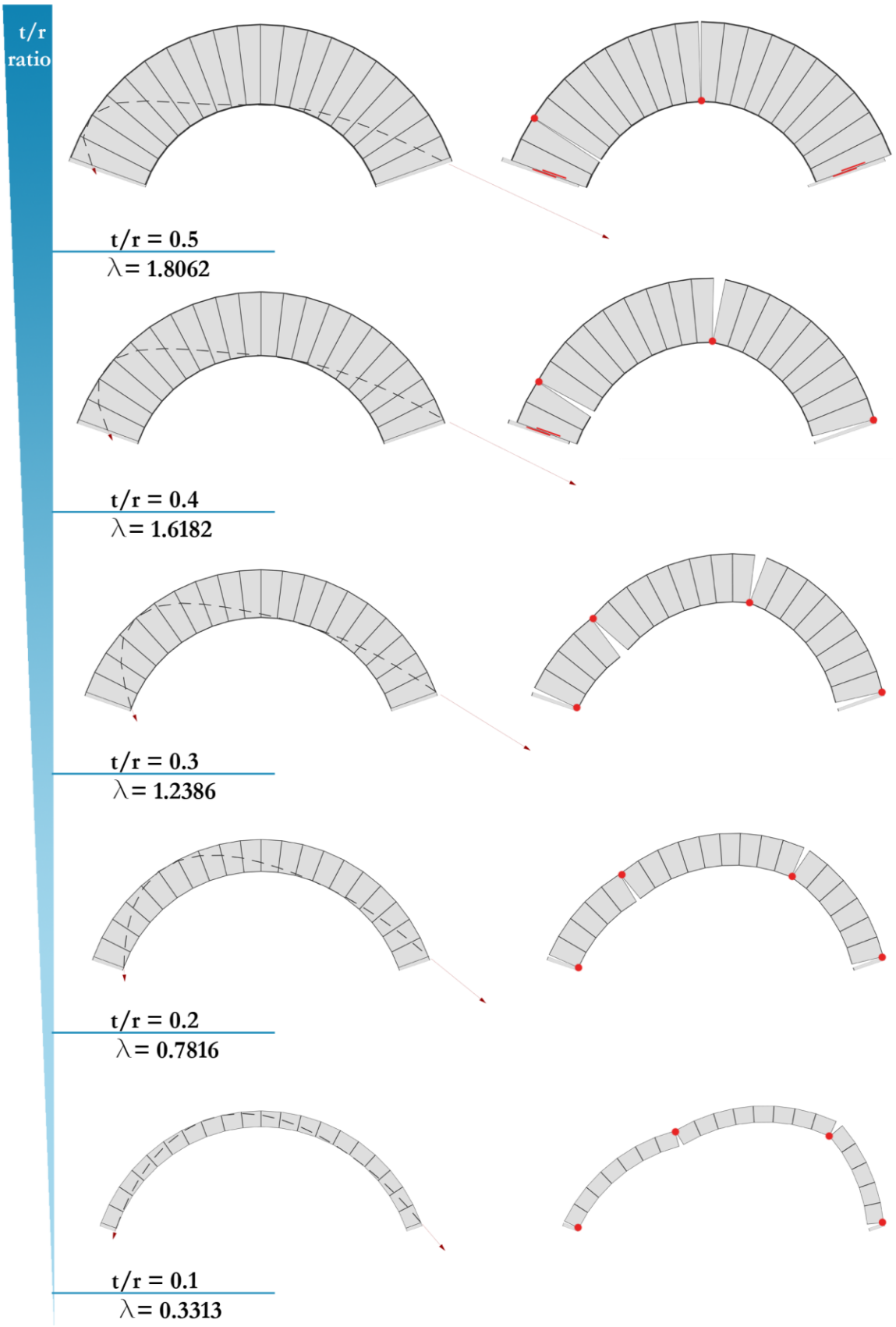

Figure 60: Collapse mechanisms and thrust lines of the masonry arch with variable thickness ratio.

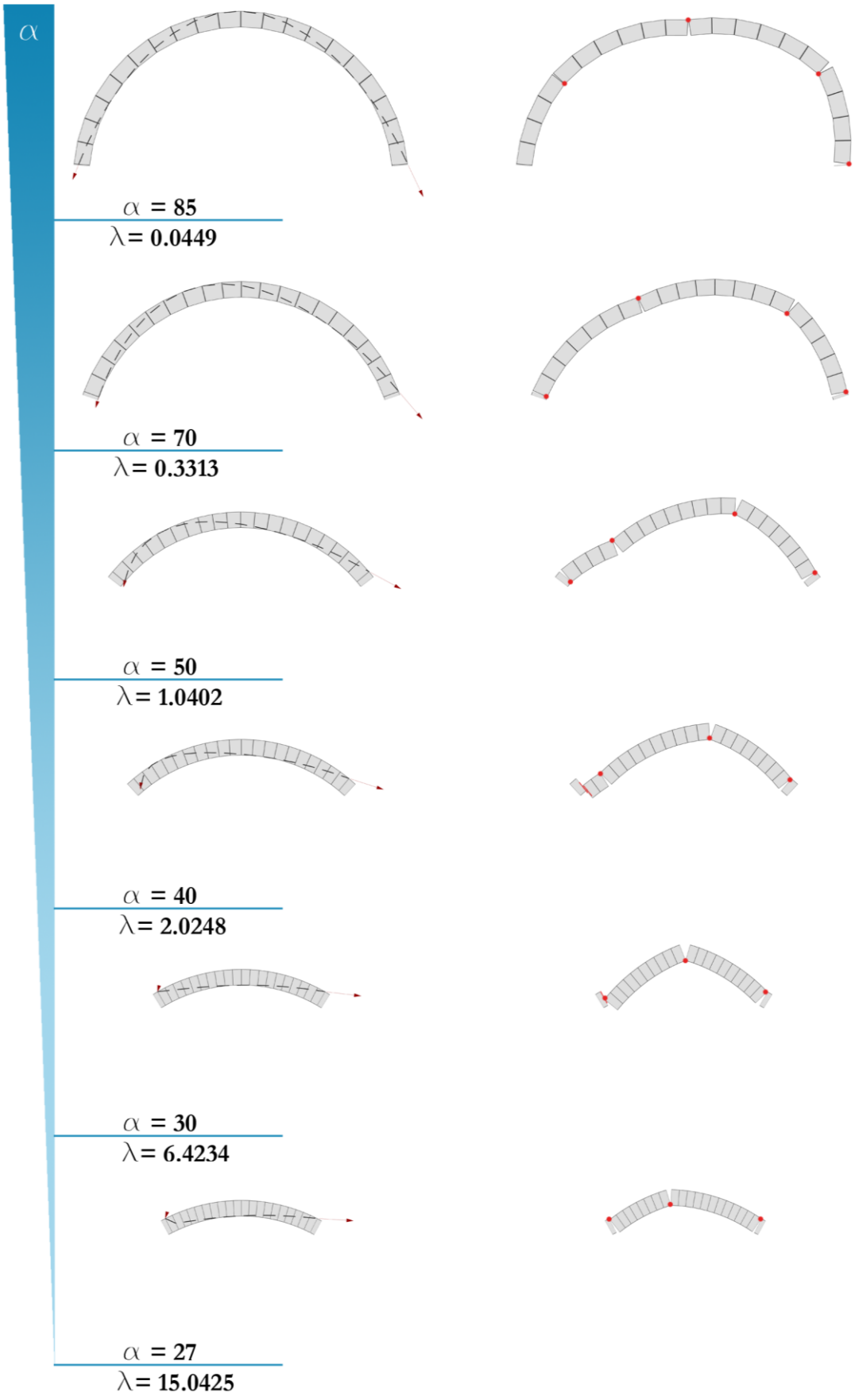

Figure 61: *Collapse mechanisms and thrust lines of the masonry arch with variable embrace angle.*

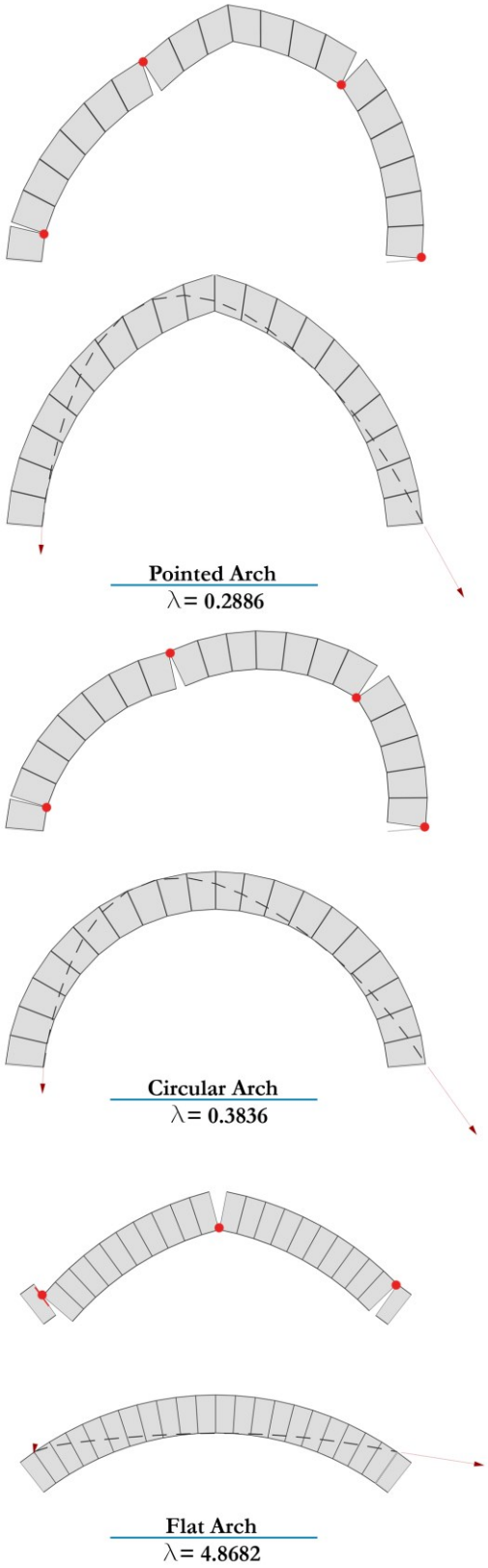

Figure 62: Comparison between pointed, circular and flat arch.

6.5. Optimal reinforcement design for masonry arches

This section is dedicated to the design of the reinforcement for masonry arches. The idea is to design appropriate reinforcement arrangements with the aim of enhancing the level of safety without altering the structural behavior of the arch. Specifically, the focus is on avoiding excessive strengthening of the masonry arch to preserve its initial structural response, that is the rocking behavior occurring under seismic action as a result of a four-hinge mechanism. Moreover, it is crucial to ensure that the reinforced elements do not transfer excessive stresses to the unreinforced sections, which could ultimately result in their failure.

The initial investigation in this study focuses on the utilization of an ideal "elastic" reinforcement for strengthening the arch. This type of reinforcement is characterized by indefinite elastic behavior and no possibility of failure. This first analysis aims to assess the response of the reinforced arch and determine the optimal locations for partial reinforcements. Then, an elastic-perfectly plastic reinforcement will be introduced, which considers the formation of hinges crucial for preserving the four-hinge collapse mechanism. This reinforcement strategy incorporates the concept of "plastic behavior" to effectively handle localized displacements and facilitate the redistribution of forces.

6.5.1. Elastic reinforcement design for masonry arch

This section will discuss the strengthening of a masonry arch by the application of elastic reinforcements located at the intrados or the extrados. In both cases, the reinforcement is applied on a masonry arch made of stone $\gamma = 1700$ kg/m^3 and discretized into 21 voussoirs connected through rough interfaces. The thickness ratio t/r is set equal to 0.1 with a midline radius r of 2 m while the embrace angle α is equal to 78,75. As for the load and constraints conditions, the arch is fixed at the springer and subjected to self-weight $\mathbf{P}_d$ and horizontal load $\mathbf{P}_l$, equal in magnitude to the self-weight and proportional to λ, both applied at the centroid of each voussoir. Moreover, with the purpose of considering the change in direction of the seismic action, represented by the horizontal force $\mathbf{P}_l$ proportional to λ, the reinforcement is applied symmetrically.

To consider the introduction of this kind of reinforcement, an additionally constraint equation is provided in the optimization problem as explained in Section 5.11. The MATLAB code implemented to design the reinforcement allow the user to add one single reinforcement for each iteration choosing the interface and the side of application, intrados or extrados, step by step.

The design of the elastic reinforcement located at the extrados is presented in Figure 63. The graph on the left shows the increase in the load multiplier λ with each iterative addition of the reinforcement. It is evident that a well-distributed reinforcement configuration achieves a 50% increment in the load multiplier.

The design procedure for the reinforcement at the intrados is presented in Figure 64, following a similar approach. In this case, the specific area to be reinforced to achieve a 50% increment in the load multiplier λ corresponds to the area at the crown. This strategic arrangement ensures that the desired level of strengthening is achieved while preserving the integrity of the arch structural behavior.

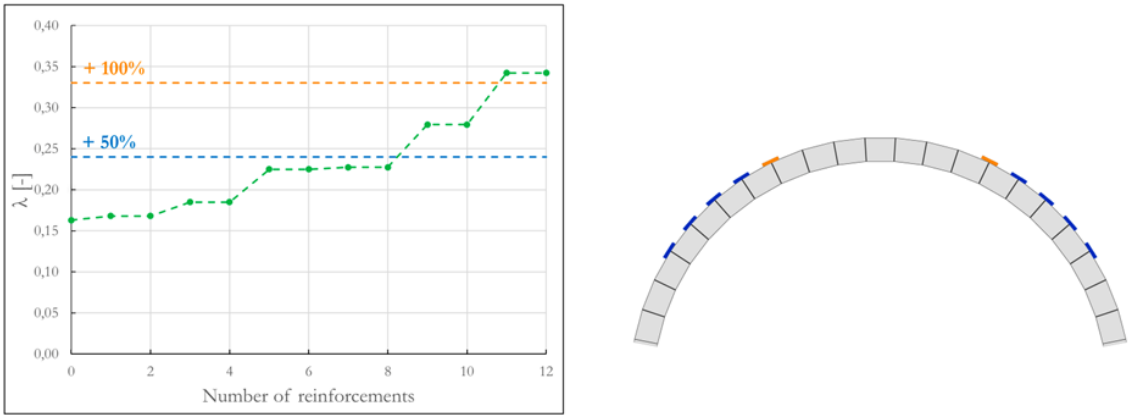

Figure 63: Load multiplier increment λ due to the iterative application of an elastic reinforcement on a masonry arch located at the extrados (left), final optimal reinforcement design (right).

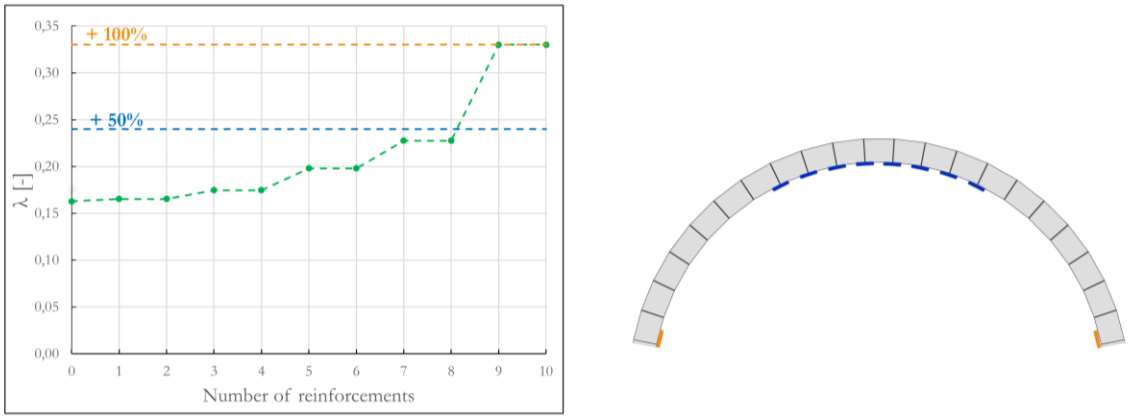

Figure 64: Load multiplier increment λ due to the iterative application of an elastic reinforcement on a masonry arch located at the intrados (left), final optimal reinforcement design (right).

In both Figure 65 and Figure 66 is possible to observe how the mechanism and the collapse load multiplier can change with the iterative addition of a reinforcement.

The first mechanism and the related collapse load multiplier λ correspond to the unreinforced arch. In the following iterations, at each step, a new reinforcement is added both on the interface where a hinge opens and on the symmetrical interface arranged on the other half of the arch.

The analysis conducted does not account for changes in the direction of the seismic load. To address this limitation and to design a reinforcement that can withstand dynamic load conditions, the insertion of a reinforcement on the symmetrical interface located on the other half of the arch is proposed. Since the horizontal load does not change direction, the load multiplier remains unaffected in most cases, as the symmetric reinforcement does not impact the structural response for the current specific mechanism.

As depicted in Figure 65 and Figure 66, the introduction of the reinforcement, as well as its symmetrical counterpart (in green), corresponds to a step in which the load multiplier remains unchanged. However, the presence of the symmetric reinforcement will influence the subsequent iterations, when the mechanism changes due to the insertion of a new reinforcement and the formation of a hinge in that area is prevented, thereby altering the behavior of the arch.

In Figure 67 is illustrated the optimal reinforcement design in detail. In the case of reinforcement at the extrados, the area at the crown and near to the springers is not reinforced, in order to avoid sliding and preserving the structural response in presence of seismic action and settlements. On the other hand, for the strengthening of an arch at the intrados, the areas to be reinforced are essentially located at the crown. In fact, the presence of the elastic reinforcement in these areas prevents the opening of a hinge, precluding the arch to accommodate the displacement due to settlements and seismic actions. The design of the reinforcement with this arrangement allows to increase the value of the load multiplier, while preserving the four-hinge mechanism.

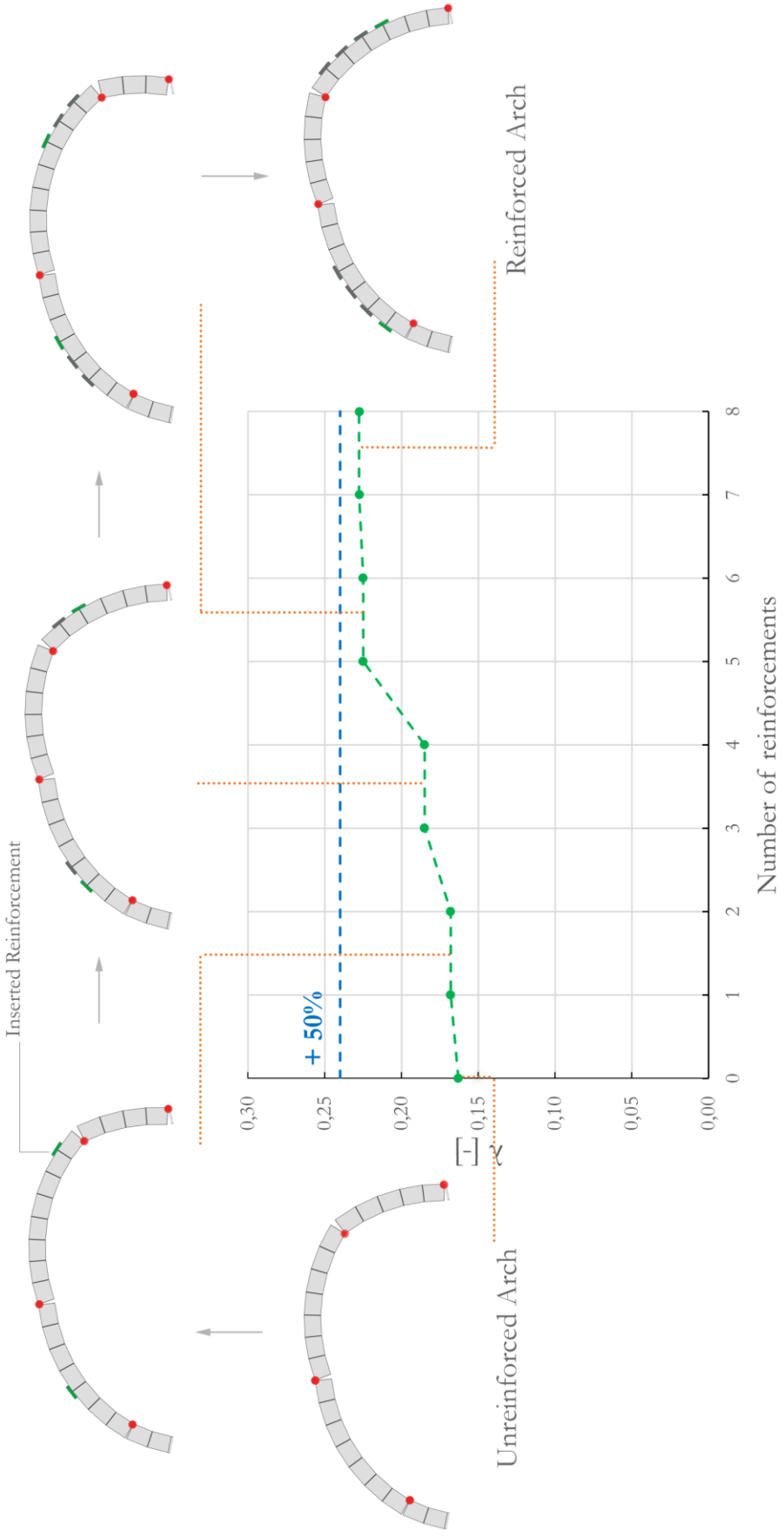

Figure 65: Mechanism and collapse load multiplier trend for the elastic reinforcement at the extrados.

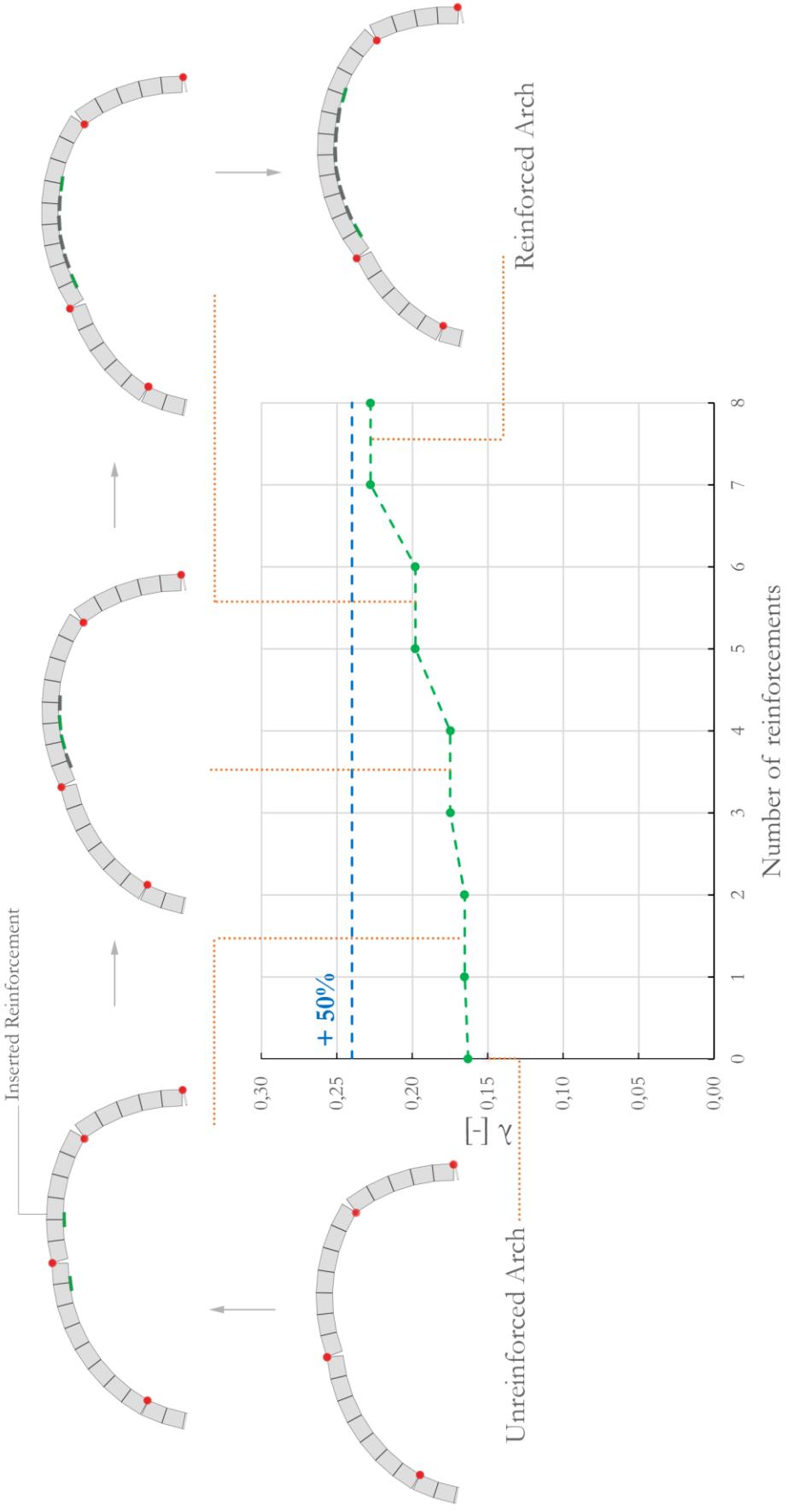

Figure 66: Mechanism and collapse load multiplier trend for the elastic reinforcement at the intrados.

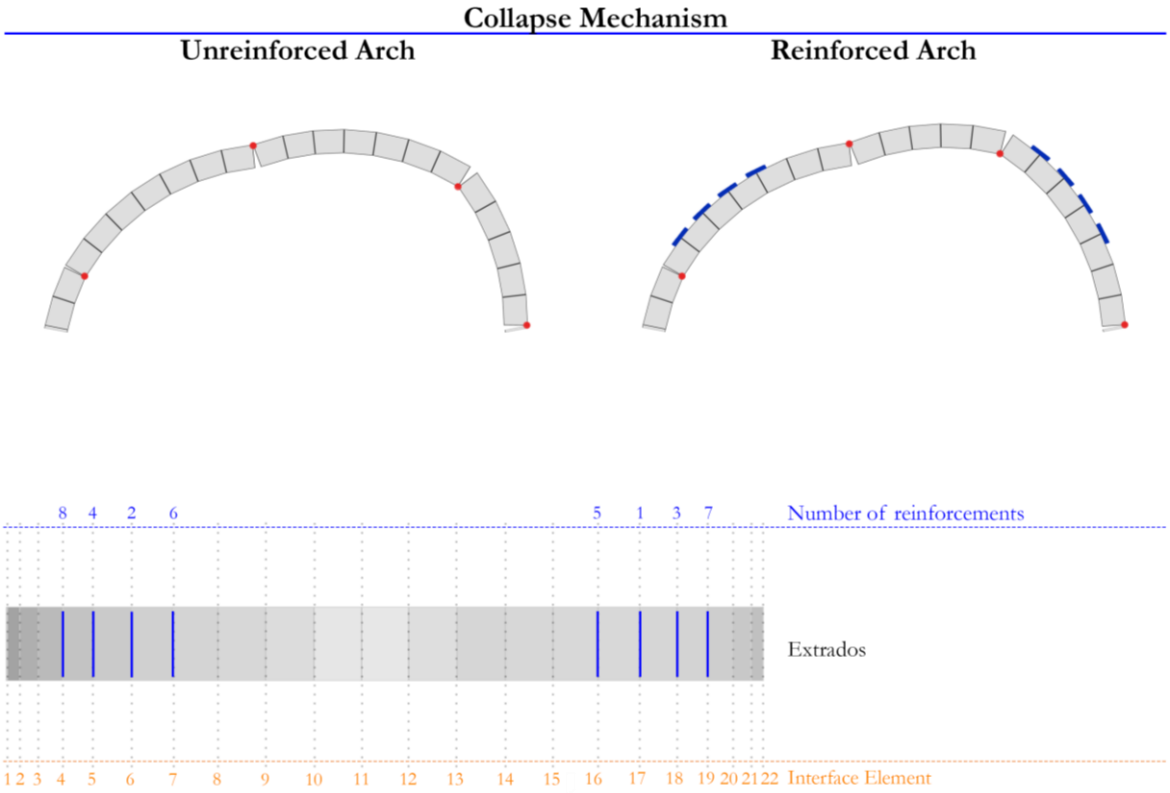

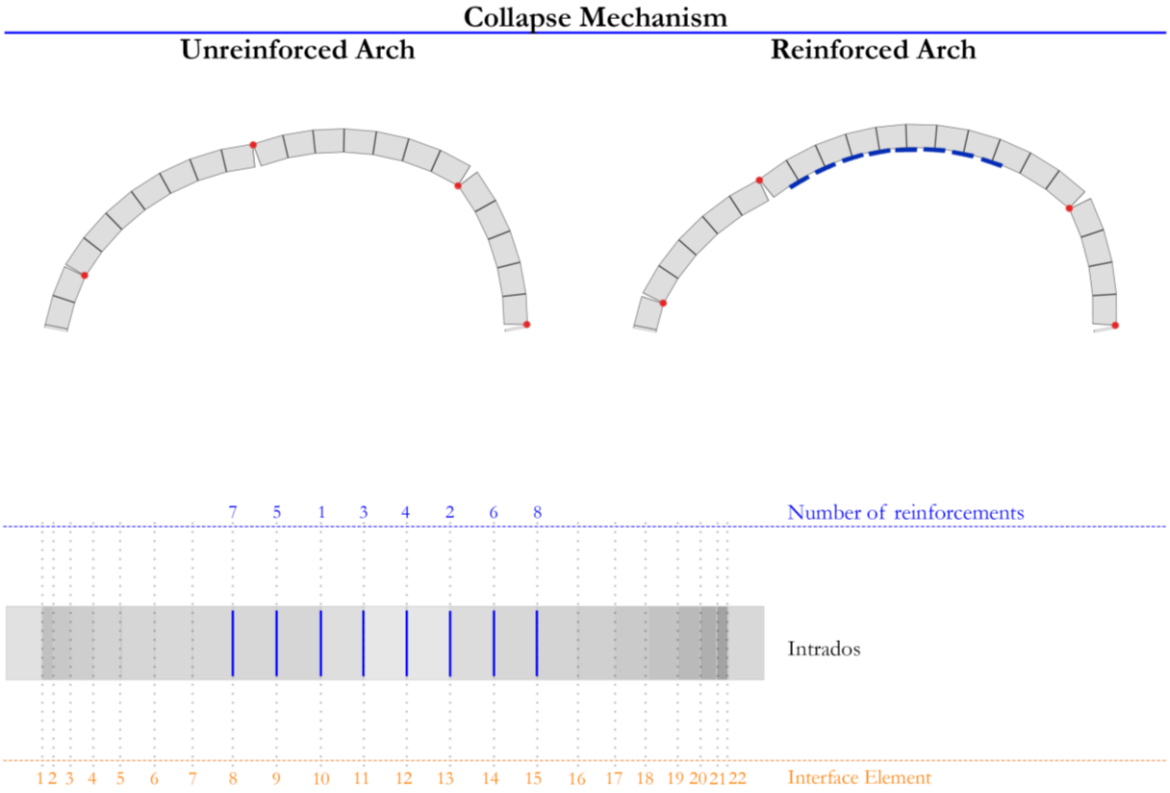

Figure 67: Design of the elastic reinforcement for the extrados (top) and the intrados (down).

6.5.2. Elastic-perfectly plastic reinforcement design for masonry arch

In this second section, the design of an elastic-perfectly plastic reinforcement for a masonry arch will be proposed. The reinforcement, applied once at the intrados and once at the extrados only, is assumed to be characterized by an elastic-perfectly plastic response as defined in Section 5.12. Conversely the elastic reinforcement, the elastic-perfectly plastic reinforcement enables a certain rate of the displacement at the reinforced interface corresponding to a reactive force for the reinforcement F_y. This allows to take into account the formation of hinges that enable the preservation of the four-hinge collapse mechanism. In fact, by integrating the concept of "plastic deformation" into the design approach, the strengthening strategy accounts for the capacity of the reinforcement to collapse. Enabling the formation of hinges and a redistribution of stresses, this "plastic behavior" allows to effectively maintain structural integrity in the face of significant loading conditions.

For the arch shown in the previous section, with same geometry, constraints and load conditions, the design of an elastic-perfectly plastic reinforcement will be defined following the same procedure followed in Section 6.5.1.

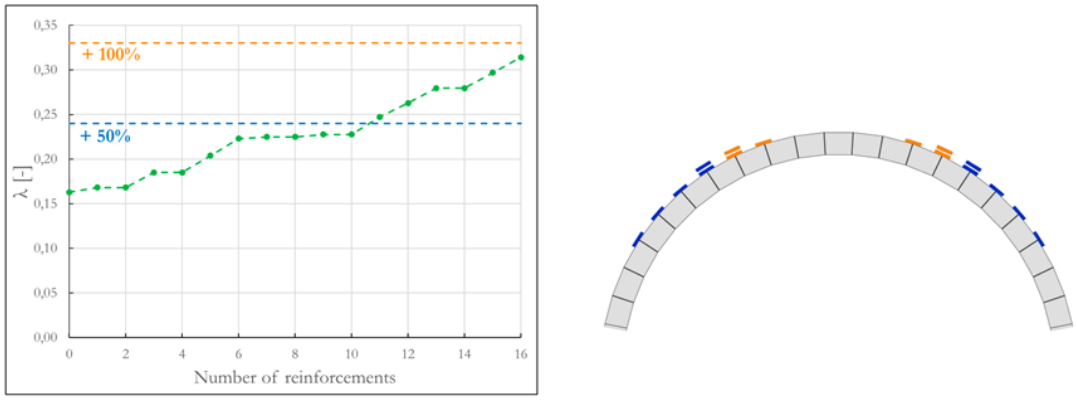

Figure 68: Load multiplier λ increment due to the iterative application of an elastic-perfectly plastic reinforcement on a masonry arch located at the extrados (left), final optimal reinforcement design (right).

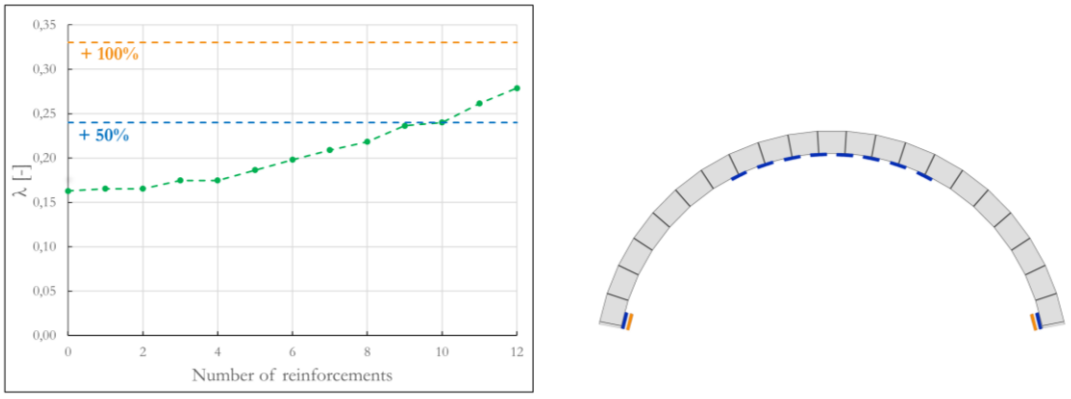

Figure 69: Load multiplier λ increment due to the iterative application of an elastic-perfectly plastic reinforcement on a masonry arch located at the intrados (left), final optimal reinforcement design (right).

As depicted in Figure 68 and Figure 69, the application of an elastic-perfectly plastic reinforcement at the extrados or at the intrados allows to gradually increment the value of the load multiplier, if compared to the outcomes obtained employing a reinforcement with an elastic response. This is essentially due to the fact that the plastic reinforcement can fail at a certain interface, allowing a hinge to occur. For this reason, comparing the design defined for the elastic reinforcement in Section 6.5.1, more than one layer of plastic reinforcement can be applied at the extrados or the intrados.

Figure 70 and Figure 71 show the iterative reinforcement procedure in detail. Similarly to the previous case of the reinforcement with elastic behavior, in the design of the elastic-perfectly plastic reinforcement at the extrados, the areas at the crown and near to the springers are left unreinforced. On the other hand, the strengthening design at the intrados provides the insertion of plastic reinforcements, located not only at the crown, but also on the internal side of the interface close to the support of the arch. Therefore, the main difference with the elastic reinforcement is that the plastic reinforcement can be applied with a reduced increment in the load multiplier λ.

Based on the current analysis conducted, it is possible to state that the magnitude of the reactive force F_y exerted by the reinforcement has a significant impact not only on the magnitude of the load multiplier, but also on its rate of increase. The same effect holds for the number of reinforcements required to achieve the desired level of safety enhancement. In fact, when a low reactive force F_y is measured in the reinforcement, then small variations in the load multiplier are obtained. Under the same assumption, a greater number of reinforcements is generally required.

As shown in Figure 72, the plastic reinforcement accommodates in a more efficient way a seismic action or a settlement, if compared with the elastic reinforcement, since the rocking mechanism is allowed even where the reinforcement is applied, thus preventing crushing or sliding of the blocks in the masonry arch.

Therefore, the employment of the elastic-perfectly plastic reinforcement reduces the increment in the load multiplier, allowing a more controlled insertion of the reinforcement. Indeed, the application of a plastic reinforcement as a strengthening intervention has proven to be highly effective in preserving the characteristic mechanical behavior of a masonry arch. This approach allows for a controlled increase in the collapse multiplier without excessively constraining the structural system. Additionally, it prevents the transfer of excessive stresses to the unreinforced sections, reducing the risk of failure in those areas.

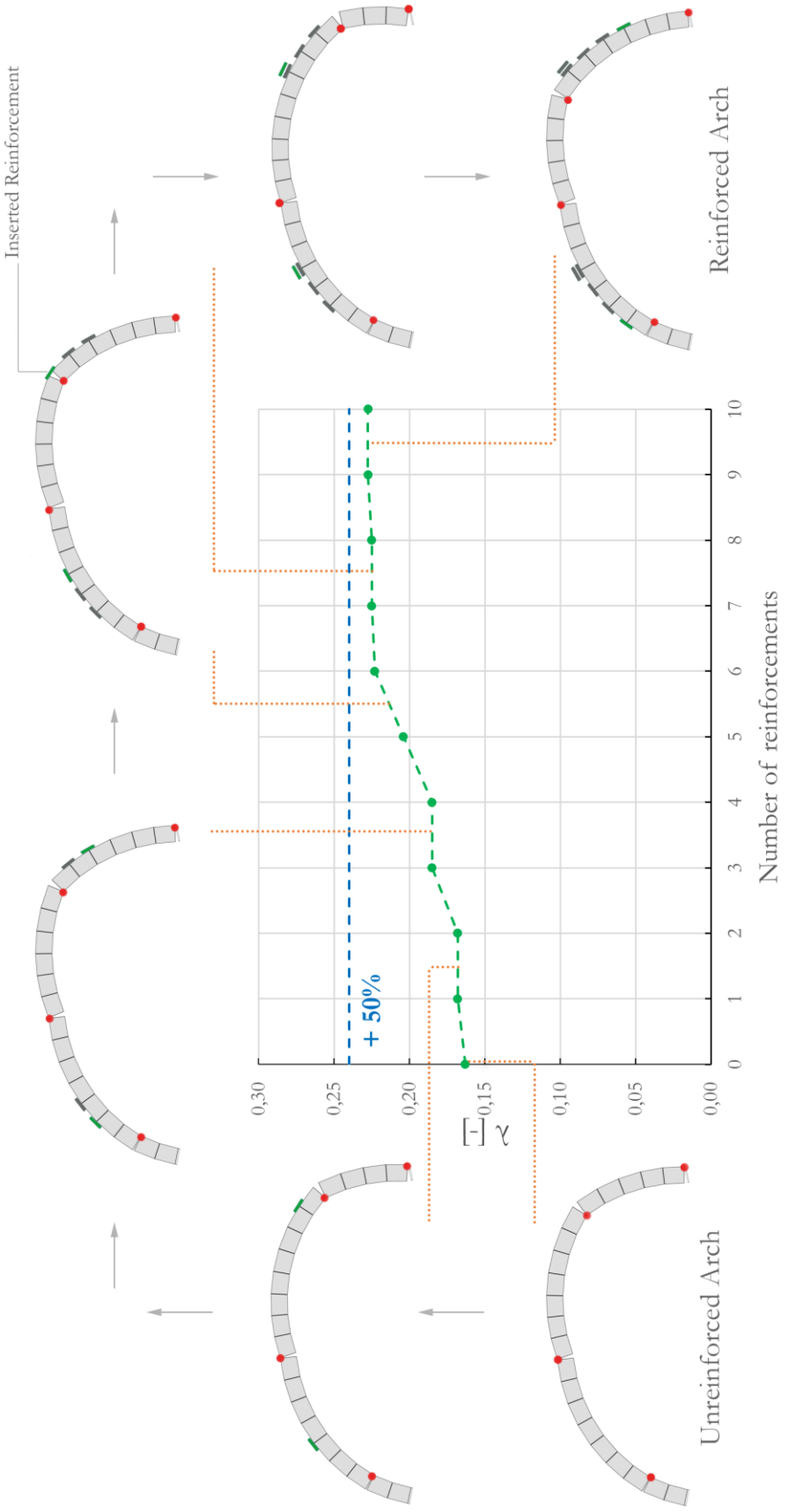

Figure 70: Mechanism and collapse load multiplier trend for the elastic-perfectly plastic reinforcement at the extrados.

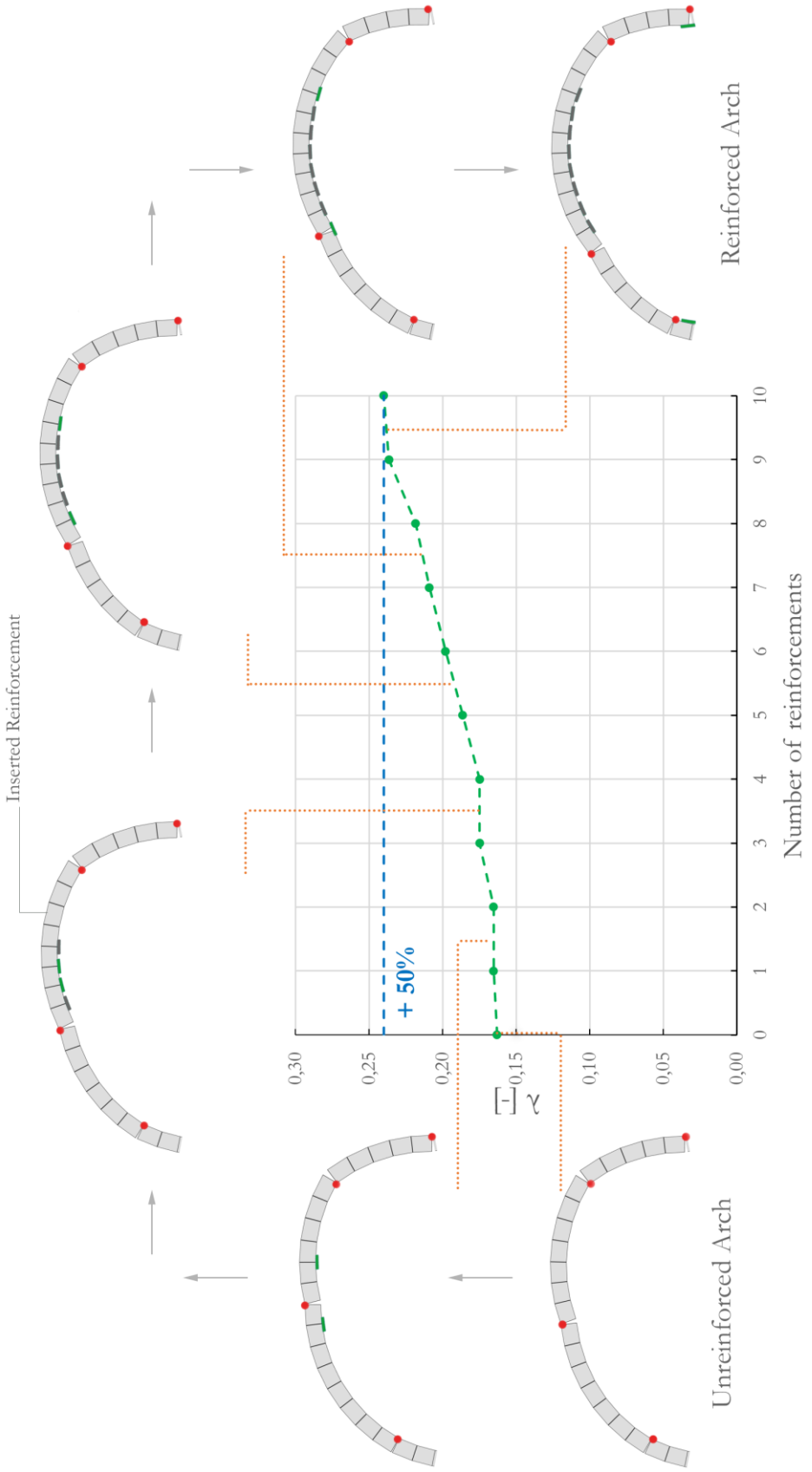

Figure 71: Mechanism and collapse load multiplier trend for the elastic-perfectly plastic reinforcement at the intrados.

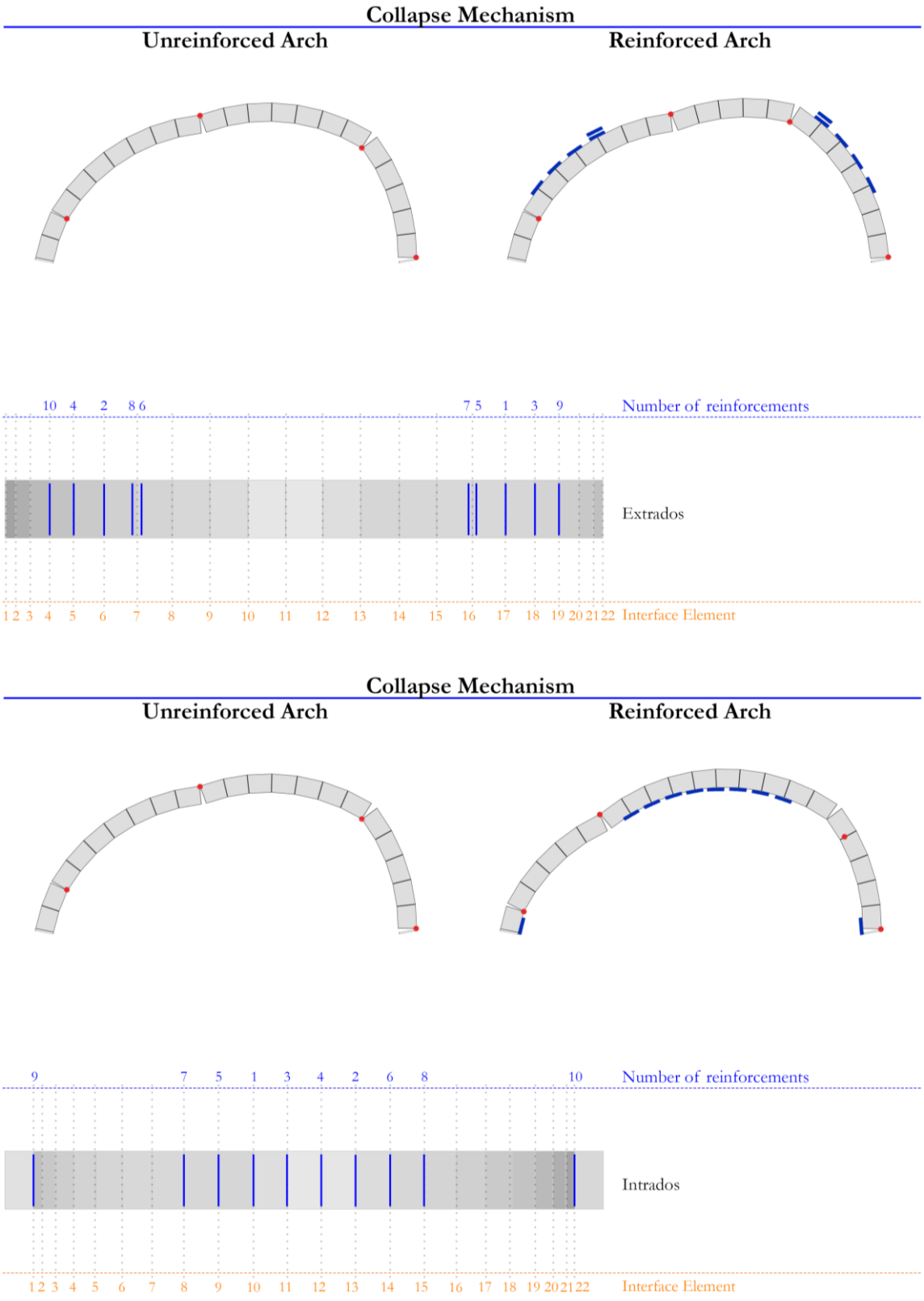

Figure 72: Design of the elastic-perfectly plastic reinforcement for the extrados (top) and the intrados (down).

6.5.3. Effect of the reinforcement on arch-pier interaction

In this section is discussed the effect of a strengthening intervention for a masonry arch on piers. The masonry arch is discretized in 21 blocks with a midline radius of 2 m and thickness ratio of 0.1. Each pier is 0.7 m large and 3.20 m height.

In Figure 73 is illustrated the increment in the load multiplier due to the insertion of elastic reinforcements at the intrados of the arch and at the base of the supports. The insertion of an extensive reinforcement consistently alters the structural behavior of the arch on its piers. As illustrated in the graph, with a lower number of inserted reinforcements it is possible to see a great increment in the load multiplier. As shown in Figure 74, if the arch is entirely reinforced at the intrados the hinges are constrained to occur at the internal side of the support. Therefore, this outcome demonstrates how strengthening a part of a masonry structure, in this case the arch, can weaken other elements, the supports, and trigger unpredicted collapse mechanism.

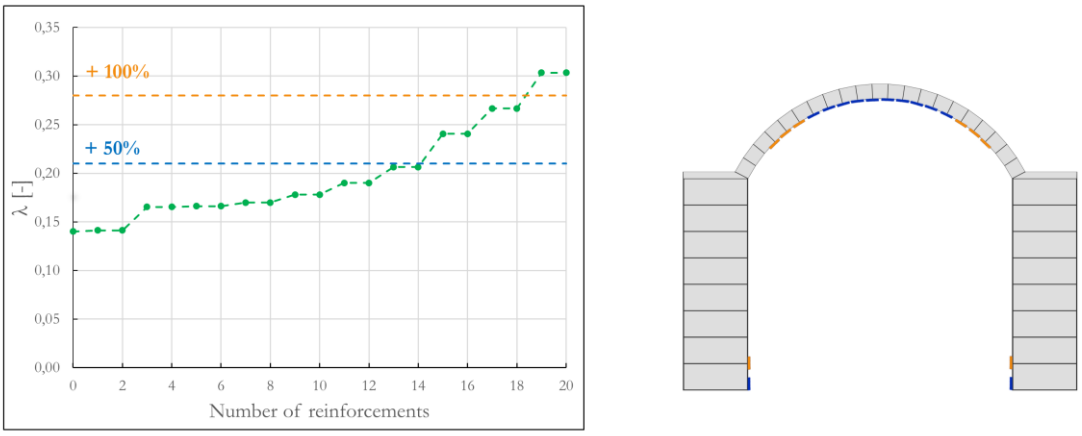

Figure 73: Load multiplier increment (left) and optimal reinforcement with elastic behavior located at the intrados and internal pier side of a masonry arch on supports.

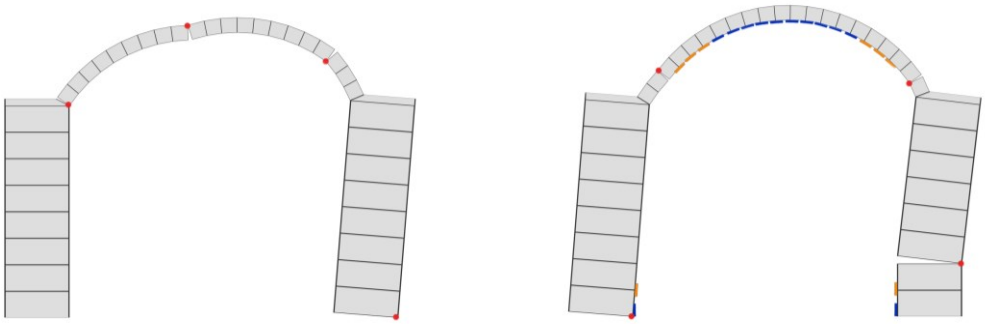

Figure 74: Collapse mechanism for a unreinforced (left) and reinforced (right) of a masonry arch on supports.

CONCLUSIONS

In the present thesis, an algorithm for the optimal reinforcement design of masonry arches is proposed.

Whitin the framework of the limit analysis with non-associative flow rule, an algorithm is implemented for describing the collapse mechanisms and collapse load increase in reinforced arches, discretized with two-dimensional rigid blocks mutually connected through unilateral and rough interfaces.

The limit analysis problem with non-associative flow rule is formulated as a sequence of linear programming problems (LP) and then enhanced with an additional constraint equation to take into account the inserted reinforcements. An iterative framework for the optimized placement of ad-hoc localized reinforcements is conceptualized and implemented. This is utilized to simulate and verify all the possible suitable configurations ensuring the safety of the masonry arches.

In section 6.5.1, a first solution using an ideal "elastic" reinforcement is proposed to limit the opening at the interface where the reinforcement is applied, at the extrados or at the intrados, preventing a hinge to occur on the opposite side of the interface. This provides an initial assessment of the collapse mechanism and the areas for the reinforcement.

In section 6.5.2, elastic-perfectly plastic reinforcements are employed, giving the structure some degree of ductility, since after the yielding limit the reinforcement is capable to freely deform. The design with this "plastic behavior" will consider the possibility of localized displacements to occur and a redistribution of forces. The introduction of elastic-perfectly plastic reinforcement, localized at the intrados or at the extrados, if compared to the elastic reinforcement, allows a four-hinge mechanism to occur preventing crushing and sliding

displacements. Moreover, a plastic reinforcement technique limits the transmission of excessive stresses to the unreinforced sections, thus minimizing the risk of failure.

Therefore, the use of an elastic-perfectly plastic reinforcement is a possible solution to suitably increase the value of the collapse multiplier, without completely constraint the structural system and thus achieving the purpose of the present thesis.

In conclusion, the present thesis has identified and proposed effective reinforcement strategies with the objective of enhancing safety while preserving the essential mechanical characteristics and collapse mechanism of masonry arches. By addressing the challenge of overcoming of the antinomy between structural safety and preservation, an appropriate strengthening intervention procedure has been developed that ensures the original structural behavior of historical masonry arches remains unaltered.

The optimal reinforcement configurations designed in section 6.5.1 and 6.5.2 could be further validated through experimental tests on full-scale masonry arches, by employing different composite materials and strengthening techniques.

Additionally, the proposed algorithm holds potential for application in the design of reinforcement systems for more complex historical masonry structures, as well as in evaluating the effects of a strengthening intervention on the overall structural behavior of previously damaged masonry constructions.

REFERENCES

[1] S. Timoshenko and J. N. Goodier, *Theory of elasticity*. McGraw Hill, 1951.

[2] I. J. Oppenheim, "The masonry arch as a four-link mechanism under base motion," *Earthq Eng Struct Dyn*, vol. 21, no. 11, pp. 1005–1017, Jan. 1992, doi: 10.1002/EQE.4290211105.

[3] L. De Lorenzis, M. DeJong, and J. Ochsendorf, "Failure of masonry arches under impulse base motion," *Earthq Eng Struct Dyn*, vol. 36, no. 14, pp. 2119–2136, Nov. 2007, doi: 10.1002/eqe.719.

[4] C. Modena, F. Da Porto, C. Filippo, M. Marco, and S. Elena, "Cultural Heritage Buildings and the Abruzzo Earthquake: Performance andPost-Earthquake Actions," in *Advanced Materials Research*, 2010, pp. 3–17. doi: 10.4028/www.scientific.net/AMR.133-134.3.

[5] C. F. Carocci, S. Cattari, S. Lagomarsino, and C. Tocci, "The case study of Santa Maria Paganica Church damaged by 2009 L'Aquila earthquake," in *Advanced Materials Research*, 2010, pp. 163–168. doi: 10.4028/www.scientific.net/AMR.133-134.163.

[6] V. Arcidiacono, G. P. Cimellaro, E. Piermarini, and J. Ochsendorf, "The Dynamic Behavior of the Basilica of San Francesco in Assisi Using Simplified Analytical Models," *International Journal of Architectural Heritage*, vol. 10, no. 7, pp. 938–953, Oct. 2016, doi: 10.1080/15583058.2016.1158333.

[7] G. P. Cimellaro, A. M. Reinhorn, and A. De Stefano, "Introspection on improper seismic retrofit of Basilica Santa Maria di Collemaggio after 2009 Italian earthquake," *Earthquake Engineering and Engineering Vibration*, vol. 10, no. 1, pp. 153–161, Mar. 2011, doi: 10.1007/s11803-011-0054-4.

[8] A. M. D'Altri *et al.*, "Modeling Strategies for the Computational Analysis of Unreinforced Masonry Structures: Review and Classification," *Archives of Computational Methods in Engineering*, vol. 27, no. 4, pp. 1153–1185, Sep. 2020, doi: 10.1007/s11831-019-09351-x.

[9] *Valutazione e riduzione del rischio sismico del patrimonio culturale con riferimento alle Norme tecniche per le costruzioni di cui al decreto del Ministero delle infrastrutture e dei trasporti del 14 gennaio 2008*. DPCM 9 febbraio 2011.

[10] ICOMOS, *Recommendations for the analysis, conservation and structural restoration of architectural heritage*. International Scientific Committee for Analysis and Restoration of Structures of Architectural Heritage, 2001.

[11] *Istruzioni per la Progettazione, l'Esecuzione ed il Controllo di Interventi di Consolidamento Statico mediante l'utilizzo di Compositi Fibrorinforzati a Matrice Inorganica*. CNR-DT 215/2018.

[12] A. Castellano, A. Fraddosio, J. Scacco, G. Milani, and M. D. Piccioni, "Full-scale Dynamic Tests on Unreinforced and GFRCM-reinforced Apulian Tuff Masonry Arches".

[13] A. Castellano, A. Fraddosio, J. Scacco, G. Milani, and M. D. Piccioni, "Dynamic Response of FRCM Reinforced Masonry Arches," *Key Eng Mater*, vol. 817, pp. 285–292, Aug. 2019, doi: 10.4028/www.scientific.net/KEM.817.285.

[14] J. Heyman, "The stone skeleton," *International Journal of Solid and Structures*, vol. 2, no. 2, pp. 249–279, 1966.

[15] D. Radenkovic, "Théorèmes limites pour un materiau de Coulomb à dilatation non standardisée," *Note Ac. Sciences Paris, Meeting of 12 th June*, 1961.

[16] A. Giuffrè, *Letture sulla meccanica delle murature storiche*. Rome, Italy: Kappa, 1991.

[17] G. Brandonisio, G. Lucibello, E. Mele, and A. De Luca, "Damage and performance evaluation of masonry churches in the 2009 L'Aquila earthquake," *Eng Fail Anal*, vol. 34, pp. 693–714, Dec. 2013, doi: 10.1016/j.engfailanal.2013.01.021.

[18] S. Lagomarsino, "Damage assessment of churches after L'Aquila earthquake (2009)," *Bulletin of Earthquake Engineering*, vol. 10, no. 1, pp. 73–92, Feb. 2012, doi: 10.1007/s10518-011-9307-x.

[19] S. Lagomarsino and S. Podestà, "Seismic vulnerability of ancient churches: I. Damage assessment and emergency planning," *Earthquake Spectra*, vol. 20, no. 2, pp. 377–394, 2004, doi: 10.1193/1.1737735.

[20] P. Salzano, E. Cescatti, C. Casapulla, F. Ceroni, F. da Porto, and A. Prota, "2016-17 Central Italy: Macroscale Assessment of Masonry Churches Vulnerability," in *Proceedings of the 7th International Conference on Computational Methods in Structural Dynamics and Earthquake Engineering (COMPDYN 2015)*, Athens: Institute of Structural Analysis and Antiseismic Research School of Civil Engineering National Technical University of Athens (NTUA) Greece, 2019, pp. 1000–1013. doi: 10.7712/120119.6974.19936.

[21] E. Cescatti, P. Salzano, C. Casapulla, F. Ceroni, F. da Porto, and A. Prota, "Damages to masonry churches after 2016–2017 Central Italy seismic sequence and definition of fragility curves," *Bulletin of Earthquake Engineering*, vol. 18, no. 1, pp. 297–329, Jan. 2020, doi: 10.1007/s10518-019-00729-7.

[22] L. Sorrentino, S. Cattari, F. da Porto, G. Magenes, and A. Penna, "Seismic behaviour of ordinary masonry buildings during the 2016 central Italy earthquakes," *Bulletin of Earthquake Engineering*, vol. 17, no. 10, pp. 5583–5607, Oct. 2019, doi: 10.1007/s10518-018-0370-4.

[23] *Primi elementi in materia di criteri generali per la classificazione sismica del territorio nazionale e di normative tecniche per le costruzioni in zona sismica.* O.P.C.M. 3274 del 20 marzo 2003 .

[24] *Ulteriori modifiche ed integrazioni all'ordinanza del Presidente del Consiglio dei Ministri n. 3274 del 20 marzo 2003, recante "Primi elementi in materia di criteri generali per la classificazione sismica del territorio nazionale e di normative tecniche per le costruzioni in zona sismica."* O.P.C.M. 3431 del 3 maggio 2005.

[25] ICOMOS Charter, *International Charter for the Conservation and Restoration of Monuments and Sites*. Venice,Italy, 1964.

[26] *Carta del Restauro 1972 (Carta Italiana del Restauro)*. Ministero della Pubblica Istruzione, 1972.

[27] *Interventi sul Patrimonio Monumentale a Tipologia Specialistica in Zone Sismiche: Raccomandazioni*. Ministero dei Beni Culturali e Ambientali (Com. Naz. Prev. Patr. Cult. dal Rischio Sismico), 1986.

[28] C. Brandi, *Teoria del restauro*. 1977.

[29] *Italian Building Code [Nuove Norme Tecniche per le Costruzioni]*. G.U., 2008.

[30] C. Modena, F. Da Porto, and M. R. Valluzzi, "Conservazione del patrimonio architettonico e sicurezza strutturale in zona sismica: insegnamenti dalle recenti esperienze italiane," in *Materiali e strutture : problemi di conservazione*, Edizioni Quasar, 2012, pp. 17–28.

[31] M. Tomazevic, *Earthquake-Resistant Design of Masonry Buildings*. Imperial College Press, 1999.

[32] P. B. Lourenço, N. Mendes, L. F. Ramos, and D. V. Oliveira, "Analysis of masonry structures without box behavior," *International Journal of Architectural Heritage*, vol. 5, no. 4–5, pp. 369–382, 2011, doi: 10.1080/15583058.2010.528824.

[33] E. Benvenuto, *La scienza delle costruzioni e il suo sviluppo storico*. Firenze, Italy, 1981.

[34] M. Nocera, C. Gatta, D. Addessi, and D. Liberatore, "Micromechanical Modeling of Unreinforced Masonry Arches Accounting for Flexural Hinges and Shear Slidings," *International Journal of Architectural Heritage*, vol. 16, no. 10, pp. 1608–1619, Oct. 2022, doi: 10.1080/15583058.2021.1908445.

[35] J. A. Ochsendorf, "Collapse of masonry structures," Jul. 2002, doi: 10.17863/CAM.14048.

[36] M. R. Valluzzi, F. da Porto, and C. Modena, "Behavior and modeling of strengthened three-leaf stone masonry walls," *Mater Struct*, vol. 37, no. 3, pp. 184–192, Apr. 2004, doi: 10.1007/bf02481618.

[37] D. V Oliveira and P. B. Lourenço, "Repair of stone masonry arch bridges," in *Proceedings of the Arch Bridges '04*, Barcelona, Spain, 2004, pp. 451–458.

[38] G. Brandonisio, M. Angelillo, and A. De Luca, "Seismic capacity of buttressed masonry arches," *Eng Struct*, vol. 215, Jul. 2020, doi: 10.1016/j.engstruct.2020.110661.

[39] N. Masini and A. Tataranno, "Chiesa di S. Maria della Pietà a Irsina (MT)," 2003, pp. C526–C535.

[40] A. Borri and M. Corradi, "Architectural heritage: A discussion on conservation and safety," *Heritage*, vol. 2, no. 1, pp. 631–647, Mar. 2019, doi: 10.3390/heritage2010041.

[41] G. Rocchi, *La basilica di San Francesco ad Assisi : prima, durante e dopo il 1997 / Giuseppe Rocchi Coopmans De Yoldi*. Firenze, 2002.

[42] A. Borri, P. Casadei, and G. Castori, "Strengthening of Brick Masonry Arches with Externally Bonded Steel Reinforced Composites," *Journal of Composites for Construction*, vol. 13, no. 6, pp. 468–475, 2009, [Online]. Available: https://www.researchgate.net/publication/255991542

[43] A. Borri, G. Castori, P. Casadei, and S. Ebaugh, "Rinforzo di Archi in Muratura con Materiali Compositi Innovativi".

[44] P. Foraboschi, "Strengthening of Masonry Arches with Fiber-Reinforced Polymer Strips," *Journal of Composites for Construction*, vol. 8, no. 3, pp. 191–202, Jun. 2004, doi: 10.1061/(asce)1090-0268(2004)8:3(191).

[45] M. Corradi, A. Borri, G. Castori, and K. Coventry, "Experimental analysis of dynamic effects of FRP reinforced masonry vaults," *Materials*, vol. 8, no. 12, pp. 8059–8071, 2015, doi: 10.3390/ma8125445.

[46] A. Borri, G. Castori, and M. Corradi, "Intrados strengthening of brick masonry arches with composite materials," *Compos B Eng*, vol. 42, no. 5, pp. 1164–1172, Jul. 2011, doi: 10.1016/j.compositesb.2011.03.005.

[47] E. Bertolesi, G. Milani, F. G. Carozzi, and C. Poggi, "Ancient masonry arches and vaults strengthened with TRM, SRG and FRP composites: Numerical analyses," *Compos Struct*, vol. 187, pp. 385–402, Mar. 2018, doi: 10.1016/j.compstruct.2017.12.021.

[48] A. Avorio, A. Borri, and G. Cangi, "Riparazione e consolidamento degli edifici in muratura," in *Manuale per la riabilitazione e la ricostruzione post sismica degli edifici Regione dell'Umbria*, Rome: DEI, 1999.

[49] M. Angelillo, *Mechanics of Masonry Structures*, vol. 551. Springer International Publishing., 2014.

[50] A. Borri, M. Corradi, G. Castori, and A. De Maria, "A method for the analysis and classification of historic masonry," *Bulletin of Earthquake Engineering*, vol. 13, no. 9, pp. 2647–2665, Sep. 2015, doi: 10.1007/s10518-015-9731-4.

[51] P. B. Lourenço, "Computational strategies for masonry structures," PhD dissertation, Delft University of Technology, 1996.

[52] P. Roca, M. Cervera, G. Gariup, and L. Pela', "Structural analysis of masonry historical constructions. Classical and advanced approaches," *Archives of Computational Methods in Engineering*, vol. 17, no. 3, pp. 299–325, 2010, doi: 10.1007/s11831-010-9046-1.

[53] P. B. Lourenço and J. G. Rots, "Multisurface Interface Model for Analysis of Masonry Structures," *Journal of Engineering Mechanics-asce*, vol. 123, pp. 660–668, 1997.

[54] D. Baraldi and A. Cecchi, "Discrete approaches for the nonlinear analysis of in plane loaded masonry walls: Molecular dynamic and static algorithm solutions," *European Journal of Mechanics - A/Solids*, vol. 57, pp. 165–177, May 2016, doi: 10.1016/j.euromechsol.2015.12.008.

[55] D. Baraldi and A. Cecchi, "A full 3D rigid block model for the collapse behaviour of masonry walls," *European Journal of Mechanics - A/Solids*, vol. 64, pp. 11–28, Jul. 2017, doi: 10.1016/j.euromechsol.2017.01.012.

[56] P. A. Cundall and O. D. L. Strack, "A discrete numerical model for granular assemblies," *Geotechnique*, vol. 29, pp. 47–65, 1979.

[57] J. Lemos, R. D. Hart, and P. A. Cundall, "A generalized distinct element program for modelling jointed rock mass," *Proceedings of the International Symposium on Fundamentals of Rock Joints*, pp. 335–343, Apr. 1985.

[58] C. Papantonopoulos, I. N. Psycharis, D. Y. Papastamatiou, J. V. Lemos, and H. P. Mouzakis, "Numerical prediction of the earthquake response of classical columns using the distinct element method," *Earthq Eng Struct Dyn*, vol. 31, no. 9, pp. 1699–1717, Sep. 2002, doi: 10.1002/eqe.185.

[59] T. Forgács, V. Sarhosis, and K. Bagi, "Minimum thickness of semi-circular skewed masonry arches," *Eng Struct*, vol. 140, pp. 317–336, Jun. 2017, doi: 10.1016/j.engstruct.2017.02.036.

[60] V. Sarhosis and J. V. Lemos, "A detailed micro-modelling approach for the structural analysis of masonry assemblages," *Comput Struct*, vol. 206, pp. 66–81, Aug. 2018, doi: 10.1016/j.compstruc.2018.06.003.

[61] A. Page, "Finite element model for masonry," *ASCE J Struct Div*, vol. 104, pp. 1267–1285, Apr. 1978, doi: 10.1061/JSDEAG.0005406.

[62] Sk. S. Ali and A. W. Page, "Finite Element Model for Masonry Subjected to Concentrated Loads," *Journal of Structural Engineering-asce*, vol. 114, pp. 1761–1784, 1988.

[63] R. Serpieri, M. Albarella, and E. Sacco, "A 3D microstructured cohesive–frictional interface model and its rational calibration for the analysis of masonry panels," *Int J Solids Struct*, vol. 122–123, pp. 110–127, Sep. 2017, doi: 10.1016/j.ijsolstr.2017.06.006.

[64] K. F. Abdulla, L. S. Cunningham, and M. Gillie, "Simulating masonry wall behaviour using a simplified micro-model approach," *Eng Struct*, vol. 151, pp. 349–365, 2017.

[65] C. Zhai, X. Wang, J. Kong, S. Li, and L. Xie, "Numerical Simulation of Masonry-Infilled RC Frames Using XFEM," *Journal of Structural Engineering*, vol. 143, no. 10, Oct. 2017, doi: 10.1061/(ASCE)ST.1943-541X.0001886.

[66] D. Addessi, C. Gatta, S. Marfia, and E. Sacco, "Multiscale Analysis of in-plane Masonry Walls Acounting for Degradation and Frictional Effects," *Int J Multiscale Comput Eng*, vol. 18, no. 2, pp. 159–180, 2020, doi: 10.1615/IntJMultCompEng.2020031235.

[67] D. Addessi, P. Di Re, C. Gatta, and E. Sacco, "Multiscale analysis of out-of-plane masonry elements using different structural models at macro and microscale," *Comput Struct*, vol. 247, p. 106477, Apr. 2021, doi: 10.1016/j.compstruc.2020.106477.

[68] J. G. Rots, B. Belletti, and S. Invernizzi, "Robust modeling of RC structures with an 'event-by-event' strategy," *Eng Fract Mech*, vol. 75, no. 3–4, pp. 590–614, Feb. 2008, doi: 10.1016/j.engfracmech.2007.03.027.

[69] R. W. Clough and J. Penzien, *Dynamics of Structures*. Berkeley: Computers and Structures, Inc., 2003.

[70] S. Huerta, "Mechanics of masonry vaults: The equilibrium approach," 2001, pp. 47–69.

[71] A. Giuffre and C. F. Carocci, "Statica e dinamica delle costruzioni murarie storiche," 1993.

[72] F. Marmo and L. Rosati, "Reformulation and extension of the thrust network analysis," *Comput Struct*, vol. 182, pp. 104–118, 2017.

[73] A. Chiozzi, G. Milani, and A. Tralli, "A Genetic Algorithm NURBS-based new approach for fast kinematic limit analysis of masonry vaults," *Comput Struct*, vol. 182, pp. 187–204, 2017.

[74] R. Hill, *The Mathematical Theory of Plasticity*. Oxford: Clarendon Press, 1950.

[75] W. Prager and P. G. Hodge, *Theory of Perfectly Plastic Solids*. University of California, 1951. Accessed: Jan. 01, 2023. [Online]. Available: https://books.google.it/books?id=x8VPAQAAIAAJ

[76] D. C. Drucker, "Coulomb Friction, Plasticity, and Limit Loads," *J Appl Mech*, vol. 21, no. 1, pp. 71–74, Mar. 1954, doi: 10.1115/1.4010821.

[77] D. C. Drucker and W. Prager, "Soil Mechanics and Plastic Analysis on Limit Design," *Q Appl Math*, vol. 10, pp. 157–165, 1952.

[78] W.-F. Chen, *Limit analysis and soil plasticity*. Elsevier Scientific Pub. Co, 1975.

[79] J. Lubliner and B. Moran, "Plasticity Theory," *J Appl Mech*, vol. 59, no. 1, pp. 245–246, Mar. 1992, doi: 10.1115/1.2899459.

[80] J. (Jean) Lemaître and J.-Louis. Chaboche, *Mechanics of solid materials*. Cambridge University Press, 1990. doi: 10.1017/CBO9781139167970.

[81] A. Kooharian, "Limit Analysis of Voussoir and Concrete Arches," *Proceedings of the American Concrete Institute*, vol. 4, pp. 317–328, 1953.

[82] R. K. Livesley, "Limit analysis of structures formed from rigid blocks," *Int J Numer Methods Eng*, vol. 12, no. 12, pp. 1853–1871, 1978, doi: 10.1002/nme.1620121207.

[83] R. K. Livesley, "A computational model for the limit analysis of three-dimensional masonry structures," *Meccanica*, vol. 27, no. 3, pp. 161–172, 1992, doi: 10.1007/BF00430042.

[84] G. Del Piero, "Limit analysis and no-tension materials," *Int J Plast*, vol. 14, pp. 259–271, 1998.

[85] G. Del Piero, "Constitutive equation and compatibility of the external loads for linear elastic masonry-like materials," *Meccanica*, vol. 24, pp. 150–162, 1989.

[86] S. Di Pasquale, "Statica dei solidi murari: teorie ed esperienze," in *Reports Dipartimento di Costruzioni*, Università di Firenze, 1984.

[87] M. Como and A. Grimaldi, "A unilateral model for the limit analysis of masonry walls," in *Unilateral problems in structural analysis*, Del Piero G. and Maceri F., Eds., Springer, 1985.

[88] M. Como, *Statics of Historic Masonry Constructions*, vol. 1. in Springer Series in Solid and Structural Mechanics, vol. 1. Heidelberg: Springer Berlin Heidelberg, 2013. doi: 10.1007/978-3-642-30132-2.

[89] L. Nunziante, L. Gambarotta, and A. Tralli, *Scienza delle costruzioni*. 2008.

[90] R. Baldacci, G. Ceradini, and E. Giangreco, *Plasticità*. 1974.

[91] D. C. Drucker, "Technical Publications," in *Mechanics of Material Behavior*, G. J. Dvorak and R. T. Shield, Eds., in Studies in Applied Mechanics, vol. 6. Elsevier, 1984, pp. 6–14. doi: https://doi.org/10.1016/B978-0-444-42169-2.50007-3.

[92] J. Salencon, "Sur le prolongement statique des champs de Prandtl pour le matériau de Coulomb.," *Archives of Mechanics*, vol. 25, pp. 643–648, Apr. 1973.

[93] A. C. Palmer, "A limit theorem for materials with non-associated flow laws," *J. de Mecanique*, vol. V, no. 2, pp. 217–222, Jun. 1966.

[94] G. Sacchi and M. Save, "A note on the limit loads of non-standard materials," *Meccanica*, vol. 3, no. 1, pp. 43–45, 1968, doi: 10.1007/BF02173992.

[95] J. salençon, "Plasticite pour la Mecanique des Sols," *Limit Analysis and Rheological Approach in Soil Mechanics*, pp. 95–166, 1978, doi: 10.1007/978-3-7091-4352-0_3.

[96] J. Heyman, *The masonry arch*. Chichester: Ellis Horwood, 1982.

[97] J. Heyman, "Couplet's engineering memoirs 1726-33," *Hist Technol*, vol. 44, pp. 1–21, 1976.

[98] C. A. Coulomb, "Essai sur une application des regles de maximis et minimis a quelques problemes de statique relatifs a 1'architecture," *Mem. Div. Sav. Acad.*, 1773.

[99] J. Heyman, *The Stone Skeleton*. Cambridge University Press, 1995. doi: 10.1017/CBO9781107050310.

[100] J. Heyman, "THE S A F E T Y OF MASONRY ARCHES," *Pergamon Press*, vol. 11, no. November 1968, pp. 363–385, 1969.

[101] J. Heyman, "Hooke's cubico–parabolical conoid," *Notes Rec R Soc Lond*, vol. 52, pp. 39–50, 1998.

[102] C. Culmann, *Die graphische Statik*. Zurich: Verlag von Meyer & Zeller, 1866.

[103] L. Cremona, *Graphical Statics: Two Treatises on the Graphical Calculus and Reciprocal Figures in Graphical Statics*. Oxford: Clarendon Press, 1890.

[104] D. W. O'Dwyer, "Funicular analysis of masonry vaults," *Computers and Structures* , vol. 73, no. 1–5, pp. 187–197, 1999.

[105] A. Andreu, L. Gil, and P. Roca, "Computational Analysis of Masonry Structures with a Funicular Model," *J Eng Mech*, vol. 133, no. 4, pp. 473–480, Apr. 2007, doi: 10.1061/(ASCE)0733-9399(2007)133:4(473).

[106] I. J. Oppenheim, D. J. Gunaratnam, and R. H. Allen, "Limit State Analysis of Masonry Domes," *Journal of Structural Engineering*, vol. 115, no. 4, pp. 868–882, Apr. 1989, doi: 10.1061/(ASCE)0733-9445(1989)115:4(868).

[107] P. Block, "Thrust network analysis: exploring three-dimensional equilibrium," Massachusetts Institute of Technology, Cambridge, MA, 2009.

[108] P. Block, T. Ciblac, and J. Ochsendorf, "Real-time limit analysis of vaulted masonry buildings," *Comput Struct*, vol. 84, no. 29–30, pp. 1841–1852, Nov. 2006, doi: 10.1016/J.COMPSTRUC.2006.08.002.

[109] F. Marmo, D. Masi, and L. Rosati, "Thrust network analysis of masonry helical staircases," *International Journal of Architectural Heritage*, vol. 12, no. 5, pp. 828–848, Jul. 2018, doi: 10.1080/15583058.2017.1419313.

[110] F. Fraternali and G. Rocchetta, "Shape Optimization of Masonry Vaults," Apr. 2002.

[111] F. Fraternali, M. Angelillo, and A. Fortunato, "A lumped stress method for plane elastic problems and the discrete-continuum approximation," *Int J Solids Struct*, vol. 39, no. 25, pp. 6211–6240, Dec. 2002, doi: 10.1016/S0020-7683(02)00472-9.

[112] F. Fraternali, "A thrust network approach to the equilibrium problem of unreinforced masonry vaults via polyhedral stress functions," *Mech Res Commun*, vol. 37, no. 2, pp. 198–204, Mar. 2010, doi: 10.1016/J.MECHRESCOM.2009.12.010.

[113] M. Angelillo, E. Babilio, and A. Fortunato, "Singular stress fields for masonry-like vaults," *Continuum Mechanics and Thermodynamics*, vol. 25, no. 2–4, pp. 423–441, Mar. 2013, doi: 10.1007/s00161-012-0270-9.

[114] M. Angelillo, "Static analysis of a Guastavino helical stair as a layered masonry shell," *Compos Struct*, vol. 119, pp. 298–304, Jan. 2015, doi: 10.1016/J.COMPSTRUCT.2014.09.007.

[115] A. Fraddosio, N. Lepore, and M. D. Piccioni, "Lower Bound Limit Analysis of Masonry Vaults Under General Load Conditions," 2019, pp. 1090–1098. doi: 10.1007/978-3-319-99441-3_118.

[116] P. Smars, "Influence of friction and tensile resistance on the stability of masonry arches," in *Structural Analysis of Historic Construction: Preserving Safety and Significance*, CRC Press, 2008, pp. 1191–1206. doi: 10.1201/9781439828229.ch138.

[117] N. A. Nodargi and P. Bisegna, "Thrust line analysis revisited and applied to optimization of masonry arches," *Int J Mech Sci*, vol. 179, p. 105690, Aug. 2020, doi: 10.1016/j.ijmecsci.2020.105690.

[118] Circolare 25 marzo 2016, "Valutazione e riduzione del rischio sismico del patrimonio culturale con riferimento alle norme tecniche per le Costruzioni di cui al DM 14.1.2008.," *n. 18*.

[119] G. Milani, "Upper bound sequential linear programming mesh adaptation scheme for collapse analysis of masonry vaults," *Advances in Engineering Software*, vol. 79, pp. 91–110, Jan. 2015, doi: 10.1016/J.ADVENGSOFT.2014.09.004.

[120] A. Chiozzi, G. Milani, N. Grillanda, and A. Tralli, "A fast and general upper-bound limit analysis approach for out-of-plane loaded masonry walls," *Meccanica*, vol. 53, no. 7, pp. 1875–1898, May 2018, doi: 10.1007/s11012-017-0637-x.

[121] A. Chiozzi, N. Grillanda, G. Milani, and A. Tralli, "UB-ALMANAC: An adaptive limit analysis NURBS-based program for the automatic assessment of partial failure mechanisms in masonry churches," *Eng Fail Anal*, vol. 85, pp. 201–220, Mar. 2018, doi: 10.1016/j.engfailanal.2017.11.013.

[122] C. Baggio and P. Trovalusci, "Limit Analysis for No-Tension and Frictional Three-Dimensional Discrete Systems*," *Mechanics of Structures and Machines*, vol. 26, no. 3, pp. 287–304, Jan. 1998, doi: 10.1080/08905459708945496.

[123] C. Baggio and P. Trovalusci, "Collapse behaviour of three-dimensional brick-block systems using non-linear programming," *Structural Engineering and Mechanics*, vol. 10, no. 2, pp. 181–195, Aug. 2000, doi: 10.12989/sem.2000.10.2.181.

[124] M. C. Ferris and F. Tin-Loi, "Limit analysis of frictional block assemblies as a mathematical program with complementarity constraints," *Int J Mech Sci*, vol. 43, no. 1, pp. 209–224, Jan. 2001, doi: 10.1016/S0020-7403(99)00111-3.

[125] C. Melbourne and M. Gilbert, "The application of limit analysis techniques to masonry arch bridges," in *Bridge Assesment Management and Design. Proceedings of the Centenary Year Bridge Conference, (HELD) 26-30 September 1994, Cardiff*, 1994.

[126] M. Gilbert and C. Melbourne, "Rigid-block analysis of masonry structures," *Structural engineer*, vol. 72, no. 21, 1994.

[127] M. Gilbert, "Limit analysis applied to masonry arch bridges: State-of-the-art and recent developments," Apr. 2007, pp. 13–28.

[128] C. Casapulla, "Dry rigid block masonry: safe solutions in presence of Coulomb friction," *Transactions on the Built Environment*, vol. 55, 2001, Accessed: May 01, 2023. [Online]. Available: www.witpress.com,

[129] M. Gilbert, C. Casapulla, and H. M. Ahmed, "Limit analysis of masonry block structures with non-associative frictional joints using linear programming," *Comput Struct*, vol. 84, no. 13–14, pp. 873–887, May 2006, doi: 10.1016/J.COMPSTRUC.2006.02.005.

[130] F. Portioli, C. Casapulla, L. Cascini, M. D'Aniello, and R. Landolfo, "Limit analysis by linear programming of 3D masonry structures with associative friction laws and torsion interaction effects," *Archive of Applied Mechanics*, vol. 83, no. 10, pp. 1415–1438, Oct. 2013, doi: 10.1007/s00419-013-0755-4.

[131] F. Portioli, C. Casapulla, M. Gilbert, and L. Cascini, "Limit analysis of 3D masonry block structures with non-associative frictional joints using cone programming," *Comput Struct*, vol. 143, pp. 108–121, Sep. 2014, doi: 10.1016/j.compstruc.2014.07.010.

[132] D. J. Sutcliffe, H. S. Yu, and A. W. Page, "Lower bound limit analysis of unreinforced masonry shear walls," *Comput Struct*, vol. 79, no. 14, pp. 1295–1312, Jun. 2001, doi: 10.1016/S0045-7949(01)00024-4.

[133] A. Orduña and P. B. Lourenço, "Cap Model for Limit Analysis and Strengthening of Masonry Structures," *Journal of Structural Engineering*, vol. 129, no. 10, pp. 1367–1375, Oct. 2003, doi: 10.1061/(ASCE)0733-9445(2003)129:10(1367).

[134] A. Orduña and P. B. Lourenço, "Three-dimensional limit analysis of rigid blocks assemblages. Part I: Torsion failure on frictional interfaces and limit analysis formulation," *Int J Solids Struct*, vol. 42, no. 18–19, pp. 5140–5160, Sep. 2005, doi: 10.1016/j.ijsolstr.2005.02.010.

[135] A. Orduña and P. B. Lourenço, "Three-dimensional limit analysis of rigid blocks assemblages. Part II: Load-path following solution procedure and validation," *Int J Solids Struct*, vol. 42, no. 18–19, pp. 5161–5180, Sep. 2005, doi: 10.1016/J.IJSOLSTR.2005.02.011.

[136] G. Milani, "3D upper bound limit analysis of multi-leaf masonry walls," *Int J Mech Sci*, vol. 50, no. 4, pp. 817–836, Apr. 2008, doi: 10.1016/J.IJMECSCI.2007.11.003.

[137] G. Milani, K. Beyer, and A. Dazio, "Upper bound limit analysis of meso-mechanical spandrel models for the pushover analysis of 2D masonry frames," *Eng Struct*, vol. 31, no. 11, pp. 2696–2710, Nov. 2009, doi: 10.1016/J.ENGSTRUCT.2009.06.015.

[138] G. Milani, F. A. Zuccarello, R. S. Olivito, and A. Tralli, "Heterogeneous upper-bound finite element limit analysis of masonry walls out-of-plane loaded," *Comput Mech*, vol. 40, no. 6, pp. 911–931, Aug. 2007, doi: 10.1007/s00466-006-0151-9.

[139] N. A. Nodargi, C. Intrigila, and P. Bisegna, "A variational-based fixed-point algorithm for the limit analysis of dry-masonry block structures with non-associative Coulomb friction," *Int J Mech Sci*, vol. 161–162, p. 105078, Aug. 2019, doi: 10.1016/J.IJMECSCI.2019.105078.

[140] S. W. Sloan and P. W. Kleeman, "Upper bound limit analysis using discontinuous velocity fields," *Comput. Methods Appl. Mech. Engrg*, vol. 127, pp. 293–314, 1995.

[141] G. De Felice, "Strutture a blocchi Applicazioni di calcolo a rottura." Università Roma Tre.

[142] J. Heyman, "The safety of masonry arches," in *Masonry Bridges, Viaducts and Aqueducts*, Routledge, 2017, pp. 329–352. doi: 10.4324/9781315249513-20.

ACKNOWLEDGEMENTS

Having come to the end of my doctoral journey, I would like to thank some of the people who contributed significantly to the completion of this thesis work.
First of all, I would like to extend my heartfelt thanks to my supervisors, Prof. Mario Daniele Piccioni and Prof. Aguinaldo Fraddosio, for giving me the opportunity to undertake this doctoral journey, for the trust they placed in me and for their valuable advice and suggestions.
I would like to express my sincerest and deepest gratitude to Prof. Elio Sacco for his constant support and for his fundamental and decisive contribution to this thesis.
Special thanks also go to my fellow travelers, who have been more than just colleagues: PhD students, fellows and researchers with whom I have shared the delights and natural anxieties of this common journey. Their presence and support have been crucial in facing challenges and overcoming obstacles along the way.
Finally, I thank my family for their ever-present support.

Giunta a conclusione del mio percorso di dottorato, desidero ringraziare alcune tra le persone che hanno contribuito in modo significativo alla stesura del presente lavoro di tesi.
Innanzitutto, vorrei rivolgere un sentito ringraziamento ai miei relatori, il Prof. Mario Daniele Piccioni e il Prof. Aguinaldo Fraddosio, per avermi dato l'opportunità di intraprendere questo percorso di dottorato, per la fiducia che hanno riposto in me, per i preziosi consigli e suggerimenti.
Desidero esprimere la mia più sincera e profonda gratitudine al Prof. Elio Sacco per il suo costante sostegno e per il contributo fondamentale e decisivo che ha dato a questa tesi.
Un ringraziamento particolare va anche i miei compagni di viaggio, che sono stati più di semplici colleghi: dottorandi, assegnisti e ricercatori con i quali ho condiviso le gioie e le naturali ansie di questo cammino comune. La loro presenza e il loro supporto sono stati fondamentali per affrontare le sfide e superare gli ostacoli lungo il percorso.
Infine, ringrazio la mia famiglia per l'immancabile sostegno.